AD-A138 242 CONDITIONS FOR TWO-CELL STRUCTURE IN SEVERE VORTICAL STORMS(U) TRW SPACE AND TECHNOLOGY GROUP REDONDO BEACH CA G F CARRIER ET AL. FEB 84 TRW-35524-6003-UT-00 1/2

UNCLASSIFIED N00014-79-C-0508 F/G 4/2 NL

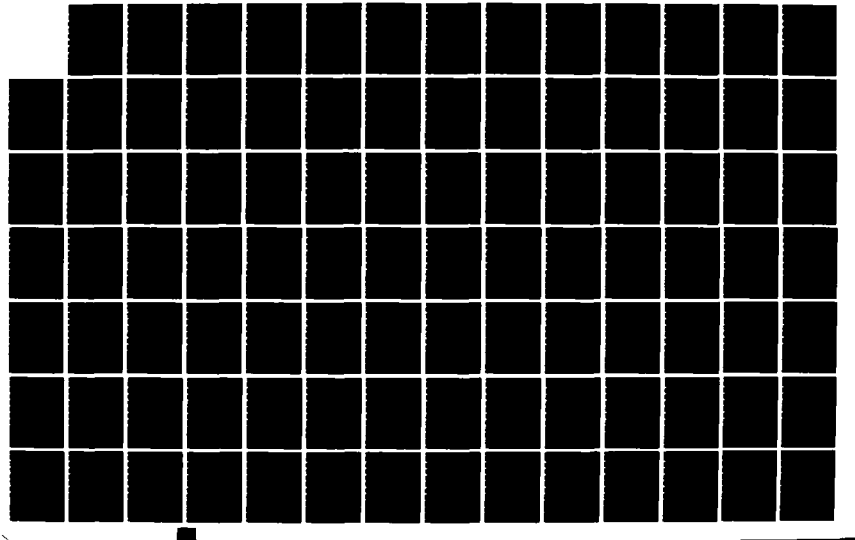

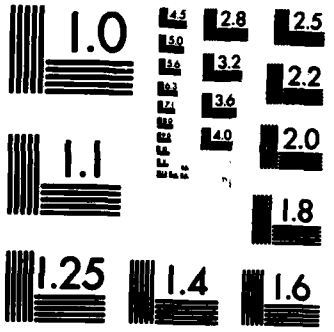

MICROCOPY RESOLUTION TEST CHART
NATIONAL BUREAU OF STANDARDS-1963-A

(12)

TRW Report 35524-6003-UT-00
ONR Contract N00014-79-C-0508
Final Report
February 1984

CONDITIONS FOR TWO-CELL STRUCTURE IN SEVERE VORTICAL STORMS

by

G. F. Carrier, F. E. Fendell, P. S. Feldman, and S. F. Fink
TRW Space and Technology Group, Redondo Beach, CA 90278

UNCLASSIFIED

SECURITY CLASSIFICATION OF THIS PAGE

REPORT DOCUMENTATION PAGE

1a. REPORT SECURITY CLASSIFICATION: UNCLASSIFIED	1b. RESTRICTIVE MARKINGS
2a. SECURITY CLASSIFICATION AUTHORITY	3. DISTRIBUTION/AVAILABILITY OF REPORT: Distribution unlimited
2b. DECLASSIFICATION/DOWNGRADING SCHEDULE	
4. PERFORMING ORGANIZATION REPORT NUMBER(S): 35524-6003-UT-00	5. MONITORING ORGANIZATION REPORT NUMBER(S)
6a. NAME OF PERFORMING ORGANIZATION: TRW Electronics & Defense Sector; 6b. OFFICE SYMBOL (If applicable)	7a. NAME OF MONITORING ORGANIZATION: Office of Naval Research
6c. ADDRESS (City, State and ZIP Code): Redondo Beach, CA 90278	7b. ADDRESS (City, State and ZIP Code): Arlington, VA 22217
8a. NAME OF FUNDING/SPONSORING ORGANIZATION; 8b. OFFICE SYMBOL (If applicable)	9. PROCUREMENT INSTRUMENT IDENTIFICATION NUMBER: N00014-79-C-0508
8c. ADDRESS (City, State and ZIP Code)	10. SOURCE OF FUNDING NOS. — PROGRAM ELEMENT NO. / PROJECT NO. / TASK NO. / WORK UNIT NO.
11. TITLE (Include Security Classification): Conditions for Two-Cell Structure in Severe Vortical Storms (U)	

12. PERSONAL AUTHOR(S): Carrier, G. F. (Harvard U.); Fendell, F. E.; Feldman, P. S.; and Fink, S. F.

13a. TYPE OF REPORT	13b. TIME COVERED	14. DATE OF REPORT (Yr., Mo., Day)	15. PAGE COUNT
Final Report	FROM 7/9/83 TO 3/2/84	1984 February	112

16. SUPPLEMENTARY NOTATION

17. COSATI CODES			18. SUBJECT TERMS (Continue on reverse if necessary and identify by block number)	
FIELD	GROUP	SUB. GR.	Hurricane	Tornado Cyclone
			Severe Local Storm	Tropical Cyclone
			Tornado	Typhoon

19. ABSTRACT (Continue on reverse if necessary and identify by block number)

Predictive capability for the intensity of severe vortical storms of the troposphere entails anticipation of which systems will undergo transition from one-cell to two-cell structure, and which will not. Roughly half of all tropical storms, and nearly half of all mesocyclones, undergo this transition, in which the low-level pressure differential between periphery and center may increase from O(1%) to O(10%) of atmospheric pressure, and the peak swirl speed may increase from O(50 m/s) to O(100 m/s). The transition entails insertion of relatively dry, nonrotating, compressionally heated, tropopause-level air at the axis of the vortex, such that slowly recirculating air (an eye) displaces to an annulus (the eyewall) the rapidly swirling cloudy updraft arising from separation of the low-level inflow layer. This investigation inquires whether the vertical stratification of the circulation at the periphery of the vortex (which varies only slowly in time) might not provide a relatively accessible observable that suggests whether two-cell structure can be sustained by the vortex. To this end, an integral-type (transversely averaged) numerical

20. DISTRIBUTION/AVAILABILITY OF ABSTRACT	21. ABSTRACT SECURITY CLASSIFICATION
UNCLASSIFIED/UNLIMITED ☐ SAME AS RPT. ☒ DTIC USERS ☐	Unclassified

22a. NAME OF RESPONSIBLE INDIVIDUAL	22b. TELEPHONE NUMBER (Include Area Code)	22c. OFFICE SYMBOL
Robert F. Abbey, Jr.	(202 696-4125	Code 422MM

DD FORM 1473, 83 APR — EDITION OF 1 JAN 73 IS OBSOLETE.

UNCLASSIFIED

SECURITY CLASSIFICATION OF THIS PAGE

19. (Abstract, continued)

solution is obtained to an inviscid, thin-layer formulation for the position, thickness, wind-speed components, and thermodynamic state of the separated inflow layer. The free layer for the tornadic mesocyclone, of relatively limited radial extent, is described conveniently in two segments: (1) a low-level portion, termed the turnaround, in which (with increasing altitude) the separated layer undergoes an incursion toward the axis of rotation and then an excursion away from the axis, such that the layer is inferred to become unstable and undergo a breakdown when the fluid recovers a radial distance comparable to that at separation; and (2) a vertically extensive portion (extending to near-tropopause height) in which the layer remains of fairly constant thickness but is situated modestly further from the axis with increasing altitude. Peripheral circulation constant with altitude characterizes solutions compatible with two-cell structure. For the relatively broad horizontal expanse of a tropical cyclone, the turnaround alone describes virtually the entire ascent through the troposphere of the separated inflow layer; furthermore, the separated layer thickens until it is no longer treated well by the thin-strip-type formulation undertaken here. Nevertheless, the theory does give insight into what balance of forces describes conservation of momentum in a typhoon eyewall.

Acknowledgments

The authors are grateful to Walter Martin and James Hughes for the opportunity to pursue this investigation under Office of Naval Research contract N0014-79-0508. The authors also wish to thank Ann McCollum for preparation of the manuscript and Asenatha McCauley for preparation of the figures.

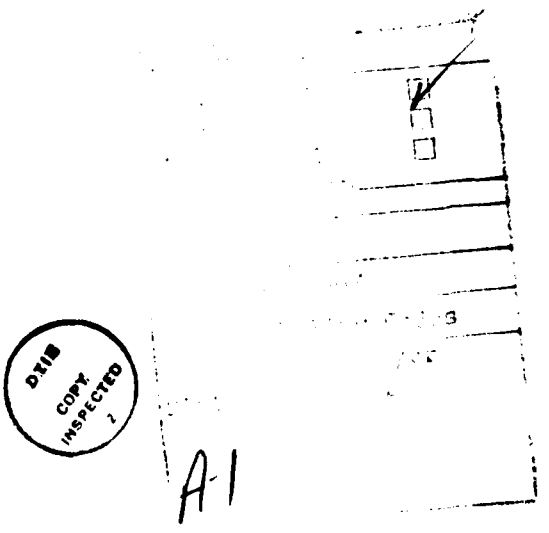

TABLE OF CONTENTS

TABLE OF CONTENTS (Continued)

ABSTRACT

Predictive capability for the intensity of severe vortical storms of the troposphere entails anticipation of which systems will undergo transition from one-cell to two-cell structure, and which will not. Roughly half of all tropical storms, and nearly half of all mesocyclones, undergo this transition, in which the low-level pressure differential between periphery and center may increase from O(1%) to O(10%) of atmospheric pressure, and the peak swirl speed may increase from O(50 m/s) to O(100 m/s). The transition entails insertion of relatively dry, nonrotating, compressionally heated, tropopause-level air at the axis of the vortex, such that slowly recirculating air (an eye) displaces to an annulus (the eyewall) the rapidly swirling cloudy updraft arising from separation of the low-level inflow layer. This investigation inquires whether the vertical stratification of the circulation at the periphery of the vortex (which varies only slowly in time) might not provide a relatively accessible observable that suggests whether two-cell structure can be sustained by the vortex. To this end, an integral-type (transversely averaged) numerical solution is obtained to an inviscid, thin-layer formulation for the position, thickness, wind-speed components, and thermodynamic state of the separated inflow layer. The free layer for the tornadic mesocyclone, of relatively limited radial extent, is described conveniently in two segments: (1) a low-level portion, termed the turnaround, in which (with increasing altitude) the separated layer undergoes an incursion toward the axis of rotation and then an excursion away from the axis, such that the layer is inferred to become unstable and undergo a breakdown when the fluid recovers a radial distance comparable to that at separation; and (2) a vertically extensive portion (extending to near-tropopause height) in which the layer remains of fairly constant

thickness but is situated modestly further from the axis with increasing altitude. Peripheral circulation constant with altitude characterizes solutions compatible with two-cell structure. For the relatively broad horizontal expanse of a tropical cyclone, the turnaround alone describes virtually the entire ascent through the troposphere of the separated inflow layer; furthermore, the separated layer thickens until it is no longer treated well by the thin-strip-type formulation undertaken here. Nevertheless, the theory does give insight into what balance of forces describes conservation of momentum in a typhoon eyewall.

1. Introduction

Progress in forecasting the intensity of already organized vortical storms requires identifying observable(s) that foretell whether or not evolution from one-cell to two-cell structure will occur. Very roughly, about half of all tropical storms (Fendell 1974), and about one-quarter to one-half of mesocyclones (Brooks 1949; Houze, Jr. and Hobbs 1982), undergo transition from a Rankine-type radial profile for swirling (with low-level inflow, central updraft, and upper-level outflow). Specifically, with the insertion of a central column of relatively dry, clear, nonrotating, slowly recirculating, originally tropopause-level air, the region of intensely swirling, cloudy updraft becomes an annulus displaced from the axis of symmetry. The full insertion of an "eye" within an "eyewall" implies that ground-level pressure deficits from the center to the ambient edge of the vortex, on the order of one-or-two percent of atmospheric pressure (and peak swirl of not much over 50 m/s, at most) prior to insertion of an eye, increase to deficits on the order of five-to-ten percent of atmospheric pressure (and peak swirl modestly in excess of 100 m/s) (Miller 1958). Is there an accessible observable that would permit anticipating whether a tropical storm will become a supertyphoon and/or whether a tornado cyclone will spawn one or more virulent tornadoes ($\sim$1 h duration, 150 km path, 100 m/s peak swirl)? Of course, the intensity of a tropical storm is not a simple monotonic intensification, followed by a simple monotonic decay; rather, cyclic strengthening-weakening suggests several partial insertions and retractions of an "eye" (Carrier 1971b); damage along the path of a tornado [and peak swirl speed inferred from funnel-cloud length (Dergarabedian and Fendell 1971a, 1971b)] suggests similar behavior.

Accessibility suggests seeking the observable at the periphery of the vortex; e.g., the upper-tropospheric cloud cover can frustrate passive sensors of a meteorological satellite. It is well known that a midtropospheric minimum in the total static enthalpy (the sum of static enthalpy, latent-heat equivalent of water-vapor content, and gravitational potential energy) portends severe weather (Darkow 1967); however, the nature, time scale, and degree of severity usually cannot be anticipated simply on the basis of a local, convectively unstable stratification. Thus, one turns to the wind magnitude and direction: specifically, is the variation with altitude of the circulation at the edge of a moderate one-cell vortex indicative of the capacity of the system for intensification to two-cell structure? It is anticipated that the vertical profile of the circulation at the edge of the vortex (1) varies but modestly over system lifespan and (2) varies but modestly over radial position (until one reaches the central regions, or "core", of the vortex). Thus, the stability of the vortex, if it were to undergo transition to two-cell structure, plausibly may be indicated by one sampling of variation of peripheral circulation with altitude.

Application of linear stability theory to a nascent weak disturbance to identify criteria for intensification is difficult because many processes maintaining the ambient today must be described by parameterizations of uncertain validity; also, early entrance of nonlinear effects frustrates identification of the state to which the system evolves. Applying linear stability to an already well-defined vortical storm would seem more relevant for identifying conditions for evolution to two-cell structure; however, the same difficulties with parameterizations (can sub-vortex-scale phenomena such as cumulus convection, turbulent

diffusion and, possibly relevantly, radiative transfer be parameterized in terms of vortex-scale variables and, if so, what are the correct parameterizations?) and with small-perturbation theory hold--and adequate, yet simple, description of a one-cell configuration, for facile perturbation, is not a trivial matter. Instead of a temporal development, a steady analysis is undertaken that inquires whether "eye-within-an-eyewall" configuration is consistent with only certain ambient stratifications of circulation. If it turns out that two-cell structure is compatible with virtually any variation of ambient circulation with altitude, then no discriminant has been identified. Also, it must turn out (1) that the analysis is insensitive to parameterization details, or else it suffers from limitations already noted, and (2) that results are insensitive to geometric details, or else the approximate analysis to be undertaken is too crude.

Finally, it is remarked that the translational path of the vortex is an entirely separate matter that can be approached by statistical data from historical record, or by embedding the vortex in larger-scale atmospheric dynamics. Attention here is confined to anticipating intensity.

2. Structure of a Severe Atmospheric Vortex

2.1 Four-Part Structure of a Two-Cell Vortex

Since the possible transition from one-cell to two-cell structure primarily concerns alteration in the more rapidly swirling "core" of the vortex, a time-averaged axisymmetric analysis is undertaken. It seems premature to account for gustiness and asymmetries [e.g., manifestation of large-scale coherent structure (Roshko 1976) such as suction vortices (Fujita et al 1976)] until a more

elementary description is established. It is taken that time-dependent investigation of intensification and of decay would yield results consistent with the structure proposed for a postulated quasisteady mature stage.

A closed model is adopted, such that diffusive (but not convective) transport across domain boundaries may occur. These boundaries are a lateral edge at which the swirl has diminished to virtually ambient value; an isobaric, isothermal slippery lid set at the altitude to which ground- (or sea-) level air would rise, in view of its total static enthalpy (in the convectively unstable stratification), upon moist-adiabatic ascent[1]; and the ground plane or sea surface, approximated as an isothermal boundary enforcing a virtual no-slip constraint on the velocity field. In a numerical approach, a uniformly valid boundary-value problem would be posed and solved for the postulated quasisteady mature stage of a severe

---

[1] In the locus of thermodynamic states referred to as the moist adiabat, air expands and cools as it rises, until it becomes saturated. Thenceforth during ascent, sufficient water vapor condenses to maintain saturation at the locally prevailing temperature. The air retains the heat of phase transition, and the condensed water substance either falls out or is conveyed along, but reversal of the process (evaporative cooling) is precluded. Ascent is idealized as too rapid to permit dilution of the updraft with drier and/or cooler air. The level of neutral stability entails recovery of ground-level (or sea-level) total static enthalpy; identification of the system "lid" at such an altitude deviates from conventional definition of the tropopause. In fact, of course, in idealizing the eyewall as characterized by a moist adiabat, one is ignoring structure within the eyewall, and is omitting dilution of eyewall air with air from the eye and/or with air from the potential vortex (Appendix A).

atmospheric vortex. In the subdivisional approximate analyses to be undertaken here, only the locally dominant processes are retained, and enforcing appropriate continuity of fields and fluxes at subdivisional interfaces yields a global solution; selfconsistency is established by a posteriori substitution of the solution to confirm that the locally dominant processes have been anticipated correctly. It is recognized that some relaxation of the closed nature of the model may be required (e.g., possible downflux of stratospheric air into an eye, upper-tropospheric outflow of eyewall air, etc.); nevertheless, the closed, subdivisional model is a convenient vehicle for presentation.

A previously adopted three- or four-part structure for a mature, quasisteady axisymmetric severe atmospheric vortex (Carrier 1970; Carrier et al. 1971) is briefly reviewed to permit the presentation to be selfcontained (figure 1). The bulk of the vortex consists of rapidly swirling air (region I), the radial variation of the azimuthal velocity component being approximated adequately as that of a potential vortex; the ultimate source of the swirl is the rotation of the earth. Whereas there is appreciable radial influx in the bulk of the vortex during spin-up, in the quasisteady mature stage of interest here, the radial influx need preclude only outward movement of the central-ascent region, and since only a very small influx is required for that, the radial influx seems negligible. Thus, after spin-up, there is a cyclostrophic balance [holding radially between the central updraft and peripheral edge, holding axially between the surface-layer inflow and upper-troposphere outflow (see below)], such that the radial pressure gradient balances the centrifugal force; the more meticulous (so-called) gradient-wind balance does not seem required

for present purposes. The angular momentum at any radial position in the bulk of the vortex is that holding at the periphery at the same height. Whereas there may be local transient updrafts and downdrafts, on average there is a slow downdraft of air from the bulk vortex to the surface inflow layer; while the local downflux may be modest in magnitude, the total downflux, upon summing over area, suffices to furnish the "throughput" of the vortex (i.e., the secondary flow, associated with low-level influx, central updraft, and upper-level outflow). The thermodynamic fields throughout the "throughput-supply" region (i.e., the bulk-vortex region) are those prescribed to hold at the peripheral edge; the major exception is the isobars, which are horizontal at the periphery (where hydrostatics holds), but which dip groundward (or seaward) with enhanced swirling (i.e., with decreasing radial distance from the axis of symmetry). While the thermodynamic stratification of the bulk-vortex region is indicative of the ambient in which the vortex was formed, sea-to-air transfer maintains the stratification for the tropical cyclone over the trades in a manner precluded for a continental mesocyclone. In any case, the throughput supply is finite, and the later throughput may be drier and cooler than earlier throughput; however, other phenomena may enter to disrupt the system prior to throughput exhaustion (e.g., disruption by orographic lifting).

The low-level inflow region (II) is the only one in which angular momentum is not conserved; it is dissipated in part, owing to the no-slip boundary condition that engenders a swirling influx (so-called "tea-cup effect"). Thus, indeed there must be a modest downdrift on average into the surface layer, in which radial and azimuthal velocity components are comparable and significant. In fact, there is

an accelerating radial pressure gradient acting on the inflow layer; thus it is not surprising that, under the high-speed portion of the vortex, the diffusive-like processes are confined to a thin sublayer contiguous to the ground or sea--a sublayer that becomes ever thinner as the axis of rotation is approached, even though the total inflow-layer thickness grows (albeit modestly) with decreasing radial distance from the axis (Burggraf et al 1971; Carrier 1971a; Carrier and Fendell 1978). Specifically, over the bulk of the inflow layer, inviscid processes are controlling; at fixed radial distance from the axis, as one descends vertically downward, the virtual pure swirling of the bulk vortex gradually becomes virtual pure radial influx of the same magnitude (appropriate for the radial distance from the axis). Only across the sublayer does the velocity fall abruptly to zero. This established behavior is belabored because (1) it justifies an inviscid treatment of most of the inflow layer if it separates to form an eyewall; (2) it emphasizes that the portion of the eyewall contiguous to the eye may shear the eye into recirculation, but can impart little rotation to the eye fluid; (3) it emphasizes that the portion of the eyewall contiguous to the potential vortex but modestly shears the potential vortex; (4) it emphasizes the nature of the (sublayer) fluid that lies below the eye, if the eye does not extend from the tropopause down the full extent of the troposphere to the sea surface (or ground); and (5) it characterizes the velocity-component profiles holding in the inflow layer at separation.

Whereas the quantitative description of the bulk vortex and surface-inflow layer seems already adequately in hand for present purposes, the description of the turnaround [whereby the separating inflow layer turns vertical (lowest

portion of III)] and the eyewall [whereby the vertical inflow layer rises the extent of the troposphere (middle and upper portion of III)] has been but very roughly examined, and is the subject of closer scrutiny here. It may be noted that for a one-cell vortex, the surface-inflow layer continues into the axis ($r^*=0$) without separation, and then turns upward by necessity. The emphasis on inflow-layer separation into a free shear layer (the position of whose inner boundary/interface with the eye, and the position of whose outer boundary/interface with the bulk vortex, are set by requiring continuity of pressure and are ascertained in the course of solution) anticipates that two-cell structure is to be scrutinized below. It may also be noted that a moist-adiabatic locus of thermodynamic states holds in the separated layer, that angular momentum is conserved along its streamlines, that the total head along its streamlines is constant (aside from the gravitational-potential term), that a cyclostrophic-like force balance holds in the layer, and that the separating-inflow-layer thickness and the turnaround-and-eyewall thickness are probably roughly comparable (at least up to midtroposphere). Thus, the turnaround and eyewall involve a relatively thin layer across which the transverse pressure gradient is significant; frequently in highly subsonic flow, the transverse pressure gradient is small across thin layers, so the present context is not entirely conventional, and fortunately integral-type (transversely averaged) treatment is adequate for present purposes. Whereas the upper-tropospheric turning of the eyewall into an outflow layer is to be the subject of closer scrutiny in future work, here attention is concentrated on the lower troposphere and midtroposphere.

The locus of thermodynamic states that characterize the inflow layer and turnaround/eyewall is given by the moist adiabat based on ground-level (or sea-

level) ambient; the ambient altitude is assigned to the level of neutral stability, $z^*=z_t^*$. The eye (IV) is idealized as completely dry, so its locus of thermodynamic states is based on a dry adiabat, referenced to the neutral-stability-lid altitude and state. Mass exchange, from the eye to the eyewall at the lower altitude and from the eyewall to the eye at greater altitude, is to be included in future investigations; incidentally, the net eye/eyewall exchange need not be in perfect balance, though imbalance implies net flux across the ceiling lid. It is in the emphasis on the significance of the eye for the intense vortex that the structure presented here is distinguished from other treatments (e.g., Barcilon 1967).

2.2 Implications of Lateral Scale on Vortex-Core Analysis

The severe atmospheric vortex has been characterized as a once-through cycle, in which a throughput supply is exhausted as air is processed[2]; the processed air is too dry for effective recycling, and recycling on the scale of vortex lifetime might entail compressional heating (during descent at the periphery) incompatible with a central-pressure deficit at ground level (or sea level).

As already noted, specification of the ambient stratification (holding at $r^*=r_o^*$) implies the amount of lateral, low-altitude reduction of pressure at the axis of symmetry from the value of pressure holding at the periphery, on the basis of moist adiabatic ascent (one-cell vortex), and the amount of further pressure reduction on the basis of dry-adiabatic compression of air from the neutral-stability level (two-cell vortex) (Lilly 1969; Gray 1970; Dergarabedian

---

[2]The closed model with a "captured" throughput supply is more appropriate for the large lateral scale of the tropical cyclone than for the limited lateral scale of a rotating thunderstorm.

and Fendell 1970, 1977). The eye air need not be recompressed eyewall air, but could be descending stratospheric air (partly or entirely). Contrary to postulations of earlier models (Malkus and Riehl 1960), recent satellite photography (Black 1977) confirms sufficient outward slope of the eye/eyewall interface (Haurwitz 1935), so that the augmented pressure deficit from ambient (associated with eye insertion) is available to support enhanced eyewall swirl speeds. In particular, if one cencentrates attention just above the surface inflow layer, ignores lateral density variations at low altitude in the dynamics, and adopts a radial profile for the swirl, integration of the cyclostrophic approximation to the conservation of radial momentum yields the peak swirl for a thermo-hydrostatically computed low-level pressure deficit. For example, a Rankine-vortex model, such that the pressure deficit is expended in equal amounts to sustain the rigidly rotating core and the outer potential vortex, is plausible for a one-cell vortex; since the eye is nonrotating in two-cell structure, the entire (larger) pressure deficit sustains an outer-potential-vortex profile (only). In any case, one obtains a peak swirl speed holding near ground level at the innermost radius of the potential vortex, V*. As already noted, V* is about 50 m/s or less for one-cell structure (moist-adiabatic ascent near the axis), and over 100 m/s for two-cell structure (dry-adiabatic eye near the axis)--since tornado-prone and hurricane-prone ambients often yield comparable low-level central pressure deficits from ambient.

The other parameter that characterizes a vortex is r_1*, the radial distance from the axis at which V* holds; also at $r^*=r_1^*$, the inflow layer (II) separates to constitute the turnaround (lowest portion of III) for cases of

two-cell structure (i.e., cases in which region IV exists). For an intense tornado, this distance is taken to be O(170 m), while for a typhoon this distance is taken to be O(16 km). From knowledge of V* and r_1*, and of the circulation and thermodynamic state as a function of altitude at the vortex periphery (where r_0*>>r_1*, so that the periphery may be taken to be at infinity, without significant error, for many purposes), one expects to be able to deduce all other mean properties of the vortex.

Clearly, both tornado and hurricane extend through the troposphere, or O(14 km) vertically; however, the vast difference in radial scale between a devastating tornado arising from evolution to two-cell structure in a mesocyclone and a devastating typhoon from evolution to two-cell structure in a tropical cyclone necessitates special provision for treatment of the two vortices within one formulation. In particular, it is anticipated that the separating inflow layer (perhaps 50 m thick for a tornado, and perhaps 1 km thick for a typhoon) continues radially inward as it rises after separation, reaches a minimum finite distance from the axis, and then turns outward from the axis. It is further anticipated that the <u>altitude</u> over which this inward, outward (turnaround) excursion occurs is O(r_1*). For a tornado, the entire turnaround involves the lowest 170 m or so of the troposphere. The overwhelming preponderance of the description of the fate of the separated inflow layer lies subsequent to the turnaround, in what was termed the eyewall. For a typhoon, the turnaround might involve a vertical distance of 14 km or so, the entire depth of the trophsphere; if the entire fate of the separated inflow layer is given by the turnaround, then there is no sequential eyewall region after separation.

2.3 The Turnaround for the Typhoon and for the Hurricane

For the typhoon, one anticipates the need to retain the gravitational potential, the variation of the bounding eye and eyewall pressures with altitude, and the change of density with altitude, in treatment of the turnaround. However, for the tornado, one may ignore change of the gravitational potential, change of the bounding eye and eyewall pressures with altitude, and the change of density with height; indeed, one may ignore even the variation of thickness of the separated layer with height for the tornado, since the thickness is so small. Thus, a simple, semianalytic incompressible model may be derived for the tornado, since its only purpose is to furnish conditions holding at the end of the inward-outward excursion of the separated inflow layer in the turnaround; such conditions hold at the start of the more vertical rise of the eyewall. However, it turns out that analysis of the turnaround for the tornado may be superfluous for even this objective. The reason is that completion of the inward-outward excursion of the turnaround leads to a configuration such that the streamlines of the separated layer are concave in the direction of increasing streamwise velocity. The associated instability is taken here to imply occurrence of the still incompletely understood vortex-breakdown phenomenon. Thus, no attempt is made to infer conditions at the outset of the tornado eyewall; rather, plausible conditions holding after the breakdown are estimated.

The density decreases with altitude, so by simple continuity considerations, one anticipates that the displacement of the eyewall from the axis of symmetry increases with height; however, the multiple of density decrease

limits the multiple of increase. While the direct procedure for investigating the eyewall would be to specify the stratification of ambient circulation and to deduce the radial displacement of the eyewall from the axis, it turns out more tractable to solve the inverse problem in which the displacement is specified and the associated stratification of circulation is inferred.

3. The Turnaround

3.1 The Tornado

An inviscid incompressible steady axisymmetric flow with swirl could be adopted to describe the lowest portion of region III; in general, a quasilinear second-order elliptical partial differential equation for the streamfunction would satisfy nonlinear gradient-type constraints on both the streamsurface contiguous to the eye (IV) and also the streamsurface contiguous to the outer potential vortex (I) (see, e.g., Batchelor 1967, pp. 543-546). Such a challenging free-boundaries problem would require numerical solution; even then, it would not be of particular value, since retention of density variation seems essential to any treatment that aspires to describe region III through the extent of the troposphere.

A transversely averaged, integral-type treatment of the variable-density separated shear layer is developed in succeeding sections. Here a constant-density treatment of the lowest portion of region III is presented. As noted in Section 2, such a treatment can pertain only to the tornado, in which the turnaround entails a region that extends from ground level to but 170 m or so (such that hydrostatic effects, and variation of ambient circulation, are negligible over the vertical extent of interest). Furthermore, the turnaround for the tornado evolves to an unstable state that does not furnish definitive guidance for the eyewall calculation (the solution for region III over the rest of the troposphere). Thus, the constant-density treatment that immediately follows serves mainly as a preparation for the variable-density treatment required for the typhoon turnaround (that occurs over a height that extends many kilometers up from the sea surface); the reader familiar with turnarounds needs but skim quickly over the remainder of Section 3.1 for notation.

The momentum balance in an axisymmetric, separated boundary layer without structure is sought (figure 2). If the lowest portion of a fully inserted eye is isobaric at pressure p^*_{eye}, then the pressure in the potential vortex is (density ρ^* const.)

$$p^*(r^*,z^*) = p^*_{eye} + \frac{1}{2}\rho^* V^{*2}\left[1 - \left(\frac{r_1^*}{r^*}\right)^2\right] , \qquad (3.1.1)$$

where super asterisk denotes a dimensional quantity; at the separation radius, $p^*(r_1^*,z^*) = p^*_{eye}$, in the absence of hydrostatic effects. For $r^* < r_1^*$, the radial pressure gradient adds to the centrifugal force associated with swirling v^*, such that the sum of two forces is balanced witn a centrifugal force associated with the (radial and axial) motion q^*; thus q^* is the velocity component in a plane containing the axis of symmetry, and is perpendicular to v^*.

Accordingly, if $R^*(z^*)$ denotes the radial distance from the axis to the outer surface of the eyewall, at any point $[R^*(z^*),z^*]$, the force balance perpendicular to the thin sheet gives

$$-\frac{\partial}{\partial h^*}\left(\frac{p^*}{\rho^*}\right) = \frac{q^{*2}\,R^{*\prime\prime}}{[1 + (R^{*\prime})^2]^{3/2}} - \frac{v^{*2}}{R^*\,[1 + (R^{*\prime})^2]^{1/2}} , \qquad (3.1.2)$$

where h^* represents a coordinate running across the sheet, prime denotes ordinate derivative, and the two principal radii of curvature have been introduced. If $\Gamma^* \equiv r_1^*\,V^* = R^*v^*$,

$$\int v^{*2}dh^* = \Gamma^{*2}\int \frac{dh^*}{[R^*(h^*)]^2} = \frac{r^{*2}_1\,V^{*2}\,A^*}{R^{*2}} \text{ if } \frac{A^*}{R^{*2}} \equiv \int \frac{dh^*}{[R^*(h^*)]^2} ; \qquad (3.1.3)$$

$$\int q^{*2}\,dh^* = V^{*2}\,B^* \Rightarrow B^* = \int \left[\frac{q^*(h^*)}{V^*}\right]^2 dh^* . \qquad (3.1.4)$$

From these definitions (A*,B* consts.), and from (3.1.1) applied at r* = R*, (3.1.2) integrates to

$$\frac{V^{*2}}{2}\left[1 - \frac{r_1^{*2}}{R^{*2}}\right] = \frac{A^* V^{*2} r_1^{*2}}{R^{*3}[1 + (R^{*\prime 2})]^{1/2}} - \frac{B^* V^{*2} R^{*\prime\prime}}{[1 + (R^{*\prime})^2]^{3/2}} . \tag{3.1.5}$$

The following nondimensionalization is introduced:

$$R = \frac{R^*}{r_1^*} , \; z = \frac{z^*}{r_1^*} , \; h = \frac{h^*}{r_1^*} , \; \alpha = \frac{2A^*}{r_1^*} , \; \beta = \frac{2B^*}{r_1^*} . \tag{3.1.6}$$

If $A^* \doteq h^*$, $B^* \doteq (h^*/2)$, seemingly reasonable values, then $(\alpha/2) = \beta = h$, where h is O(0.2). In any case, under (3.1.6), (3.1.5) becomes (with α,β specified)

$$1 - \frac{1}{R^2} = \frac{\alpha}{R^3(1 + R'^2)^{1/2}} - \frac{\beta R''}{(1 + R'^2)^{3/2}} \Rightarrow R'' = \frac{\alpha}{\beta}\left(\frac{1 + R'^2}{R^3}\right) - \frac{1}{\beta}\left(\frac{R^2 - 1}{R^2}\right)\left(1 + R'^2\right)^{3/2} . \tag{3.1.7}$$

For this translationally invariant (in z) equation, which yields R periodic in z (see below), solution is sought for positive and negative z, where the boundary conditions are taken to be

$$R(0) = 1, \tag{3.1.8}$$

$$R'(0) = R_o' \text{, given const (taken positive).} \tag{3.1.9}$$

The boundary conditions preclude odd or even solution for R(z). Sought are R^+, the largest value of R, which occurs at R'= 0, and R^-, the smallest value of R, which also occurs at R'= 0. Since $R^- < 1$, $v^*(R^{*-})/v^*(r_1^*) = [v^*(R^{*-})/V^*] > 1$; the magnitude of this "overshoot" of swirl is sought as a function of (plausible values for) the parameters α,β.

While numerical treatment of (3.1.6) - (3.1.9) ultimately is used, some preliminary phase-plane analysis is useful (figure 3):

$$\frac{dR}{dz} \equiv P(R) \Rightarrow \frac{d^2R}{dz^2} = \frac{dP}{dz} = \frac{dR}{dz}\frac{dP}{dR} = P\frac{dP}{dR} \quad ; \tag{3.1.10}$$

hence

$$\frac{\beta PP'}{(1+P^2)^{3/2}} = \frac{\alpha}{R^3(1+P^2)^{1/2}} + \frac{1}{R^2} - 1 \quad . \tag{3.1.11}$$

---

[3] Although the following development is not pursued here to the extent of obtaining results, it may be worth noting that if

$$H(R) = (1+P^2)^{-1/2},$$

then (3.1.11) becomes

$$-\beta H' = \frac{\alpha H}{R^3} + \frac{1}{R^2} - 1 \quad .$$

If

$$\tau = R^{-2} \quad ,$$

then

$$2\beta\frac{dH}{d\tau} - \alpha H = \tau^{-1/2} - \tau^{-3/2} \quad ,$$

or

$$H = (\beta\tau^{1/2})^{-1} - \left(\frac{\pi}{2\alpha\beta}\right)^{1/2}\left(1+\frac{\alpha}{\beta}\right)\exp\left(\frac{\alpha\tau}{\beta}\right)\operatorname{erfc}\left(\frac{\alpha\tau}{2\beta}\right)^{1/2} + E\exp\left(\frac{\alpha\tau}{2\beta}\right) \quad ,$$

where E is a const. of integration. Since P = (dR/dz),

$$\frac{dR}{dz} = \left\{1 + [H(\tau)]^{-2}\right\}^{1/2} = \frac{d(\tau^{-1/2})}{dz} \Longrightarrow$$

$$dz = \frac{d(\tau^{-1/2})}{\left\{1 + [H(\tau)]^{-2}\right\}^{1/2}} \quad ,$$

where $H(\tau)$ is given above.

The slope P' is infinite at $P = 0$, and is zero for R satisfying

$$\frac{\alpha}{R^3(1 + P^2)^{1/2}} + \frac{1}{R^2} - 1 = 0 \quad ; \tag{3.1.12}$$

The intersection of the curve of (3.1.12) with the ray $P = 0$ is given by

$$\frac{\alpha}{R_*^3} + \frac{1}{R_*^2} - 1 = 0 \quad , \tag{3.1.13}$$

where $R_* = 1$ for $\alpha = 0$ and $R_* > 1$ for $\alpha > 0$. For $1 >> \alpha > 0$, $R_* = 1 + (\alpha/2) - (3\alpha^2/8) + \ldots$.

For the special case of no swirl $\alpha = 0$, multiplication of (3.1.11) by R' yields the integral

$$\frac{\beta}{(1 + R'^2)^{1/2}} = \frac{(R - 1)^2}{R} + \frac{\beta}{m} \quad , \tag{3.1.14}$$

where the constant of integration has been written as (β/m), with

$$m = (1 + R_0'^2)^{1/2} \tag{3.1.15}$$

for consistency with the boundary conditions (3.1.8) and (3.1.9). Since, from (3.1.14), R' is maximum at $R = 1$, $(1 + R_0'^2)^{1/2}$ is the maximum value of $(1 + R'^2)^{1/2}$, whence the symbol m. At $R' = 0$,

$$R^{\pm} = 1 + \frac{\beta}{2}\left(1 - \frac{1}{m}\right) \pm \left[\frac{\beta}{2}\left(1 - \frac{1}{m}\right)\right]^{1/2}\left[2 + \frac{\beta}{2}\left(1 - \frac{1}{m}\right)\right]^{1/2} . \tag{3.1.16}$$

For $R_0' \to 0$ so $m \to 1$, $R^{\pm}$ merge to unity; this case involves a vertically separating surface inflow layer, and hence no overshoot. For $R_0' \to \infty$ so $m \to \infty$, $R^{\pm}$ remain bounded:

$$R^{\pm} = 1 + \frac{\beta}{2} \pm \left(\frac{\beta}{2}\right)^{1/2} \left[2 + \frac{\beta}{2}\right]^{1/2} \quad ; \qquad (3.1.17)$$

this case involves effectively horizontal inflow of the separating surface layer and leads to the minimum value of R^- for fixed β. For $\beta = 0.1$, $R^+ \doteq 1.37$ and $R^- \doteq 0.73$; for $\beta \doteq 0.2$, $R^+ = 1.56$ and $R^- \doteq 0.64$. Since $\beta = O(0.2)$ is a plausible value, these values suggest what proves to be a general trend: R^- decreases as β increases and as R_o' increases.

Finite values for α indicate finite swirl; increasing α yields larger values of R^- and hence smaller overshoot of swirl. From results of numerical integration given in table 1 and supplemented by figures 4 and 5, for finite α, $R^{\pm}$ approach finite values as $R_o' \to \infty$ for fixed β. For the plausible values $\alpha = 0.1$, $\beta = 0.2$, for $R_o' = 2, 5, 10$, the corresponding values of R^- are 0.748, 0.695, 0.677. Hence, swirl overshoots in the range of about 30% seem plausible, but not much more. Estimates (Lewellen 1977, p. 109) that the swirl in the turnaround can exceed swirl at $R = 1$, $z = h$ by 100% are excessive according to this analysis.

As suggested earlier, the periodic nature of the mathematical solution is not observed physically because of known instability of flows under centrifugal forces acting on concave streamlines. Soon after one incursion and return of the separated shear layer, "vortex breakdown" (Hall 1972; Leibovich 1978) enters, and no attempt is undertaken here to describe details of this process. What emerges is taken to be a vertical free layer, the evolution of which with height entails a more inclusive model (holding through a considerable depth of the troposphere) attempted in Section 4 below.

3.2 The Typhoon

As already noted, if the vertical extent of the turnaround for the two-cell tropical-storm case is $O(r_1^*)$ where r_1^* is the radius of peak swirl in the potential vortex (region I), then accounting for axial stratification in the eye and in the ambient, and accounting for the gravitational potential, are appropriate. The generalization of the presentation of Section 3.1 to be now undertaken is pertinent not only to the tropical-cyclone turnaround; while the initial conditions holding at the starting value of the axial coordinate z^* may be altered, and while the roles of some prescribed and deduced variables may be interchanged for more efficient solution (inverse-problem methodology), still the ordinary differential equations to be derived are as pertinent to the eyewall (mid and upper portion of region III) as to the "compressible turnaround" (lower portion of region III).

First, some properties of the pressure field in region I are required; this field is denoted $p_1^*(r^*,z^*)$, where $p_1^*(r_o^*,z^*) \equiv p_{amb}^*(z^*)$, given, where "amb" abbreviates ambient. Also $p_1^*[R^*(z^*),z^*] \equiv p_{ae}^*[R^*(z^*),z^*]$, where "ae" denotes "ambient-side edge of the separated layer." If, for brevity, the subscript unity is discarded temporarily, then in region I, with subscripts r^* and z^* denoting partial differentiation,

$$p_{r^*}^* \doteq \rho^* \, v^{*2}/r^* \quad , \tag{3.2.1}$$

$$-p_{z^*}^* \doteq \rho^* \, g^* \quad ; \tag{3.2.2}$$

hence,

$$g^* \, p_{r^*}^* = - \frac{v^{*2}}{r^*} \, p_{z^*}^* = - \frac{\Gamma^{*2}(z^*)}{r^{*3}} \, p_{z^*}^* \quad . \tag{3.2.3}$$

If one seeks solution in the form

$$p^*(\eta^*) = p^*\left[m^*(z^*) - s^*(r^*)\right] \quad , \tag{3.2.4}$$

then

$$p^*_{\eta^*}(\eta^*) \left[g^* \, s^*_{r^*}(r^*) \, r^{*3} - \Gamma^{*2}(z^*) \, m^*_{z^*}(z^*) \right] = 0 \quad ; \tag{3.2.5}$$

i.e., without loss of generality,

$$s^*(r^*) = - 1/(2 \, g^* \, r^{*2}) \quad , \tag{3.2.6}$$

$$m^*(z^*) = \int^{z^*} \Gamma^{*-2}(z^1) \, dz^1 \quad . \tag{3.2.7}$$

For the special case of a vortex that is invariant with altitude, $\Gamma^* = \Gamma_o{}^*$, const., $m^*(z^*) = z^*/\Gamma_o{}^{*2}$. The choice of $p^*(\eta^*)$ which matches the ambient atmosphere at $r^{*-2} << 1$ is (upon restoration of the subscript unity)

$$p_1{}^* = p^*_{amb} \left[z^* + \Gamma_o{}^{*2}/(2g^* \, r^{*2}) \right] \quad . \tag{3.2.8}$$

In this approximation the ambient formally is taken to hold at an infinite radial distance, but the discrepancy from a match to an ambient at a value of $(r_o{}^*/r_1{}^*)$ of only ten results in an error of about merely one percent.

The more general case of a vortex, the angular momentum of which decreases linearly from a value of $\Gamma_o{}^*$ at sea level to the value of $[(M-1)/M]\Gamma_o{}^*$, $M \gg 1$, at the tropopause $z^* = z_t{}^*$, i.e.,

$$\Gamma^*(z^*) = \Gamma_o{}^* \, \frac{M \, z_t{}^* - z^*}{M \, z_t{}^*} \Rightarrow \eta^* = \frac{M \, z_t{}^*}{M \, z_t{}^* - z^*} + \frac{\Gamma_o{}^{*2}/(M \, z_t{}^*)}{2g^* \, r^{*2}} \quad , \tag{3.2.9}$$

such that as $r^* \to \infty$,

$$z^* = M \, z_t{}^* \, (\eta^* - 1)/\eta^* \quad . \tag{3.2.10}$$

Thus, a solution of the first-order partial differential equation, $p^*(\eta^*)$, any function of η^*, also satisfies the boundary condition,

$$p_1^*(\eta^*) \to p_{amb}^*(z^*) \text{ for } r^* \to \infty \quad , \tag{3.2.11}$$

if one takes as the function

$$p_1^*(\eta^*) = p_{amb}^* \left[\frac{z^* + \dfrac{\Gamma_o^{*2}(M z_t^* - z^*)}{2g^* r^{*2} M z_t^*}}{1 + \dfrac{\Gamma_o^{*2}(M z_t^* - z^*)}{2g^* r^{*2} M^2 z_t^{*2}}} \right] . \tag{3.2.12}$$

For $M \to \infty$, this case degenerates to the previous one.

More generally, if $\Gamma^*(z^*) = \Gamma_o^*[(M z_t^* - z^*)/(M z_t^*)]^n$, $n \geqslant 0$, then

$$p_1^*(\eta^*) = \begin{cases} p_{amb}^* \left\{ M z_t^* - (M z_t^* - z^*) \left[1 - \dfrac{(1-2n)}{(M z_t^* - z^*)^{1-2n}} \dfrac{\Gamma_o^{*2}}{2g^* r^{*2} (M z_t^*)^{2n}} \right]^{\frac{1}{1-2n}} \right\}, n \neq \frac{1}{2} \\ p_{amb}^* \left\{ M z_t^* - (M z_t^* - z^*) \exp\left[- \Gamma_o^{*2}/(2g^* r^{*2} M z_t^*) \right] \right\} , \; n = \frac{1}{2} \end{cases} . \tag{3.2.13}$$

Finally, if $\Gamma^*(z^*) = \Gamma_o^* \exp(-a^* z^*)$, then

$$p_1^*(\eta^*) = p_{amb}^* \left\{ z^* + (2a^*)^{-1} \ell n \left[1 + \frac{a^* \Gamma_o^{*2}}{g^* r^{*2} \exp(2a^* z^*)} \right] \right\} . \tag{3.2.14}$$

Thus, deviation of the isobars (from the asymptotic horizontal planes holding in the hydrostatic ambient) owing to rotation is known formally throughout region I for any physically interesting stratification of the angular momentum, and several examples have been presented explicitly. This deviation is significant in ascertaining the pressure differential at any altitude between the edge

of the eyewall contiguous to the vortex of region I and the edge of the eyewall contiguous to the eye of region IV, where the eyewall is envisioned as a narrow layer. More explicitly, in region III the pressure on the streamsurface contiguous to region IV must match the known eye pressure $p^*_{eye}(z^*)$, and the pressure on the streamsurface contiguous to region I must match the pressure in the potential vortex at the eyewall edge $p_1{}^*[R^*(z^*),z^*]=p^*_{amb}\{m^{*-1}[m^*(z^*)-s^*(r^*)]\}$. These statements constitute the boundary conditions for the eyewall calculation, to which attention is now turned.

The symbol $R^*(z^*)$ henceforth denotes the radial displacement of the outer surface of the eyewall with structure; the symbol $h^*(z^*)$ denotes the transverse thickness of the eyewall, such that $h^*(z^*)$ is measured inward from $R^*(z^*)$ and perpendicular to $R^*_{z^*}(z^*)$. The eyewall is taken as thin, so in general $h^*(z^*) << R^*(z^*)$; under this inequality, transversely averaged analyses of the eyewall suffices.

The symbol z^*_* denotes the altitude down to which hydrostatic, adiabatic compression (of air whose reference thermodynamic state is that of the ambient at $z_t{}^*$) characterizes $p^*_{eye}(z^*)$, where it is recalled that $z_t{}^*$ is the altitude of the tropopause (assigned here to be the ambient altitude at which the pressure and temperature of the ambient match that of ground-level air which has risen on a moist adiabat). For $z^*_* \geq z^* \geq 0$, $p^*_{eye}(z^*)$ is given by hydrostatics, and by moist-adiabatic states such that the pressure is continuous at $z^* = z^*_*$. If $z^*_* = 0$, then in $R^*(z^*) > r^* \geq 0$, the dry-adiabatic relation holds throughout the entire depth of the troposphere (for a moisture-free, fully inserted eye). It is perhaps worth recalling that standard thermohydrostatic calculation yields $p^*_{eye}(z^*)$ and $z_t{}^*$ from specification of a storm-prone ambient $p^*_{amb}(z^*)$; in the course of such a calculation the triplet $(\rho^*_{moist}, T^*_{moist}, p^*_{moist})$ has been associated, where

$p^*_{amb}(0) \geq p^*_{moist}(z^*) \geq p^*_{amb}(z_t^*)$, and where subscript "moist" designates the moist adiabatic based on ground-level (or sea-level) ambient conditions.

It is convenient to introduce the concept of a series of calculations, $i = 1,2,3...$ for known $p^*_{amb}(z^*), T^*_{amb}(z^*), \rho^*_{amb}(z^*)$, and given $\Gamma^*(z^*)$. These calculations are based on different completeness of "flushing" of moist-adiabatic air from the eye as denoted by $z_*^{*(i)}$, $i = 1,2,3...$ For example, one could study

$$z_*^{*(i)} = \frac{i-1}{N} z_t^* \ , \ 1,2,3...,N+1 \ , \qquad (3.2.15)$$

where $i = 1$ would constitute a fully inserted eye flushed of moist air, and $i = N+1$ would constitute the degenerate case of an eye-free structure. The theory advanced here is limited to cases in which z_*^* is a large fraction of z_t^*; i.e., attention is at the outset confined to fully, or near fully, developed eyes.

Under the cyclostrophic and potential-vortex approximations, the peak swirl speed (of a two-cell vortex with a nonrotating core) supportable by surface-level pressure deficit between eye and ambient, is estimated by

$$p^*_{amb}(0) - p^{*(i)}_{eye}(0) \doteq \frac{1}{2} \rho^*_{amb}{}^{(0)} \left[V^{*(i)}\right]^2 \ , \qquad (3.2.16)$$

where the density has been taken as fixed at its ambient value, and the superscript i is recalled to denote the completeness of eye flushing. For $i = 1$, the swirl speed is maximum, and this value is used for nondimensionalization below. While the explicitness of (3.2.16) is convenient as a tentative approximation, a more accurate formula (that accounts for the variation of density with radius in the potential vortex and that acknowledges that the peak swirl is achieved above the surface inflow layer--rather than at $z^* = 0$) ultimately is required and is introduced below.

The reference value for the angular momentum Γ_o^* is taken to be

$$\Gamma_o^* = r_1^* V^{*(1)} \quad , \tag{3.2.17}$$

where r_1^* is the (specified) radius at which the surface inflow layer separates. If Γ_o^* is held fixed for all i, then, if

$$r_o^{*(i)} V^{*(i)} = \Gamma_o^* \Rightarrow r_o^{*(i)} = \Gamma_o^*/V^{*(i)} \quad , \tag{3.2.18}$$

it follows that

$$r_o^{*(1)} = r_1^* \; ; \; r_o^{*(i)} > r_o^{*(1)} \text{ , since } V^{*(1)} > V^{*(i)} \text{ , } i > 1 \; . \tag{3.2.19}$$

Also, reference values for the streamwise and swirl components of velocity in the eyewall are taken as follows:

$$q_o^{*(i)} = K V^{*(i)} \; , \; v_o^{*(i)} = C V^{*(i)} \text{ , where } 0 < C, K < 1. \tag{3.2.20, 3.2.21}$$

It may be noted that

$$\left[q_o^{*(i)}\right]^2 + \left[v_o^{*(i)}\right]^2 \leqslant \left[V^{*(i)}\right]^2 \Rightarrow (C^2 + K^2) \leqslant 1 \; . \tag{3.2.22, 3.2.23}$$

The equality implies no kinetic-energy losses after separation, whereas the inequality implies losses (associated with vortex breakdown). While formally a large range of values for C,K may be explored, in fact $C \doteq K \doteq 2^{-\frac{1}{2}}$ seems plausible.

By conservation of angular momentum for the eyewall

$$\left[R^{*(i)}{}_{z^*)}\right] \left[v^{*(i)}{}_{(z^*)}\right] = r_o^{*(i)} \, v_o^{*(i)} \; . \tag{3.2.24}$$

It is consistent with nondimensionalization introduced in Section 3.1 to adopt:

$$R^{(i)}(z) = \frac{R^{*(i)}(z^*)}{r_o^{*(1)}} \ , \ v^{(i)}(z) = \frac{v^{*(i)}(z^*)}{V^{*(1)}} \ , \ z = \frac{z^*}{r_o^{*(1)}} \ . \tag{3.2.25}$$

Hence,

$$\left[R^{(i)}(z)\right] \left[v^{(i)}(z)\right] = \Sigma_1^{(i)} \ , \ \Sigma_1^{(i)} = \frac{r_o^{*(i)} \ v_o^{*(i)}}{r_o^{*(1)} \ V^{*(1)}} = C \ . \tag{3.2.26}$$

By conservation of mass for the eyewall,

$$\left[\rho^*_{moist}(z^*)\right] \left[q^{*(i)}(z^*)\right] \left[R^{*(i)}(z^*)\right] \left[h^{*(i)}(z^*)\right] \doteq \rho^{(i)}_{eye}(0) \ q_o^{*(i)} \ r_o^{*(i)} \ h_o^{*(i)} \ , \tag{3.2.27}$$

where, for a thin layer, it is reasonable to adopt

$$h_o^{*(i)} = \kappa \ r_o^* \ , \text{ given} \ , \tag{3.2.28}$$

where r_o^* = 300 - 500 miles for a typhoon, r_o^* = 6 - 8 miles for a tornado, and κ = 0.0025 for both. If one defines

$$\rho_{moist}(z) = \frac{\rho^*_{moist(z^*)}}{\rho^{*(1)}_{eye}(0)} \ , \ q^{(i)}(z) = \frac{q^{*(i)}(z^*)}{V^{*(1)}} \ , \ h^{(i)}(z) = \frac{h^{*(i)}(z^*)}{r_o^{*(1)}} \ , \tag{3.2.29}$$

then

$$\left[\rho_{moist}(z)\right] \left[q^{(i)}(z)\right] \left[R^{(i)}(z)\right] \left[h^{(i)}(z)\right] = \Sigma_2^{(i)} \ , \tag{3.2.30}$$

$$\Sigma_2^{(i)} = K \frac{\rho^{*(i)}_{eye}(0)}{\rho^{*(1)}_{eye}(0)} \frac{V^{*(i)}}{V^{*(1)}} \frac{r_o^{*(i)}}{r_o^{*(1)}} \frac{\kappa \ r_o^*}{r_o^{*(1)}} \tag{3.2.31}$$

$$= K \kappa \frac{\rho^{*(i)}_{eye}(0)}{\rho^{*(1)}_{eye}(0)} \frac{r_o^*}{r_o^{*(1)}} \ . \tag{3.2.32}$$

In fact, the value of κ is not well set, and $\rho^*_{eye}{}^{(i)}(0)$ does not well characterize the density of the eyewall at separation; thus, some convenient reassignment of the value of $\Sigma_2^{(i)}$ is adopted below to avoid iteration of transcendental equations in establishing initial conditions. However, the essential point is that $\Sigma_2^{(i)}$ is a known constant. It may also be worth noting that the density of the moist adiabat ρ^*_{moist} is tabulated as a function of p^*_{moist}, and thus ρ^*_{moist} is really known only indirectly as a function of altitude z^*.

Aside from gravitational effects, there is a constant head across all streamsurfaces of the separating inflow layer that constitutes the turnaround and eyewall (region III). Thus, Bernoulli's equation for the moist-adiabatic locus appropriate for region III becomes (g^* is the magnitude of the gravitational acceleration)

$$\frac{\left[q^{*(i)}(z^*)\right]^2 + \left[v^{*(i)}(z^*)\right]^2}{2} + g^* \frac{(z^* + z^{*\prime})}{2} + \int_{p^{*(i)}(h^*)}^{p^{*(i)}(z^*)} \frac{dp_2^*}{\rho^*_{moist}(p_2^*)}$$

$$= \frac{\left[q_o{}^{*(i)}\right]^2 + \left[v_o{}^{*(i)}\right]^2}{2} + \frac{g^* h_o{}^{*(i)}}{2} , \qquad (3.2.33)^4$$

where $z^{*\prime}$ characterizes the height on the eye side of the separated layer that corresponds to height z^* on the eyewall side, in view of the fact that h^* is measured perpendicular to $R^*_{z^*}(z^*)$ and that h^* is not trivial in magnitude for the typhoon case. The formula for $z^{*\prime}$ is given below; here it is noted that at separation $z^* = h_o{}^{*(i)}$, $z^{*\prime} = 0$; also, the gravitational potential is being assigned at midheight of the layer. As previously noted, aside from the gravitational potential, the head would be constant across virtually all streamsurfaces in the separating layer, so while (3.2.33) is used here in an integral sense across the layer, for the tornado-like case it would hold in detail as well.

[4] The prime superscript here distinguishes two values of the axial coordinate, and is distinct from use of the prime to denote ordinary derivative in Section 3.1.

In (3.2.33),

$$p^{*(i)}(z^*) = \frac{1}{2}\left\{p^*_{amb}\left\{m^{*-1}\left[m^*(z^*) - s^*\left(R^{*(i)}(z^*)\right)\right]\right\} + p^*_{eye}{}^{(i)}(z^{*\prime})\right\}$$

$$= \frac{1}{2}\left\{p^*_{ae}\left[R^{*(i)}(z^*), z^*\right] + p^{*(i)}_{eye}(z^{*\prime})\right\} , \qquad (3.2.34)$$

where $p^{*(i)}(z^*)$ could be written $p^{*(i)}_{moist}(z^*)$, and $p^*_{ae}\,[R^{*(i)}(z^*), z^*]$ could be written $p_1{}^*[R^{*(i)}(z^*), z^*]$.

If one nondimensionalizes by defining

$$p^{(i)}(z) = \frac{p^{*(i)}(z^*)}{p^{*(1)}_{eye}(0)} , \qquad (3.2.35)$$

then

$$\left[q^{(i)}(z)\right]^2 + \left[v^{(i)}(z)\right]^2 + \Sigma_3 \frac{(z + z')}{2} + \Sigma_4 \int_{p^{(i)}(h)}^{p^{(i)}(z)} \frac{dp_2}{\rho_{moist}(p_2)} = \Sigma_5{}^{(i)} , \qquad (3.2.36)$$

where

$$\Sigma_3 = \frac{2g^*\, r_o{}^{*(1)}}{\left[V^{*(1)}\right]^2} , \quad \Sigma_4 = \frac{p^*_{eye}{}^{(1)}(0)/\rho^*_{eye}{}^{(1)}(0)}{\left[V^{*(1)}\right]^2/2} , \quad \Sigma_5{}^{(1)} = (C^2 + K^2)\left[\frac{V^{*(i)}}{V^{*(1)}}\right]^2 + \frac{\Sigma_3}{2}\frac{h_o{}^{*(i)}}{r_o{}^{*(1)}} . \qquad (3.2.37)$$

Finally, the balance of pressure force and accelerations acting transversely to the separated layer yields

$$\frac{\Sigma_4}{2}\frac{p_{eye}^{(i)}(z') - p_{ae}\,[R^{(i)}(z),z]}{[\rho_{moist}(z)][h^{(i)}(z)]} + \frac{\Sigma_3}{2}\frac{R_z^{(i)}(z)}{\{1+[R_z^{(i)}(z)]^2\}^{\frac{1}{2}}} + \frac{[v^{(i)}(z)]^2}{R^{(i)}(z)\{1+[R_z^{(i)}(z)]^2\}^{\frac{1}{2}}}$$

$$= \frac{[q^{(i)}(z)]^2\, R_{zz}^{(i)}(z)}{\{1+[R_z^{(i)}(z)]^2\}^{3/2}} \quad , \tag{3.2.38}$$

where

$$z' = z + h^{(i)}(z)\,\frac{R_z^{(i)}(z)}{\{1+[R_z^{(i)}(z)]^2\}^{\frac{1}{2}}} \quad . \tag{3.2.39}$$

Since z' is the altitude at the eye-contiguous side of the layer that is associated with altitude z at the potential-vortex-contiguous side of the layer, the distinction of z' and z may be significant for thick layers (i.e., for the typhoon case). As noted below (3.1.1), the eye-edge pressure exceeds the ambient-edge pressure during the turnaround ($R<1$), so the pressure difference plus the acceleration owing to the swirl are balanced by the acceleration owing to the radial-axial flow. The above formulation is convenient for the more vertical portions of the turnaround, in which R_z is zero or finite. However, near $R=1$ (i.e., near separation or near the end of the incursion), $|R_z| \to \infty$, and a computationally more convenient form of the equation is obtained by interchanging the roles of R and z, such that the erstwhile dependent variable becomes the independent variable. Specifically, if one writes

$$z' = z + h^{(i)}\,\frac{\mathrm{sgn}(z_R)}{(1+z_R^2)^{\frac{1}{2}}} \quad , \tag{3.2.40}$$

then just after separation, upon discarding the superscript i ,

$$\frac{\Sigma_4}{2}\frac{p_{eye}(z') - p_{ae}(R,z)}{\rho_{moist}\,h} - \frac{\Sigma_3/2}{(1+z_R^2)^{\frac{1}{2}}} - \frac{v^2 z_R}{R(1+z_R^2)^{\frac{1}{2}}} = \frac{q^2\, z_{RR}}{(1+z_R^2)^{3/2}} \quad . \tag{3.2.41}$$

This form is convenient as R decreases from unity until (say) $z_R \to -1$, at which point the form (3.2.38) may be used; after the minimum value of R is achieved, and (say) $R_z \to 1$, one may continue on to higher z by use of the form

$$\frac{\Sigma_4}{2}\,\frac{p_{eye}(z') - p_{ae}(R,z)}{\rho_{moist}\,h} + \frac{\Sigma_3/2}{(1+z_R^2)^{1/2}} + \frac{v^2 z_R}{R(1+z_R^2)^{1/2}} = -\frac{q^2 z_{RR}}{(1+z_R^2)^{3/2}} \quad . \tag{3.2.42}$$

The set (3.2.26), (3.2.30), (3.2.36), and (3.2.38) can be reduced by substitution of the first three into the last, to form one second-order nonlinear ordinary differential equation for R(z); admittedly, the factor q(z) is expressed in terms of an intricate functional of R(z), but the reduction is still convenient for numerical integration on a high-speed digital computer. After specification of two boundary conditions, (say) on R and R_z at some starting value of z, the initial-value problem may be marched forward in z. The form of (3.2.38) convenient at separation is (3.2.41), in which z_R, $z_{RR} \to 0$ at R = 1, z = h, z′ = 0. In dimensional form, for i = 1 and $\Gamma^*(z^*) = \Gamma_o^*$, from (3.2.8),

$$p^*_{eye}(0) - \rho^*_{moist}\, g^*\, h_o^* = p^*_{amb}\left(h_o^* + \frac{\Gamma_o^{*2}}{2g^*\, r_1^{*2}}\right) , \tag{3.2.43}$$

where $(\Gamma_o^{*2}/r_1^{*2}) = [V^{*(1)}]^2$ and here ρ^*_{moist} is the (known) density on the moist adiabat associated with

$$p^*_{moist} \doteq \frac{1}{2}\left[p^*_{eye}(0) + p^*_{amb}\left(h_o^* + \frac{(V^{*(1)})^2}{2g^*}\right)\right] . \tag{3.2.44}$$

These relations give the selfconsistent means of assigning $V^{*(1)}$, though the value varies modestly from that obtained by (3.2.16). For the turnaround, integration is initiated by taking

$$R = 1: \quad z = h,\ z_R = \varepsilon(<0) \ , \quad 0 < |\varepsilon| << 1, \tag{3.2.45}$$

or by using a locally valid series approximation.

Thus, conservation of angular momentum, conservation of mass, Bernoulli's equation, and a balance of forces, all enforced in an integral sense, constitute four equations for the four dependent variables $R^{(i)}(z)$, $v^{(i)}(z)$, $q^{(i)}(z)$, and $h^{(i)}(z)$. Five dimensionless parameters must be specified: Σ_1, $\Sigma_2^{(i)}$, Σ_3, Σ_4, and $\Sigma_5^{(i)}$; further, the thermodynamic and angular-momentum stratification of the storm-prone (convectively unstable) ambient, e.g., relative humidity and temperature circulation as a function of pressure through the depth of the troposphere, must be specified. Preliminary standard thermohydrostatic calculations give z_t, $p_{eye}^{(i)}(z)$, ρ_{moist} (p_{moist}), and the peak swirl speed achieved in the potential vortex for a fully inserted, nonrotating eye. Specification of the five above-cited dimensionless parameters actually entails specification of the thickness of the inflow layer at separation, $h_o^{*(i)}$; the radial distance from the axis of symmetry at which the surface inflow layer separates, r_1^*; the height to which moist-adiabatic air remains near the axis, $z_*^{(i)}$; and the fractions C and K characterizing distribution, of kinetic energy of the inflow layer at separation, into swirl speed and radial-axial-flow speed.

If, in the above one-layer formulation, one has the same thermodynamic stratification and angular-momentum stratification of the ambient, the same degree of flushing of the eye, the same ratio of inflow-layer vertical thickness to inflow-layer-separation radius for a fully inserted eye $(h_o^{*(i)}/r_o^{*(1)})$ and the same fractional distribution (of kinetic energy at separation) into swirl speed and radial-axial-flow speed, then the only distinction in the dimensionless formulation between two cases (one of which conceivably could be a hurricane case and the other a tornado case, within the above constraints) is the value of the dimensionless parameter Σ_3 defined in (3.2.37). The radial distance to peak swirl in the potential vortex, $r_o^{*(1)} \equiv r_1^*$, would be quite different in the two cases; Σ_3

would be two orders of magnitude smaller in the tornado than in the hurricane. This statement simply presents formally the earlier observation that the gravitational potential enters significantly only in the tropical-cyclone case. The upshot is that the constant-density, gravitational-potential-free conditions for a periodic solution in $z(\Sigma_3 = 0,\ z' = 0$ in the argument of $p_{eye},\ z = 0$ in the argument of $p_{ae})$ satisfactorily hold during the entire incursion $R < 1$ and over some altitude during the subsequent excursion $R > 1$, but such conditions do not hold for a typhoon. Also, even the simplistic analysis in Section 3.1 suggests that the separated layer becomes unstable and undergoes a breakdown during the excursion $R > 1$, i.e., at an altitude of order r_1^* or on the order of 170 m off the ground for a tornadic mesocyclone. However, variable-density and gravitation-potential effects enter significantly over the appreciably greater axial distance pertinent for the turnaround in a typhoon (here $r_1^* \simeq$ 10-16 km), and entirely different results are obtained. The results indicate that the eyewall thickness in a typhoon increases so much at midtropospheric heights that the postulated-thin-layer basis of the analysis ($R \gg h$) is seriously violated; the model then is inadequate.

3.3 Numerical Examples

In support of the statements at the end of Section 3.2, calculations are reported that are based on the mean ambient for the West Indies for September (i.e., for the peak of the hurricane season) (Jordan 1957). Figure 6 presents the temperature as a function of pressure for ambient air, for sea-level ambient air lifted on a moist adiabat (taken to be an idealized characterization of the thermodynamic states of the eyewall), and for tropopause-level air dry-adiabatically compressed down to sea-level altitude (taken to be an idealized characterization

of the thermodynamic states of the eye); constant-altitude lines are assigned on the basis of hydrostatics. From these thermohydrostatic calculations,

$$z_t^* = 13.8 \text{ km},\ p_{amb}^*(0) = 1014 \text{ mb},\ p_{eye}^*(0) = 917 \text{ mb},\ \rho_{eye}^*(0) = 9.35 \times 10^{-4} \text{ g/cm} ; \tag{3.3.1a}$$

from (3.2.16)

$$V^{*(1)} = 131.6 \text{ m/s}. \tag{3.3.1b}$$

Plausible assignment of lateral scales suggests

$$r_1^* = 1.52 \times 10^4 \text{ m} , \ \kappa = 2.5 \times 10^{-3}, \ r_o^* = 6.09 \times 10^5 \text{ m}. \tag{3.3.2}$$

Thus, from (3.2.18) and (3.2.28),

$$\Gamma_o^* = r_1^* V^{*(1)} = 2.01 \times 10^6 \text{ m}^2/\text{s}, \ h_o^{*(i)} = \kappa r_o^* = 1.72 \times 10^3 \text{ m} . \tag{3.3.3}$$

From (3.2.20) and (3.2.21), if $C \doteq K \doteq 2^{-\frac{1}{2}}$, i.e., for no kinetic-energy loss,

$$q_o^{*(1)} = K V^{*(1)} = 92.9 \text{ m/s} , \ v_o^{*(1)} = C V^{*(1)} = 92.9 \text{ m/s} \tag{3.3.4a}$$

Alternatively (and less plausibly), for about 25% loss of kinetic energy prior to any vortex breakdown, if K = 0.7 and C = 0.5,

$$q_o^{*(1)} = 91.4 \text{ m/s} , \ v_o^{*(1)} = 65.3 \text{ m/s} . \tag{3.3.4b}$$

Accordingly, under (3.3.4a), since $r_1^* = r_o^{*(1)}$ by definition,

$$\Sigma_1^{(i)} \doteq 0.707, \ \Sigma_2^{(1)} \doteq 8.83 \times 10^{-2}, \ \Sigma_3 \doteq 17.5, \ \Sigma_4 \doteq 11.4, \ \Sigma_5^{(1)} = 1, \tag{3.3.5a}$$

where these dimensionless groups are defined by (3.2.26), (3.2.32), and (3.2.37). Under (3.3.4b),

$$\Sigma_1^{(i)} = 0.5, \ \Sigma_2^{(1)} \doteq 7.49 \times 10^{-2}, \ \Sigma_3 \doteq 17.5, \ \Sigma_4 \doteq 11.4, \ \Sigma_5^{(1)} \doteq 0.74. \tag{3.3.5b}$$

Under (3.3.4b) and (3.3.5b), for a fully inserted eye, the results of numerical integration of the initial-value problem for the turnaround (described in the penultimate paragraph of Section 3.2) is given in figures 7 and 8. Actually, as discussed in the last paragraph of Section 3.2, some restrictive parametric assignments are made to permit simulation of the tornado: $\Sigma_3 = 0$, $z' = 0$ in the argument of p_{eye} (so $p_{eye} = 1$), $z = 0$ in the argument of p_{ae} as given by (3.2.8), and $z = 0$ in (3.2.45). (The hurricane ambient is seen below not to be very different from some tornado ambients.) Under the simplifications just enumerated, the compressible formulation of the turnaround (developed in Section 3.2) does degenerate essentially to the incompressible treatment (developed in Section 3.1). Explicitly, there is an incursion (from R = 1) of the separated layer toward the axis of rotation such that there is a moderate overshoot of the swirl, then an excursion such that an instability leading to vortex breakdown occurs (figure 7), all over an altitude of $z = O(1)$; furthermore, the eye-edge pressure exceeds the pressure at the ambient-edge pressure during incursion (the opposite being true during excursion), with the thickness h and radial-axial-flow speed q being rather constant with height (figure 8).

Under (3.3.4a) and (3.3.5a), again for a fully inserted eye, but <u>without</u> any of the restrictive assignments listed in the last paragraph to permit simulation of the tornado, one finds results holding for the typhoon (figures 9-11). Particularly noteworthy is the very rapid increase in thickness for $z \doteq 0.35$, such that $(h/R) \doteq 0.5$ and is increasing rapidly with altitude; the bases for the integral treatment have deteriorated.

4. The Eyewall

4.1 General Comments

The integral theory for the evolution of the separated layer (region III), after the postulated breakdown of the turnaround discussed in Section 3.1, is now given for the tornadic mesocyclone. The four basic equations remain those presented earlier: (3.2.26), (3.2.30), (3.2.36), and (3.2.38). However, while the independent variable remains the distance above ground level z, it has already been anticipated (in the last paragraph of Section 2.2) that the roles of certain specified and inferred variables would be interchanged. Specifically, only certain axial profiles of peripheral angular momentum are analytically tractable for closed-form presentation in the characteristic argument of $p_{ae}^{(i)}(R^{(i)},z)$, and study of these particular profiles often leads to results inconsistent with two-cell structure. For example, $R_z^{(i)}(z)$ may become large and negative at midtropospheric heights, upon integration forward in z after adoption of suitable starting values (see below); such behavior (deflection of the eyewall toward the axis) is inconsistent with eye insertion, since the eye extends downward from the neutral-stability altitude. It turns out to be much more computationally efficient to specify $R^{(i)}(z)$, the displacement of the separated layer from the axis of rotation, and to use the four equations to obtain $p_{ae}^{(i)}(R^{(i)},z)$, $q^{(i)}(z)$, $v^{(i)}(z)$, and $h^{(i)}(z)$ for a given ambient thermodynamic stratification [such that $p_{eye}^{(i)}(z)$ is given]. In a separate, sequential calculation one may infer the associated $\Gamma^{(i)}(z)$ by inversion of a triangular matrix (see below); in this manner, one can obtain a (piecewise-constant) profile for $\Gamma^{(i)}(z)$ for those cases for which two-cell structure is consistent with the model.

From inspection of (3.2.26), (3.2.30), (3.2.36), and (3.2.38), and from plausible physical behavior for two-cell structure, one anticipates that $R^{(i)}(z)$ increases monotonically in z, where $R^{(i)}(z) > 1$; that $\rho_{moist}(z)$, $v^{(i)}(z)$, and $p^{(i)}(z)$ decrease monotonically in z, where $p^{(i)}(z) = [p_{eye}(z') + p_{ae}^{(i)}(R^{(i)},z)]/2$; and that $q^{(i)}(z)$ and $h^{(i)}(z)$ may either increase or decrease with z, and therefore may not be monotonic in z. Since $h^{(i)}(z)$ is small for the tornadic case, distinction of z' and z seems less critical for this case.

4.2 Computational Details; Starting Conditions

The partially algebraic, partially differential set conveniently is reduced to a purely algebraic set upon specification of $R^{(i)}(z)$. Nevertheless, at each height z, a double iteration on $h^{(i)}(z)$ and $p_{ae}^{(i)}(z)$ is required because of the nonlinear, coupled nature of the equations. In particular, upon specification of $R^{(i)}(z)$, from which $v^{(i)}(z)$ follows immediately by (3.2.26), adoption of trial values for $h^{(i)}(z)$ and $p_{ae}^{(i)}(z)$ permits obtaining a compatible value for $q^{(i)}(z)$ from (3.2.36). In this connection, the inputs z' and $p_{eye}^{(i)}(z)$ are readily available from (3.2.39) and from tabulated results from standard thermohydrostatic calculations. Updated values for $p_{ae}^{(i)}(z)$ and for $h^{(i)}(z)$ are then sequentially available from (3.2.38) and (3.2.30), respectively. One than may update $q^{(i)}(z)$. Effective invariance between successive iterates for all variables is taken to indicate convergence; the value of z is incremented, and the procedure repeated. It may be remarked that adopting straight-line segments for $R^{(i)}(z)$, with neglect of the right-hand side of (3.2.38) is a plausible procedure since one anticipates very modest curvature over most of the eyewall; substitution of a smoothed profile for $R^{(i)}(z)$ should then be carried out to confirm the relative unimportance of the omitted term.

The boundary conditions are taken to be as follows:

$$z = 0: \quad R^{(i)} = 1, \; R_z^{(i)} = R_{zz}^{(i)} = 0 \; . \tag{4.2.1}$$

These conditions imply: (1) the altitude over which the turnaround occurs for the tornadic case is so much less than the height of the neutral-stability lid z_t that the eyewall might just as well be regarded as starting from ground level $z = 0$; (2) the vortex breakdown occurs so soon after the completion of the turnaround that setting $R^{(i)} = 1$, i.e., starting the eyewall at the radial distance of inflow-layer separation, is a plausible procedure; and (3) the separated layer emerges from the breakdown in nearly vertical ascent.

A significant constraint on physically acceptable profiles for $R^{(i)}(z)$, not previously discussed, is the compatibility with the stability criterion in swirling flows that (at each altitude) the angular momentum not decrease with increasing radial distance from the axis of rotation. In particular, since in the integral approach, the transversely averaged value $v^{(i)}(z)$ characterizes the eyewall rotation at each height, at the interface $r = R$ between the eyewall (region III) and the potential vortex (region I), it is required that $v^{(i)}(z) < \Gamma^{(i)}(z)/R^{(i)}(z)$. That is, the displacement of the eyewall annulus from the axis of symmetry must be such that the swirl of the fluid in the eyewall is less than the swirl of the fluid contiguous to the eyewall in the potential vortex. Only high in the troposphere, at altitudes at which outflow occurs, may this inequality be violated. Although discussion is deferred to Section 4.3 concerning how one obtains the profile of ambient circulation with altitude, $\Gamma^{(i)}(z)$, that is compatible with the eyewall standoff $R^{(i)}(z)$ adopted, nevertheless this important constraint on $R^{(i)}(z)$ should be noted.

It is of physical interest to obtain solutions for the following parametric variations: for several measured profiles of temperature and relative humidity with pressure for tornado-prone ambients; for several degrees of eye insertion in each such ambient, i = 1,2...; and (perhaps) for several characterizations of the kinetic-energy loss through the breakdown, K,C, though it may be that $K \doteq C \doteq 2^{\frac{1}{2}}$ is the case of dominant physical interest.

It may be apropos to note that the conditions for the radial displacement of edge of the eyewall contiguous to the eye, given by

$$R^{(i)}(z) - h^{(i)}(z)/\left\{1 + \left[R_z^{(i)}(z)\right]^2\right\}^{\frac{1}{2}}, \qquad (4.2.2)$$

to be constant in z, is of physical (and historic) interest. The present model loses selfconsistency as this condition is approached, because the augmented pressure deficit from ambient owing to compressional heating of the air contiguous to the axis would become unavailable to sustain swirling at speeds in excess of those compatible with moist-adiabatic ascent.

Finally, for the tornado-eyewall calculation, assignment of the peak swirl $V^{*(1)}$ by use of (3.2.43) incurs a small error, which in turn leads to a minor inconsistency in the angular-momentum field. As noted in the second paragraph of this section, the turnaround is conveniently ignored, and the eyewall is taken to rise vertically, at a prescribed distance from the axis of symmetry, at the starting altitude z = 0. Thus, the assignment of $V^{*(1)}$ at the inflow-layer-separation, as carried out in (3.2.43), is inappropriate. Indeed, comparison of (3.2.38), which is taken to hold at $z' = z = 0$, with (3.2.43) is informative. Since $R_z = R_{zz} = 0$ and the term involving Σ_3 is negligible, as is the gravitational term in (3.2.43), one sees that (3.2.38) implies a value of the pressure

at the potential-vortex edge of the thin layer, p_{ae}, that is greater after turnaround than is the analogous pressure at inflow-layer separation; the last term on the left-hand side of (3.2.38) is the basis of the discrepancy--swirl is a source of pressure difference across the post-turnaround thin layer, but not across the thin layer at separation. The upshot is that $V^{*(1)}$ is to be found by iteration by the requirement that the dimensionless angular momentum achieve its nominal value of unity at the (pseudo-) ground-level position $z = 0$. Of course, (3.2.43) provides a good first estimate for iteration. At this point, discussion of how the angular-momentum profile is obtained is appropriate.

4.3 Angular-Momentum Distribution with Altitude Consistent with a Prescribed Eyewall for a Thermodynamically Specified Ambient

Via the characteristic curve delineating the locus of an isobar extending from the outer-eyewall edge to the ambient in the hydrostatic, cyclostrophic, potential vortex (region I), one can complete the inverse solutions; i.e., one can identify the peripheral circulation compatible with an eyewall under prescribed axial profiles for radial displacement from the axis, thickness, swirl, radial-axial flow, potential-vortex-edge pressure, etc.

Since the identification is to be numerical, the sought function $x(z)$, where (recall $\Gamma_o^* = r_o^{*(1)}\, V^{*(1)}$)

$$x(z) = \frac{\Gamma_o^{*2}}{\Gamma^{*2}(z)} \Leftrightarrow \frac{\Gamma^*(z^*)}{\Gamma_o^*} = [x(z)]^{-\frac{1}{2}}, \tag{4.3.1}$$

is found in piecewise-constant approximation. Explicitly, if $H(z)$ denotes the Heaviside unit-step function,

$$x(z) = \sum_{k=1}^{M} x_k \,[H(z - z_k) - H(z_{k+1} - z)] \ , \ x_k \text{ const.}, \tag{4.3.2}$$

where for convenience

$$z_k = z_M - (M-k)(\Delta z), \quad k = M,(M-1),(M-2),\ldots,1 \ , \tag{4.3.3}$$

so $z_{k+1} > z_k$, $z_1 \geqslant 0$ and M is the number of discrete values used to sample the eyewall solution:

$$R_k \ , \ (p_{ae})_k \ , \ h_k \ , \ q_k \ , \ v_k \ , \ \ldots \text{ vs } z_k \ , \ k = 1,2,3,\ldots,M \ . \tag{4.3.4}$$

[In this section the superscript i, introduced previously to distinguish different degrees of eye insertion for a given thermodynamic stratification of the ambient, is taken as implicit, for simplicity of notation.] It turns out that choosing an interval ($\overline{\Delta z}$) and inferring M is preferred. If Z_M is defined by

$$P_{amb}(Z_M) = p_{ae}(z_M) \ ,$$

where $z_M (< z_t)$ is the greatest height to which the eyewall solution is carried (or is given creditability), and if N_{min} is the minimum positive integer satisfying the inequality

$$(N_{min})(\overline{\Delta z}) > (Z_M - z_M) \qquad (4.3.5)$$

then it is taken that

$$\Delta z \equiv (N_{min})(\overline{\Delta z}) \ . \qquad (3.4.6)$$

Then, from (4.3.3), z_k may be assigned, where z_1 is the smallest positive value assigned. The values cited in (4.3.4) may be found by interpolation in the tabulated values for the eyewall solution; in particular, the values $(p_{ae})_k$ are pertinent since one needs to tabulate

$$p_{amb}(Z_k) = p_{ae}(z_k) = (p_{ae})_k \ , \ k = M, M-1, M-2, \ldots \ . \qquad (4.3.7)$$

Another quantity required below is

$$\text{Int}\left[\frac{Z_k - z_k}{\Delta z}\right] \equiv \overline{N}_k \ , \ k = 1,2,3,\ldots,M \ , \qquad (4.3.8)$$

where the symbol "Int" indicates the largest positive integer less than or equal to the argument. In general, $\overline{N}_k$ is nonincreasing in value with increasing k.

It may be recalled from (3.2.4) - (3.2.7) that, along an isobar in region I, η^* is const., where

$$\eta^* = \int^{z^*} \frac{dz_1^*}{\Gamma^{*2}(z_1^*)} + \frac{1}{2g^*\, r^{*2}} + \text{const} \; ; \tag{4.3.9}$$

if z^* is taken to be the altitude at which $r^* = R^*$, then

$$- \int_{z^*}^{Z^*} \frac{dz_1^*}{\Gamma^{*2}(z_1^*)} + \frac{1}{2g^*\, R^{*2}(z^*)} = 0 \quad , \tag{4.3.10}$$

or, in dimensionless form, if $\Gamma(z) = \Gamma^*(z^*)/\Gamma_o^*$,

$$- \int_z^Z \frac{dz_1}{\Gamma^2(z_1)} + \frac{1}{\Sigma_3\, R^2(z)} = 0 \Rightarrow \int_z^Z x(z_1)dz_1 = \frac{1}{\Sigma_3\, R^2(z)} \quad . \tag{4.3.11}$$

In finite-difference form, using the trapezoidal rule,

$$\sum_{j=k}^{k+\bar{N}_k-1} x_j(\Delta z) + (Z_k - k_{k+\bar{N}_k})\, x_{k+\bar{N}_k} = [\Sigma_3\, R^2(z_k)]^{-1}, \tag{4.3.12}$$

or, if $\bar{N}_k > 1$,

$$x_k = - \left[\sum_{j=k+1}^{k+\bar{N}_k-1} x_j + (Z_k - z_k)(\Delta z)^{-1}\, x_{k+\bar{N}_k} \right] + \left[\Sigma_3\, (\Delta z)\, R_k^2 \right]^{-1} . \tag{4.3.13}$$

If $\bar{N}_k = 1$, then

$$x_k = - (Z_k - z_k)(\Delta z)^{-1}\, x_{k+\bar{N}_k} + [\Sigma_3\, (\Delta z)\, R_k^2]^{-1} \; ; \tag{4.3.14}$$

If $\bar{N}_k = 0$, then

$$x_k = [(Z_k - z_k)\, \Sigma_3\, R_k^2]^{-1} \quad . \tag{4.3.15}$$

In effect, Gaussian elimination (back substitution) is being used to solve a set of simultaneous linear algebraic equations with a triangular coefficient matrix. It is recalled that $\Gamma_k = x_k^{-\frac{1}{2}}$, where $z_{K+1} - z_k = (\Delta z)$ and z_M, the peak value of z, is the highest value utilized from the eyewall solution.

It seems worth recalling that in (4.3.11) the position z = 0 corresponds to the height at which the turnaround is completed. It is remarked that no solution is being furnished for the angular-momentum profile between ground level in the ambient and that height in the ambient at which (essentially) the pressure has decreased to the pressure at the base of the eye.

4.4 Numerical Examples

4.4.1 Strong Tornado

One of the most convectively unstable ambients ever measured in the vicinity of a tornado was taken near St. Cloud, MN, on July 22, 1967 at 1715Z (figure 12). At ground level, $T^*_{amb}(0) = 307.2$ K, $\rho^*_{amb}(0) = 1.12 \times 10^{-3}$ g/cm^3, $p^*_{amb}(0) = 1002.4$ mb. The pressure at the base of a moist adiabat (idealized core of a one-cell vortex) is calculated to be 930.4 mb, such that the peak swirl for a Rankine vortex sustained by this pressure deficit would be 80.0 m/s. The pressure at the base of a fully inserted eye, idealized as dry-adiabatically compressed, is calculated to be $p^{*(1)}_{eye}(0) = 839.7$ mb, such that the peak swirl for a potential vortex $V^{*(1)} = 170.3$ m/s. The tropopause height $z^*_t = 13.2$ km. The thermohydrostatic data for this ambient are presented in figure 13. It should be emphasized that the idealized processes adopted, together with this singularly unstable ambient, lead to exceptionally large peak speeds and maximum pressure deficits.

The following parametric assignments are adopted:

$$r^*_1 = 152 \text{ m}, \quad h^{*(i)}_o = 25.4 \text{ m}, \quad K = C = 2^{-\frac{1}{2}}. \tag{4.4.1}$$

Iteration reveals that the selfconsistent value for $V^{*(1)}$ discussed in the last paragraph of Section 4.2 is given by

$$V^{*(1)} = 164.0 \text{ m/s}, \tag{4.4.2}$$

or about 3.5% below the value obtained by applying cyclostrophy to the thermohydrostatically computed pressure deficit at the base of the eye. This slightly reduced value of $V^{*(1)}$ yields $\Gamma(0) \doteq 1$. If the superscripts i are discarded, it follows that the derived nondimensional groups take on the following values:

$$\Sigma_1 \doteq 0.707,\ \Sigma_2 \doteq 0.141,\ \Sigma_3 \doteq 0.111,\ \Sigma_4 \doteq 7.55,\ \Sigma_5 = 1.0\ . \qquad (4.4.3)$$

For a fully inserted eye, firgure 14 presents the eyewall geometry as a function of altitude z above ground level (more meticulously, above the height for completion of the turnaround). The outer eyewall locus R(z) is found, by trial and error (see below), in the form of straight-line segments, and the inner eyewall is then deduced by (4.2.5). It has been confirmed that smoothing the segmented profile gives very nearly the same result; i.e., the contribution from the term on the right-hand side of (3.2.38) is negligible relative to the largest terms on the left-hand side. Figure 15 presents, as a function of height z, the eyewall thickness h and radial-axial-flow speed q, for the adopted function R(z); these quantities vary modestly with height, and resotration of eye-eyewall entrainment may be anticipated to counteract the depicted thinning of the eyewall in the upper troposphere. Figure 16 presents the merging of the pressure in the eye and the pressure at the ambient edge of the eyewall, as the potential isobaric impervious "lid" at the tropopause is approached. Figure 17 presents the distribution of the angular momentum Γ as a function of altitude z; the key observation here is the constancy of the antular momentum at the (appreciable) lower-tropospheric value through much of the troposphere. Figure 17 presents the transversely averaged eyewall swirl speed v, and the swirl speed in the potential vortex at the interface between the potential vortex and the eyewall Γ/R, as functions of height z. For stability it is necessary that $(\Gamma/R) > v$, and it is seen that this inequality is violated only very high in the troposphere. It is the satisfaction of this inequality that necessitates lengthy trial-and-error numerical experimentation with profiles for R(z).

For an eye that is only 90% inserted, i.e., for the case in which (for the same ambient) the bottom 10% in height of the eye consists of moist-adiabatic

air (such that the pressure, but not density or temperature or mixing ratio, is continuous at the dry-air/moist-air interface), analogous plots of results are presented in figures 18-21. The alterations, mainly at low altitude, are selfevident and modest; consequences of the density-discontinuity interface in the eye appear in some of the profiles. For this partial insertion, the peak swirl is reduced to 155.8 m/s; for invariance of the angular momentum $\Gamma_o^* = r_1^* V^{*(1)}$, the radius of peak swirl increases to 160.4 m. Whereas Σ_1, Σ_3, and Σ_4 are unaltered from the values given in the last paragraph for the fully inserted case, $\Sigma_2 \doteq 0.144$, $\Sigma_5 \doteq 0.902$. The principal point is that the theory does seem robust enough at least to begin inquiry about less-than-complete eye insertion.

4.4.2 Moderate Tornado

A moderately convectively unstable ambient measured in the vicinity of a tornado was taken near Jackson, MS, on April 17, 1978 at 2300Z (figure 23). At ground level, $T^*_{amb}(0) = 301.2$ K, $\rho^*_{amb}(0) = 1.158 \times 10^{-3}$ g/cm^3, $p^*_{amb}(0) = 1009.9$ mb. The pressure at the base of a moist adiabat (idealized core of a one-cell vortex) is calculated to be 981.2 mb, such that the peak swirl for a Rankine vortex sustained by this pressure deficit would be 49.6 m/s. The pressure at the base of a fully inserted eye, idealized as dry-adiabatically compressed, is calculated to be $p^*_{eye}(0) = 923.9$ mb, such that the peak swirl for a potential vortex $V^{*(1)} = 122.0$ m/s. The tropopause height $z^*_t = 12.0$ km. The thermohydrostatic data for this ambient are presented in figure 24. The less severe nature of the convective instability for this ambient, relative to that introduced in Section 4.4.1, is evident.

The parametric assignments of (4.4.1) are adopted again. Iteration reveals that the selfconsistent value for $V^{*(1)}$ discussed in the last paragraph of

Section 4.2 is given by

$$V^{*(1)} = 164.0 \text{ m/s} , \tag{4.4.4}$$

or about 3.9% below the value obtained by applying cyclostrophy to the thermo-hydrostatically computed pressure deficit at the base of the eye. If the superscripts i are discarded, it follows that the derived nondimensional groups take on the following values:

$$\Sigma_1 \doteq 0.707, \ \Sigma_2 \doteq 0.133, \ \Sigma_3 \doteq 0.226, \ \Sigma_4 \doteq 14.4, \ \Sigma_5 = 1.0 . \tag{4.4.5}$$

Results for a fully inserted eye for the moderately convectively unstable ambient of figures 23 and 24 are presented in figures 25-29; these may be juxtaposed with their counterparts (figures 14-18) for a fully inserted eye for the highly convectively unstable ambient presented in figures 13 and 14. The eyewall is appreciably more vertical (and somewhat thinner) for the more unstable ambient. However, the key result that for two-cell structure the ambient circulation remains rather invariant with height, and retains its ground-level value until high in the troposphere, holds for the moderately convectively unstable ambient as well as for the highly convectively unstable ambient.

Although for brevity no figures are presented for the case of 90% eye insertion for the moderately convectively unstable ambient, in fact these calculations have been carried out and give the same trends as those reported in Section 4.4.1 for the slightly-less-than-completely-inserted eye.

5. Remarks on Possible Further Directions

Future work on the model under discussion might go on to consider the upper-level outflow of "processed throughput". However, probably further refined treatment of the two-cell structure of the vortex core is warranted. It has already been noted that addition of a model of entrainment to the inviscid analysis undertaken here would be of high priority. While entrainment models for rapidly rotating flows are not very advanced, it seems likely that the swirling and rising air of the lower eyewall annulus would entrain fluid from the virtually nonrotating eye. Indeed, such entrainment may well be necessary for selfconsistency of the model under closer scrutiny, for air from the virtually nonrotating thin diffusive sublayer of the low-level inflow region (II) is continuously being conveyed toward the axis for an incompletely inserted eye. This air would accumulate in time and obviate the postulated quasisteady nature of the mature-stage two-cell structure; thus, this steadily supplied low-momentum sublayer air must be conveyed away by entrainment into the eyewall.

Even before entrainment is introduced, it would seem worthwhile to return to the direct problem of specifying axial distributions of angular momentum compatible with two-cell structure. Experience with inverse solutions may render such an approach feasible. At least, a perturbational analysis about a distribution $\Gamma(z)$ compatible with two-cell structure might suggest the sensitivity of results to profile properties.

Finally, the current modeling of the eyewall by a moist-adiabatic locus is overidealized. It seems unlikely that the ambient stratification of total static

enthalpy holds uniformly in the potential vortex (region I) and the moist adiabat holds uniformly in the eyewall (III). Provision for some smoothing of this transition may warrant consideration.

APPENDIX A. A DERIVATION OF THE MOIST ADIABAT

Consider a volume V with surface S and surface element dS; the outward normal vector to dS is denoted n_i and fluid velocity vector is denoted u_i. Super asterisks, used in the main text to denote dimensional quantities, are dispensed with for this appendix.

For conservation of mass, consider air first. The flux of dry air through dS is in Cartesian notation, $\rho\, u_i\, n_i\, dS$, where ρ is air density. Hence, in the steady state,

$$\oint_S \rho\, u_i\, n_i\, dS = 0 \Rightarrow (\rho\, u_i)_{,i} = 0, \tag{A.1}$$

where comma denotes partial differentiation. Water vapor has the same speed, but density σ. When $\sigma < \Sigma(T)$, where $\Sigma(T)$, the saturation vapor density, is a known function of the temperature T,

$$(\sigma\, u_i)_{,i} = 0.$$

If the mixing ratio for water vapor $Y \equiv \sigma/\rho$, then

$$\rho\, u_i\, Y_{,i} = 0. \tag{A.2}$$

When T is low enough,

$$\sigma = \Sigma(T). \tag{A.3}$$

For conservation of momentum, the momentum flux associated with u_i is $(\rho + \sigma)u_j\, n_j\, u_i\, dS$, and that associated with the partial pressure of air p and with the partial pressure of vapor α is $(\alpha + p)n_i\, dS$. The production of momentum per unit volume associated with the gravitational body force (g is the magnitude of the acceleration of gravity) is $-g\, z_{,i}(\rho + \sigma)$, where the spatial coordinate z lies parallel to the body force. The loss of momentum per unit volume associated with the disappearing fluid is $-(\sigma\, u_j)_{,j}\, u_i$. Thus, using (A.1),

$$\oint_S (\rho + \sigma)u_j\, n_j\, u_i\, dS + \oint_S (\alpha + p)n_i\, dS = -g \int_V (\rho + \sigma)z_{,i}\, dV$$

$$+ \int_V (\sigma\, u_j)_{,j}\, u_i\, dV \qquad (A.4)$$

becomes

$$(\rho + \sigma)u_j\, u_{i,j} + (\alpha + p)_{,i} + (\rho + \sigma)g\, z_{,i} = 0. \qquad (A.5)$$

Incidentally, if a momentum equation had been written for each constituent, dry air and water vapor, interparticle drag of the form $D = A(u_i - v_i)$ would have been introduced, where u_i is air velocity and v_i is vapor velocity, and here $A \to \infty$ so $v_i = u_i$.

The equations of state are

$$p = \rho\, R\, T, \qquad (A.6)$$

$$\alpha = \sigma\, R'\, T, \qquad (A.7)$$

where the gas constant for vapor R' is related to the gas constant for vapor by $R' = R/(m_v/m_a)$, where m_v is the molecular weight of water vapor and m_a is the molecular weight of dry air.

The nonmechanical energy carried by the vapor can be written as $\left(L_0 + c_v^v\, T\right)$, where L_0 is the (extrapolated) value of the heat of condensation at $T = 0$, and c_v^v is the specific heat at constant volume of the vapor v. With this description, the <u>net</u> heat released by condensation at temperature T would be

$$L = L_0 + (c_v^v - c)T, \qquad (A.8)$$

where c is the specific heat of liquid water. The flux of energy across dS via u_i is

$$\left[\rho\, u_i \left(c_v\, T + \frac{v^2 + q^2}{2}\right) + \sigma\, u_i \left(c_v^v\, T + \frac{q^2 + v^2}{2} + L_0\right)\right] n_i\, dS, \tag{A.9}$$

where c_v is the specific heat at constant volume of dry air. The streamwise velocity component is denoted q and the perpendicular velocity component (swirl) is denoted v. Below, $Q^2 \equiv (v^2 + q^2)$. The work done by pressure forces across dS is $(\alpha + p)u_i\, n_i\, dS$, and the flux of potential energy is $(\rho + \sigma)g\, z\, n_i\, u_i\, dS$. The rate at which energy goes into a sink (i.e., into liquid, which, by conventional approximation in creating the moist adiabat, just vanishes) is the product of two factors: $-(\sigma\, u_j)_{,j}$, the rate of loss of mass per unit volume, and $\left\{g\, z + \left[(q^2 + v^2)/2\right] + c\, T\right\}$. It follows that

$$\left[\rho\, u_j\left(c_v\, T + \frac{Q^2}{2}\right) + \sigma\, u_j\left(c_v^v\, T + L_0 + \frac{Q^2}{2}\right) + (\rho + \sigma)u_j\, g\, z + (\alpha + p)u_j\right]_{,j}$$

$$= (\sigma\, u_i)_{,i}\left(c\, T + \frac{Q^2}{2} + g\, z\right). \tag{A.10}$$

Hence,

$$\rho\, u_j \left(g\, z + \frac{Q^2}{2}\right)_{,j} + (\sigma\, u_j)_{,j}\left[\left(c_v^v - c\right)T + L_0\right]$$

$$+ \sigma\, u_j\left(c_v^v\, T + \frac{Q^2}{2} + g\, z\right)_{,j} + \rho\, u_j (c_v\, T)_{,j}$$

$$+ \left(u_j\, p_{,j} + p\, u_{j,j}\right) + \left(u_j\, \alpha_{,j} + \alpha\, u_{j,j}\right) = 0, \tag{A.11}$$

where $(\sigma\, u_j)_{,j} = \rho\, u_j\, Y_{,j}$, $\sigma\, u_j = \rho\, Y\, u_j$, and the last line of (A.11) is

$$\rho\, u_j\left(\frac{p}{\rho}\right)_{,j} + \rho\, u_j\left(\frac{\alpha}{\rho}\right)_{,j}. \tag{A.12}$$

Thus, since $(c_v + R) = c_p$ and $(c_v^v + R') = c_p^v$,

$$\rho\, u_j(1 + Y)\left(g\, z + \frac{Q^2}{2}\right)_{,j} + \rho\, u_j(c_p\, T)_{,j} + \rho\, u_j\, Y_{,j}(L_0 - c\, T)$$

$$+ \rho\, u_j(Y\, c_p^v\, T)_{,j} = 0, \qquad (A.13)$$

where c_p^v (not c_v^v) appears because work is done on condensing gas and the enthalpy release is $\left[L_0 - (c - c_p^v)T\right]$. But

$$\rho\, u_j\left\{(1 + Y)\left[(Q^2/2) + g\, z\right]_{,j} + \frac{(p + \alpha)_{,j}}{\rho}\right\} = 0, \qquad (A.14)$$

so, if s is distance along a streamline, and since

$$Q\,\frac{\partial}{\partial s} = u_j\,\frac{\partial}{\partial x_j}\,, \qquad (A.15)$$

$$\frac{(\alpha + p)_{,s}}{\rho} - Y_{,s}(L_0 - c\, T) - (c_p\, T + Y\, c_p^v\, T)_{,s} = 0. \qquad (A.16)$$

If it is recalled that

$$\alpha = \Sigma(T)\, R'\, T,\ \rho = p/R\, T,\ Y = \Sigma(T)\, R\, T/p, \qquad (A.17)$$

the last equation becomes, if $\bar{p} \equiv (p + \alpha)$ and $\sigma \equiv (m_v/m_a)$,

$$\frac{d\, T}{d\, \bar{p}} = \frac{\dfrac{R\, T}{\bar{p} - \Sigma(T)} + \left[L_0 - (c - c_p^v)T\right]\dfrac{\sigma\,\Sigma(T)}{[\bar{p} - \Sigma(T)]^2}}{\left[c_p + \dfrac{\sigma\,\Sigma(T)\, c_p^v}{\bar{p} - \Sigma(T)}\right] + \left[L_0 - (c - c_p^v)T\right]\dfrac{\sigma\,\bar{p}\,\Sigma'(T)}{[\bar{p} - \Sigma(T)]^2}}\,, \qquad (A.18)$$

where $\Sigma'(T)$ denotes the first derivative, and all specific heats have been taken as constant. In more approximate derivations, $\bar{p} \doteq p$, $(c_p + Y\, c_p^v) \doteq c_p$, and $c_p \doteq c_p^v$ in the first term of the denominator.

APPENDIX B. THE LOW-LEVEL INFLOW LAYER

The nature of the incompressible axisymmetric flow under a potential vortex, with negligible role for Coriolis acceleration, is crucial for establishing the basis of an inviscid treatment of the separated layer. While the general character of the boundary layer already has been presented (Carrier 1971; McWilliams 1971; Burggraf et al 1971), still a simpler and more accessible argument for the laminar (constant-viscosity) case seems worth development in this appendix, which then goes on to suggest that the character of the laminar layer remains intact if a gradient-diffusion model is adopted to describe a turbulent inflow layer. The gradient-diffusion model of transfer in a boundary layer at high Reynolds number is regarded here simply as a convenient construction of empirical utility, without necessarily any basic validity.

Previous work states that the boundary layer grows monotonically, but relatively slowly, in thickness as one proceeds radially inward to the radius of maximum winds r_1 from the outer edge of the closed system r_0, where $r_0 = O(10\ r_1)$ suffices for most purposes. (The use of super asterisks to denote dimensional quantities is dispensed with in this appendix.) Near r_0, friction plays a role across the entire vertical extent of the surface inflow layer; as one approaches the axis, the role of friction in the conservation of radial momentum is confined to an ever-thinning swirl-free sublayer (immediately contiguous to the wall) across which the radial velocity component decreases to zero, in accordance with the no-slip boundary condition at the wall. The profile of the azimuthal velocity component is shaped significantly by friction across the entire thickness of the surface inflow layer, at all radial positions.

A nonoscillatory profile with distance from the wall holds for both radial and azimuthal velocity components: the maximum value of the radial velocity component can become as large as the potential-vortex swirl speed at the same radial distance from the axis of rotation, but at fixed altitude within the inflow layer the circulation is smaller, at smaller radial position. Although the swirl within the inflow layer sometimes is credited with values appreciably exceeding the asymptotic value holding above the inflow layer at the same radial position (Lewellen 1976), such behavior is not anticipated here.

B.1 Formulation

If, in cylindrical polar coordinates (r,θ,z), the corresponding velocity components are denoted (u,v,w), the conservation of mass, radial momentum, and angular momentum may be expressed as follows (with subscripts r,z denoting partial differentiation and ν denoting kinematic viscosity):

$$(ru)_r + (rw)_z = 0 \quad ; \tag{B.1.1}$$

$$\frac{(rV)^2 - (rv)^2 - (ru)^2}{r} = \left[\nu(ru)_z\right]_z - u(ru)_r - w(ru)_z \quad ; \tag{B.1.2}$$

$$\left[\nu(rv)_z\right]_z - u(rv)_r - w(rv)_z = 0 \ . \tag{B.1.3}$$

The boundary conditions are (r_0 given const.)

$$z \to \infty: \quad v \to \Gamma/r \ , \ \Gamma \text{ const} \ ; \ u \to 0 \ ; \tag{B.1.4}$$

$$z = 0: \quad u = v = w = 0 \ ; \tag{B.1.5}$$

$$r = r_0: \ u = 0, \ v \text{ specified } (\doteq \Gamma/r_0) \ . \tag{B.1.6}$$

The formulation is to be applied only in the range $r_1 \leqslant r \leqslant r_o$, where r_1 is the (finite) radius of maximum winds. Also,

$$\Gamma = r_1 V, \text{ const.} , \tag{B.1.7}$$

where V is the peak swirl speed in the potential vortex. It may be noted that the cyclostrophic balance in the potential vortex [ρ denotes density and p denotes pressure]

$$\frac{1}{\rho} p_r = \frac{V^2}{r} , \tag{B.1.8}$$

has been used to identify the radial pressure gradient in (B.1.2).

B.2 Constant-viscosity Solution

If ν is constant, solution to (B.1.1) - (B.1.7) is sought in the forms [the function form g(η) clearly is unrelated to the gravitational acceleration]

$$ru = - \Gamma\beta(r)g'(\eta) , \quad rv = \Gamma f(\eta) , \quad w = W(\eta) , \tag{B.2.1}$$

where

$$\eta = \left(\frac{\Gamma}{\nu}\right)^{\frac{1}{2}} \frac{z}{[s(r)]^{\frac{1}{2}}} . \tag{B.2.2}$$

Here, s(r) and β(r) are functions to be identified in the course of solution. One does not expect (B.2.1) - (B.2.2) to give an exact solution, but to capture the essence of the functional behavior in a useful form.

Substitution of (B.2.1) and (B.2.2) in (B.1.1) gives

$$W_\eta = (\nu\Gamma)^{\frac{1}{2}} \left[\frac{s^{\frac{1}{2}}}{r}\beta' g' - \frac{\beta s'}{2rs^{\frac{1}{2}}}\eta g''\right]$$

$$= (\nu\Gamma)^{\frac{1}{2}} \left[\frac{s^{\frac{1}{2}}}{r}\beta' g' - \frac{\beta s'}{2rs^{\frac{1}{2}}}(\eta g' - g)'\right];$$

$$W = (\nu\Gamma)^{\frac{1}{2}} \left[\left(\frac{s^{\frac{1}{2}}\beta'}{r} + \frac{\beta s'}{2rs^{\frac{1}{2}}}\right) g - \frac{\beta s'}{2rs^{\frac{1}{2}}}\eta g'\right], \qquad (B.2.3)$$

where by (B.1.5)

$$g(0) = 0. \qquad (B.2.4)$$

Substitution of (B.2.1) - (B.2.2) in (B.1.2) and (B.1.3) gives, respectively,

$$\frac{\Gamma^2}{r^2}(1 - f^2 - \beta^2 g'^2) = -\beta\Gamma^2\left[\frac{g'''}{s} - \frac{\beta'}{r} + \frac{\beta s'}{2rs} gg''\right] - \frac{\Gamma^2}{r}\beta\beta' g'^2 \quad ; \qquad (B.2.5)$$

$$\Gamma^2\left[\frac{f''}{s} - \left(\frac{\beta'}{r} + \frac{\beta s'}{2rs}\right) gf'\right] = 0 \quad . \qquad (B.2.6)$$

The terms in (B.2.5) derive, from left to right, from similarly positioned terms in (B.1.2). For selfconsistency,

$$\frac{s\beta'}{r} + \frac{s'\beta}{2r} = -1 \ , \qquad (B.2.7)$$

say; also, it is necessary, but not sufficient, to take

$$g'^2 = 1 - f^2 \ , \qquad (B.2.8)$$

$$\frac{\beta\beta'}{r} = -\frac{1-\beta^2}{r^2} \ . \qquad (B.2.9)$$

From (B.1.6), $\beta(r_0) = 0$; hence, from (B.2.9),

$$\beta^2 = \frac{r_o^2 - r^2}{r_o^2} \quad . \tag{B.2.10}$$

Equation (B.2.7) may be written

$$(\beta^2 s)' = -2r\beta \Rightarrow s = \frac{2}{3} r_o (r_o^2 - r^2)^{\frac{1}{2}} , \tag{B.2.11}$$

by use of (B.2.10).

The term in square brackets in (B.2.5) is $O(\beta\Gamma^2/s)$, while the other terms are $O(\Gamma^2/r^2)$; substitution of (B.2.10) and (B.2.11) into these expressions shows that the ratio of the bracketed to unbracketed terms is $O[(3r^2)/(2r_o^2)]$, so that for $r << r_o$, the bracketed term is negligible. The neglect of the bracketed term gives an inaccurate result where the motion is slow [i.e., where $v = O(V/10)$, $u < O(V/10)$], and an accurate result where the motion is fast. From (B.2.11), $s^{\frac{1}{2}} \sim (r_o - r)^{\frac{1}{4}}$ as $r \to r_o$; this is consistent with the more meticulous analysis of Burggraf et al (1971).

The radial momentum equation for $r_o^2 >> r^2$, i.e., for $\beta \to 1$, becomes a statement that the left-hand side of (B.1.2) vanishes; i.e., $V^2 = (u^2 + v^2)$, such that the radial component of momentum is inviscidly controlled. The two-point nonlinear third-order boundary-value problem, from (B.2.5) - (B.2.8), becomes

$$f'' + gf' = 0 \; ; \tag{B.2.12}$$

$$g'^2 = 1 - f^2 \; ; \tag{B.2.13}$$

$$f(0) = g(0) = 0 \; , \; f(\infty) \to 1 \; . \tag{B.2.14}$$

The boundary conditions follow from (B.1.4), (B.1.5), (B.1.7), (B.2.1), and (B.2.2). The problem is solved numerically; one finds

$$f'(0) \doteq 0.7456, \; g(\infty) \doteq 1.941 \; . \tag{B.2.15}$$

Results are graphed in figure 30, where it is evident that f monotonically increases (so g′ monotonically decreses).

Of course, the reduction to third order results from the discarding of the frictional term in the conservation of radial momentum (B.2.5), which was taken in the inviscid form (B.2.8). Enforcement at all r of u = 0 at z = 0, which implies $g'(0) = 0$, requires restoration of the frictional term in a thin, effectively swirl-free sublayer contiguous to the boundary.

A brief sketch of the sublayer across which u falls to zero is now presented. If

$$ru = -\Gamma\beta(r)h'(\sigma) \ , \ \sigma = \left(\frac{\Gamma}{\nu}\right)^{\frac{1}{2}} \frac{z}{m(r)} \ , \ \beta = 1 - (r/r_0)^2 \ , \tag{B.2.16}$$

then, from continuity (B.1.1),

$$(rw)_\sigma = \left(\frac{\nu}{\Gamma}\right)^{\frac{1}{2}} m\left[\Gamma\beta' h' - \Gamma\beta\left(\frac{m'}{m}\right)\sigma h''\right] \ , \tag{B.2.17}$$

$$rw = (\nu\Gamma)^{\frac{1}{2}} m\left[\beta' h - \beta\left(\frac{m'}{m}\right)\left(\sigma h' - h\right)\right] \ . \tag{B.2.18}$$

Substitution of (B.2.16) and (B.2.18) in (B.1.2) gives

$$-\left(\frac{\beta}{m^2}\right) h''' - \left(\frac{\beta\beta'}{r}\right) h'^2 + \left[\frac{\beta(\beta' + \beta m^{-1} m')}{r}\right] h h''$$

$$= -\frac{1}{r^2} - \left(\frac{\beta^2}{r^2}\right) h'^2 - \left(\frac{1}{r^2}\right) f^2 \ , \tag{B.2.19}$$

where the last term involving f^2 is dropped as uniformly negligible over the sublayer. The function m is assigned by demanding

$$\frac{\beta^2 m'}{rm} = \frac{1}{r^2} \ . \tag{B.2.20}$$

If attention is confined to $(r/r_0) << 1$, so that $\beta \to 1$, $\beta' = o(1)$, then

$$m \doteq r \ , \tag{B.2.21}$$

and

$$- h''' + (hh')' \doteq 1, \tag{B.2.22}$$

where all neglected terms are $O(r^2/r_0^2)$ or smaller. The boundary conditions are

$$h(0) = 0, \ h'(0) = 0, \ h'(\infty) \to 1 \ ; \tag{B.2.23}$$

these enforce (B.1.5) so that $u(x,0) = w(x,0) = 0$, and permit matching of frictional-sublayer and inviscid-outer-layer solutions. One arrives at a Riccati equation:

$$- h' + \frac{h^2}{2} = \frac{\sigma^2}{2} - h''(0)\sigma \ , \ h(\sigma \to \infty) \to \sigma \ , \tag{B.2.24}$$

where the boundary conditions (B.2.23) have been used to assign constants of integration. Figure 31 shows that

$$h(\sigma) \doteq \sigma + \exp(-\sigma) - 1 \Rightarrow h'(\sigma) = 1 - \exp(-\sigma) \ , \tag{B.2.25}$$

approximates the result of numerical integration satisfactorily for most purposes. Hence, a uniformly valid expression for $r^2 << r_0^2$ is given by

$$ru \doteq - \Gamma\beta(r)\left[h'(\sigma) + h'(\eta) - 1\right] \ , \tag{B.2.26}$$

where $h'(\sigma)$ is given by (B.2.24), or more facilely by (B.2.25), and $h'(\eta)$ is given by (B.2.12) - (B.2.14).

B.3 The Turbulent Boundary Layer under a Rapidly Swirling Vortex

Solution to (B.1.1) - (B.1.6) is again sought in the forms (B.2.1), but instead of (B.2.2),

$$\eta = \frac{z}{s(r)} \quad , \tag{B.3.1}$$

and $\beta(r)$, $s(r)$ are now sought in forms appropriate for a viscosity taken in the form

$$\nu = \frac{s\Gamma}{r} H(\eta) \quad , \tag{B.3.2}$$

where $H(\eta)$ is to be specified and (B.3.2) encompasses eddy-viscosity forms to be examined here. It is emphasized at the outset that selfsimilarity is not entirely adequate; nonselfsimilar contributions are not uniformly negligible and warrant retention in improvements on the preliminary development (given here to suggest that standard turbulent models for boundary layers yield results with the general characteristics of results already evolved for ν constant).

Substitution of (B.2.1) into (B.1.1) under (B.3.1) yields

$$W(\eta) = \Gamma\left[\left(\frac{s\beta'}{r} + \frac{\beta s'}{r}\right) g - \frac{\beta s'}{r} \eta g'\right] \quad . \tag{B.3.3}$$

Substitution of (B.2.1) into (B.1.3) under (B.3.1) and (B.3.2) yields

$$\frac{1}{sr}\left\{\left[H(\eta)f\right]' - (\beta s)' g f'\right\} = 0 \quad ; \tag{B.3.4}$$

consistency leads to the choice

$$(\beta s)' = -1 \Rightarrow \beta s = r_o - r \quad , \tag{B.3.5}$$

under (B.1.6). Hence,

$$(Hf')' + gf' = 0 \quad . \tag{B.3.6}$$

Substitution of (B.2.1) and (B.3.1) into (B.1.2) yields

$$\frac{\beta}{rs}\left[(H\,g'')' + gg''\right] + \frac{\beta\beta'}{r}(g')^2 = \frac{1}{r^2}\left[1 - f^2 - \beta^2(g')^2\right] . \qquad (B.3.7)$$

It is anticipated that the boundary layer associated with the azimuthal velocity component v thickens faster in the turbulent case than in the laminar case. The radial-velocity-component sublayer, in which friction enters significantly, is anticipated to occupy even less of the swirl-boundary-layer thickness than in the laminar case. Thus, in most of the inflow layer, (B.3.7) is taken as

$$\frac{\beta\beta'}{r}(g')^2 \doteq -\frac{1}{r^2}\left[1 - f^2 - \beta^2(g')^2\right] . \qquad (B.3.8)$$

For selfconsistency,

$$g'^2 = 1 - f^2 ; \qquad (B.3.9)$$

$$\frac{\beta\beta'}{r} = -\frac{1-\beta^2}{r^2} \Rightarrow \beta^2 = 1 - \left(\frac{r}{r_o}\right)^2 , \qquad (B.3.10)$$

from (B.1.6).

From (B.3.5) and (B.3.10), tentatively,

$$s = r_o\left(\frac{r_o - r}{r_o + r}\right)^{\frac{1}{2}} . \qquad (B.3.11)$$

It is anticipated that ultimately the definition of s must be modified from that given in (B.3.11) to account for nonnegligible contributions from nonself-similar terms in the equations for conservation of radial and azimuthal momentum.

Hence the boundary-value problem becomes (B.3.6) and (B.3.9), with the boundary conditions

$$f(0) = g(0) = 0 \; ; \; f(\eta \to \infty) \to 1 \quad . \tag{B.3.12}$$

It is adopted that the total viscosity $\nu = (\nu_o + \nu_e)$, where ν_o is the molecular viscosity and ν_e is the eddy viscosity and ν_e is taken in the standard form (Fendell 1972; Bush and Fendell 1972; White 1974) (figure 32)

$$\nu_e = \begin{cases} k_1 \, z^2 \, (u_z^{\,2} + v_z^{\,2})^{\frac{1}{2}} \, , & \text{in the wall layer} \\ \\ k_2 \left(\dfrac{\Gamma}{r}\right) \delta^* \, , & \text{in the defect layer;} \end{cases} \tag{B.3.13}$$

k_1 is the square of the von Karman const., or $(0.41)^2$; k_2 is the Clauser const., 0.016; and δ^* is the angular-momentum-defect thickness. A van Driest-type wall-layer correction factor and an intermittency-type defect-layer correction have been omitted as nonessential. In similarity variables, in view of (B.3.9), (B.3.13) becomes

$$\nu_e = \begin{cases} \left(\dfrac{\Gamma s}{r}\right) k_1 \, \eta^2 \, \dfrac{f'}{(1 - f^2)^{\frac{1}{2}}} \left[1 + f^2(\beta^2 - 1)\right]^{\frac{1}{2}}, & \text{wall layer} \\ \\ \left(\dfrac{\Gamma s}{r}\right) k_2 \, \sigma \, , & \text{defect layer.} \end{cases} \tag{B.3.14}$$

In the defect layer, if σ denotes a constant (to be determined),

$$\delta^* = \int_0^\infty \left(1 - \frac{rv}{\Gamma}\right) dz = s \int_0^\infty (1 - f) \, d\eta \equiv s\sigma \, . \tag{B.3.15}$$

Hence, from (B.3.2), for $r << r_o$ so $\beta \to 1$,

$$\nu = \frac{s\Gamma}{r} H(\eta) \ , \ H(\eta) = \varepsilon + k_1 \left\{ \frac{\eta^2 f'(\eta)}{[1 - f^2(\eta)]^{\frac{1}{2}}} \right\}_* \ , \tag{B.3.16}$$

where by definition subscript asterisk here defines a functional behavior:

$$\left\{ F(\eta) \right\}_* = F(\eta) \text{ for } 0 \leq \eta \leq \eta_1 \ ; \ \left\{ F(\eta) \right\}_* = F(\eta_1) \text{ for } \eta_1 \leq \eta \leq \infty \ . \tag{B.3.17}$$

Since $s \to r_o$ for $r << r_o$,

$$\varepsilon = \left[\frac{\nu_o}{\Gamma} \right] \frac{r}{s} \to \left[\frac{\nu_o}{\Gamma} \right] \frac{r_1}{r_o} \ . \tag{B.3.18}$$

For consistency with similarity, r in (B.3.18) has been taken uniformly constant at its smallest value within the range of interest. The eddy viscosity is made continuous by enforcing the following condition at the interface between the viscous sublayer (in which the mixing-length form holds) and the defect layer (in which the product of local freestream speed and an integral scale form a diffusion coefficient):

$$k_1 \eta_1^2 \frac{f'(\eta_1)}{[1 - f^2(\eta_1)]^{\frac{1}{2}}} = k_2 \sigma \ , \tag{B.3.19}$$

a relation that defines η_1.

In summary, the solution for the functions of (B.2.1) and (B.3.1), with β identified in (B.3.10) and s in (B.3.11) and W in (B.3.3), can be obtained

from (B.3.6) and (B.3.9) subject to (B.3.12), where the given parameter $\varepsilon(<<1)$ is defined by (B.3.18), the derived parameter σ is defined by (B.3.15), and the derived parameter η_1 is given by (B.3.19), with $k_1 = (0.41)^2$ and $k_2 = 0.016$.

Numerical solution entails a two-degree-of-freedom iteration in that, for example, one must anticipate both $f'(0)$ and η_1, and confirm the validity of the guesses by σ compatible with (B.3.15) and $f(\eta \to \infty)$ compatible with (B.3.12), in a shooting-type approach. Facile reduction to a one-degree-of-freedom iteration is not readily executed. Nevertheless, solutions for various values of ε are straightforward, and are presented in figures 33 and 34, with the values required for "shooting" tabulated in table 2.

REFERENCES

Barcilon, A. 1967 Vortex decay above a stationary boundary, *J. Fluid Mech.*, 27, 155-175.

Batchelor, G.K. 1967 *An Introduction to Fluid Dynamics*. Cambridge University Press, 543-546.

Black, P.G. 1977 Some aspects of tropical storm structure revealed by hand-held-camera photographs from space. *Skylab Explores the Earth*. U.S. Government Printing Office, Washington, D.C., 417-461.

Brooks, E.M. 1949 The tornado cyclone. *Weatherwise*, 2, 32-33.

Burggraf, O.R., Stewartson, K. & Belcher, R. 1971 Boundary layers induced by a potential vortex. *Phys. Fluids*, 14, 1821-1833.

Carrier, G.F. 1970 Singular perturbation theory and geophysics. *SIAM (Soc. Industr. Appl. Math) Rev.*, 12, 175-193.

Carrier, G.F. 1971a Swirling flow boundary layers. *J. Fluid Mech.*, 49, 133-144.

Carrier, G.F. 1971b The intensification of hurricanes. *J. Fluid Mech.*, 49, 145-158.

Carrier, G.F. & Fendell, F.E. 1978 Analysis of the near-ground wind field of a tornado with steady and spatially varying eddy viscosity. *Wind Field and Trajectory Models for Tornado-Propelled Objects*. Electric Power Research Institute, Palo Alto, CA, Project 308, Report NP-748, A-1 - A-45.

Carrier, G.F., Hammond, A.L., & George, O.D. 1971 A model of the mature hurricane. *J. Fluid Mech.*,47, 145-170.

Darkow, G.L. 1967 The total energy environment of severe storms. *Preprints of Papers Presented at the Fifth Conference on Severe Local Storms*. American Meteorological Society, Boston, MA, 99-108.

Dergarabedian. P. & Fendell, F. 1970 On estimation of maximum wind speeds in tornadoes and hurricanes. *J. Astronaut. Sci.*, 17, 218-236.

Dergarabedian, P. & Fendell, F. c1977 One- and two-cell structure in tornadoes. *Proceedings of the Symposium on Tornadoes: Assessment of Knowledge and Implications for Man*. Institute for Disaster Research, Texas Tech University, Lubbock, TX, 501-521.

Dergarabedian, P. & Fendell, F.E. 1971a Estimation of maximum wind speeds in tornadoes. *Tellus*, 22, 511-516.

Dergarabedian, P. & Fendell, F.E. 1971b A method for rapid estimation of maximum tangential wind speed in tornadoes. *Mon. Wea. Rev.*, 99, 143-145.

Fendell, F.E. 1974 Tropical cyclones. *Advances in Geophysics*, Vol. 17, Academic, 1-100.

Fujita, T.T., Forbes, G.S. & Umenhofer, T.Z. 1976 Close-up view of 20 March 1976 tornadoes: sinking cloud tops to suction vortices. *Weatherwise*, 29, 117-131, 145.

Gray, W.M. 1969 Hypothesized importance of vertical wind shear in tornado genesis. *Preprints of Papers presented at the Sixth Conference on Severe Local Storms*, American Meteorological Society, Boston, MA, 230-237.

Hall, M.G. 1972 Vortex breakdown. *Ann. Rev. Fluid Mech.*, 4, 195-217.

Haurwitz, B. 1935 The height of tropical cyclones and the "eye" of the storm. *Mon. Wea. Rev.*, 63, 45-49.

Houze, Jr., R.A. & Hobbs, P.V. 1982 Organization and structure of precipitating cloud systems. *Advances in Geophysics*, Vol. 22, Academic, 225-315.

Jordan, C.L. 1957 A mean atmosphere for the West Indies area. *National Hurricane Research Project Report No. 6.* U.S. Department of Commerce, Washington, D.C.

Leibovich, S. 1978 The structure of vortex breakdown. *Ann. Rev. Fluid Mech.*, 10, 221-246.

Lewellen, W.S. 1977 Theoretical models of the tornado vortex. *Proceedings of the Symposium on Tornadoes: Assessment of Knowledge and Implications for Man*, R.E. Peterson, ed., 107 - 143. Lubbock, TX: Institute for Disaster Research, Texas Tech University.

Lilly, D.K. 1969 Tornado dynamics. National Center for Atmospheric Research, Boulder, CO, research manuscript 9-117.

McWilliams, J.C. 1971 The boundary layer dynamics of symmetric vortices. Ph.D. thesis. Cambridge, MA: Harvard University.

Miller, B.I. 1958 On the maximum intensity of hurricanes. *J. Meteorol.*, 15, 184-195.

Roshko, A. 1976 Structure of turbulent shear flows: a new look. AIAA J., 14, 1349-1357.

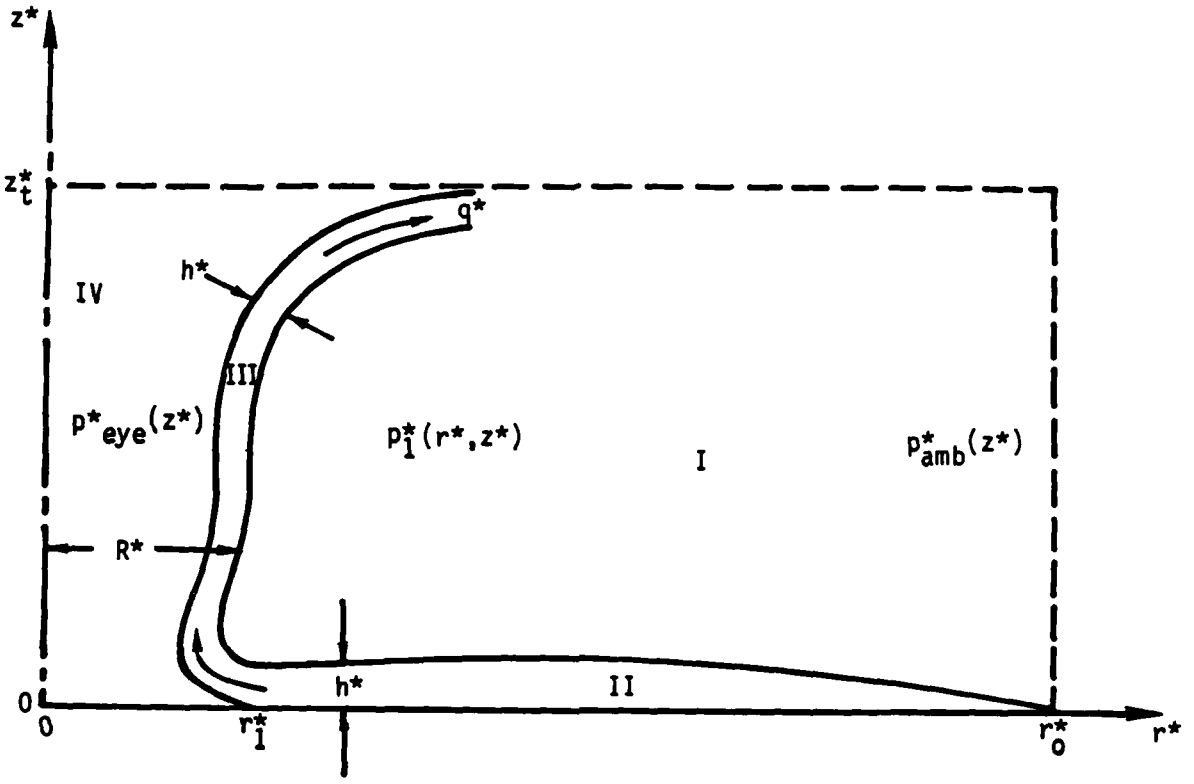

FIGURE 1. Schematic of the postulated four-part model of the structure mature two-cell vortex, of radial extent r_o^* and axial extent z_t^* (the height of the tropopause).

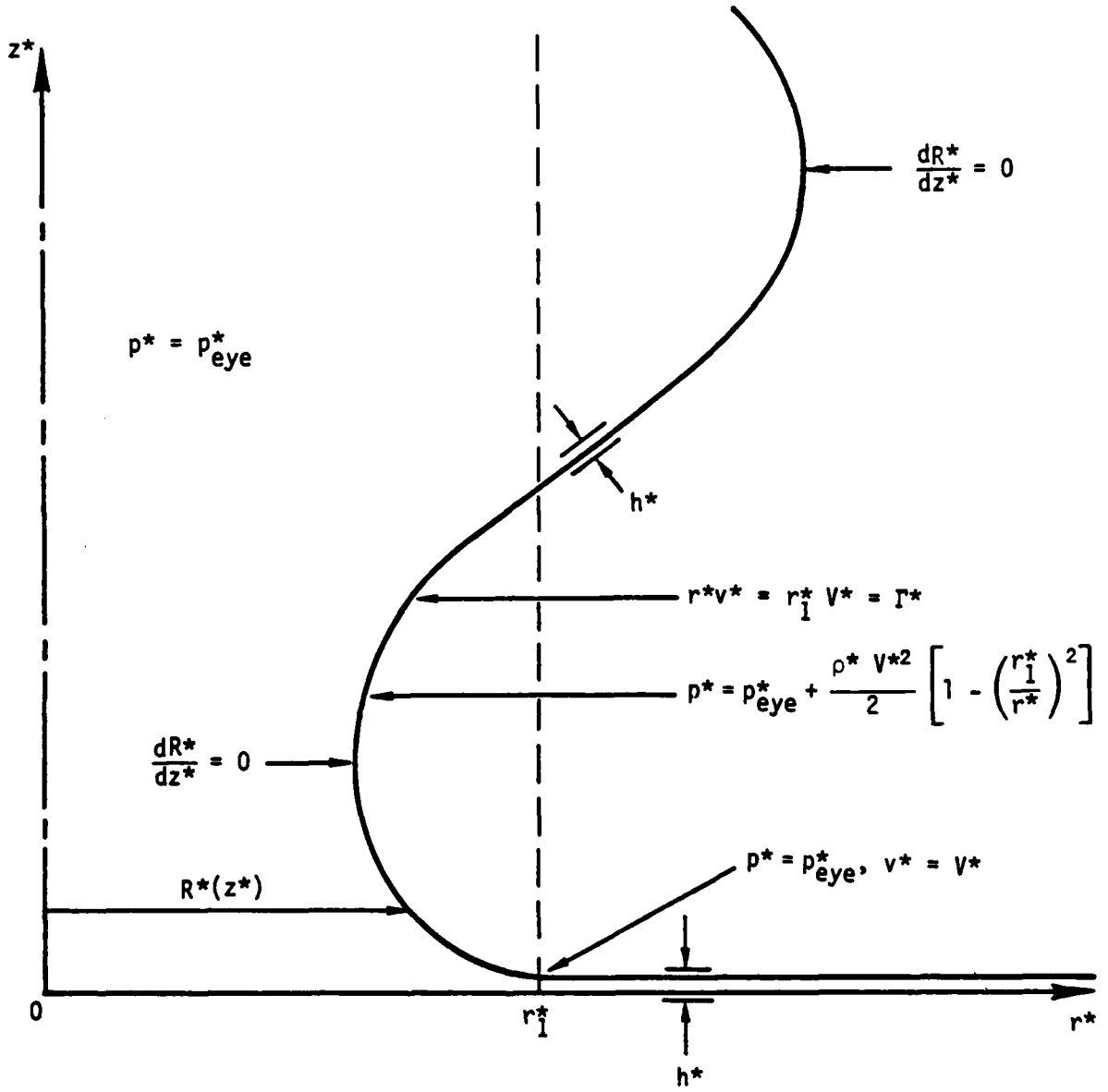

FIGURE 2. Schematic of the location of an inviscid eyewall without structure demarcating the interface between an isobaric nonswirling eye at pressure p^*_{eye} and a potential vortex. The sheet representing the eyewall has thickness $h^* \to 0$; in the turnaround region, its displacement from the axis, as a function of height above the ground plane, is denoted $R^*(z^*)$.

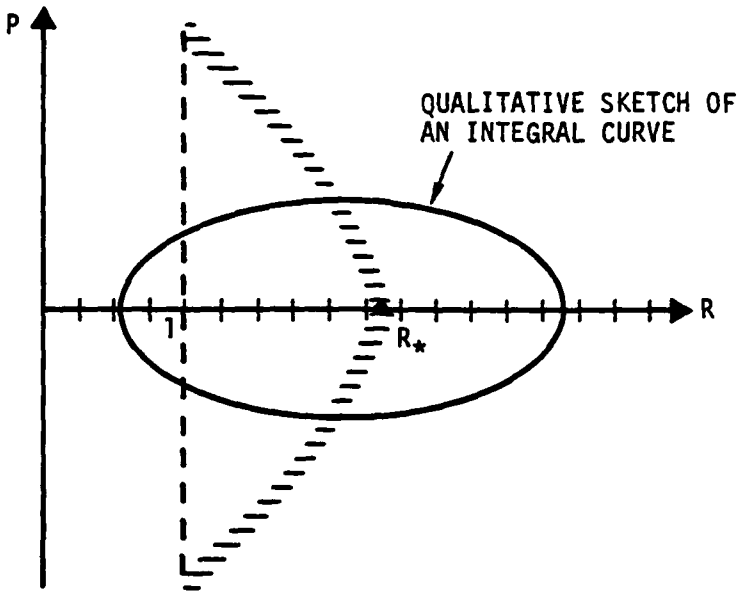

FIGURE 3. Phase-plane properties of equation (3.1.11), where $P = (dR/dz)$, with R the dependent variable ($R > 0$) and z the independent variable. Isoclines of zero and infinite slope are noted. At $R = 1$, the distance from the axis of symmetry at which the surface inflow layer separates, a finite positive slope is adopted. For $\alpha > 0$, $R_* > 1$; for $\alpha = 0$, $R_* = 1$. The sketched trajectory (solution curve) is a limit cycle (closed curve indicative of periodic behavior). The periodicity is not of physical interest.

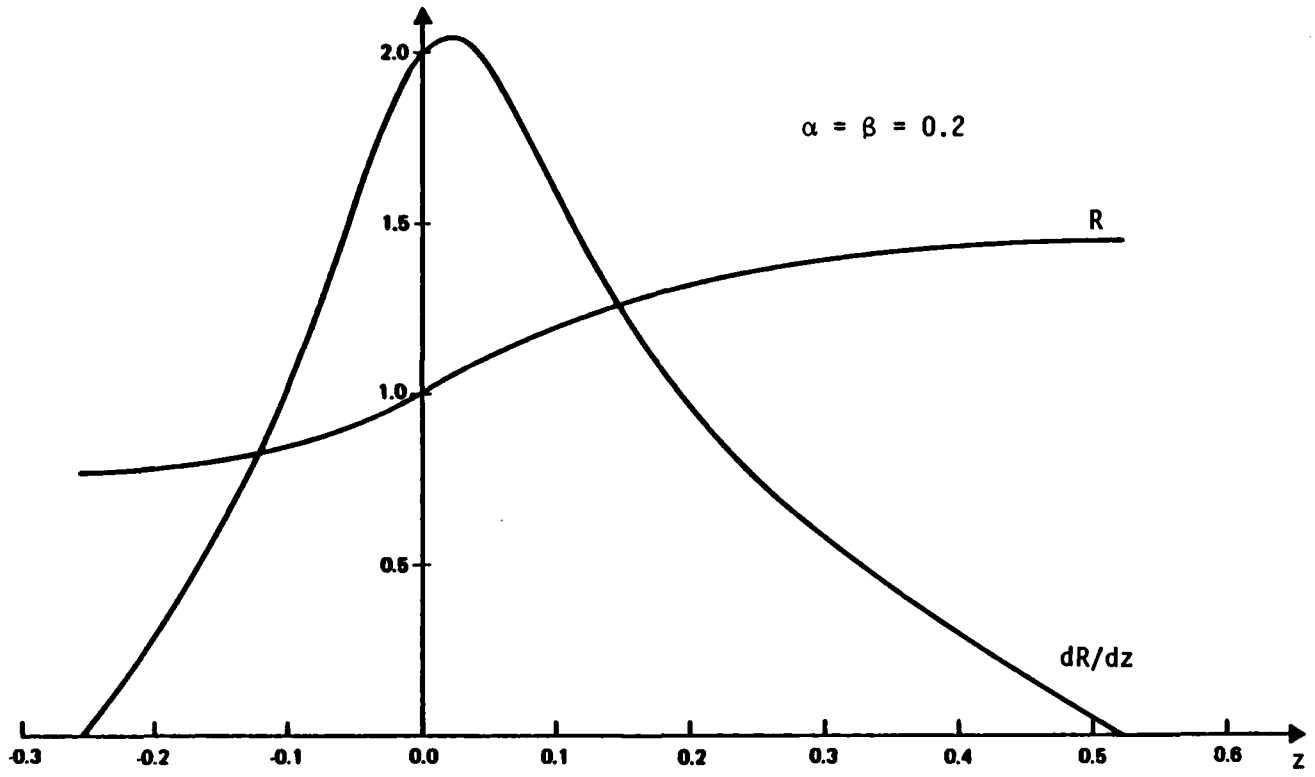

FIGURE 4. The solution to the boundary-value problem posed by equations (3.1.7) - (3.1.9), for $R_0' = 2$; the solution may be completed by symmetry considerations to constitute a full cycle.

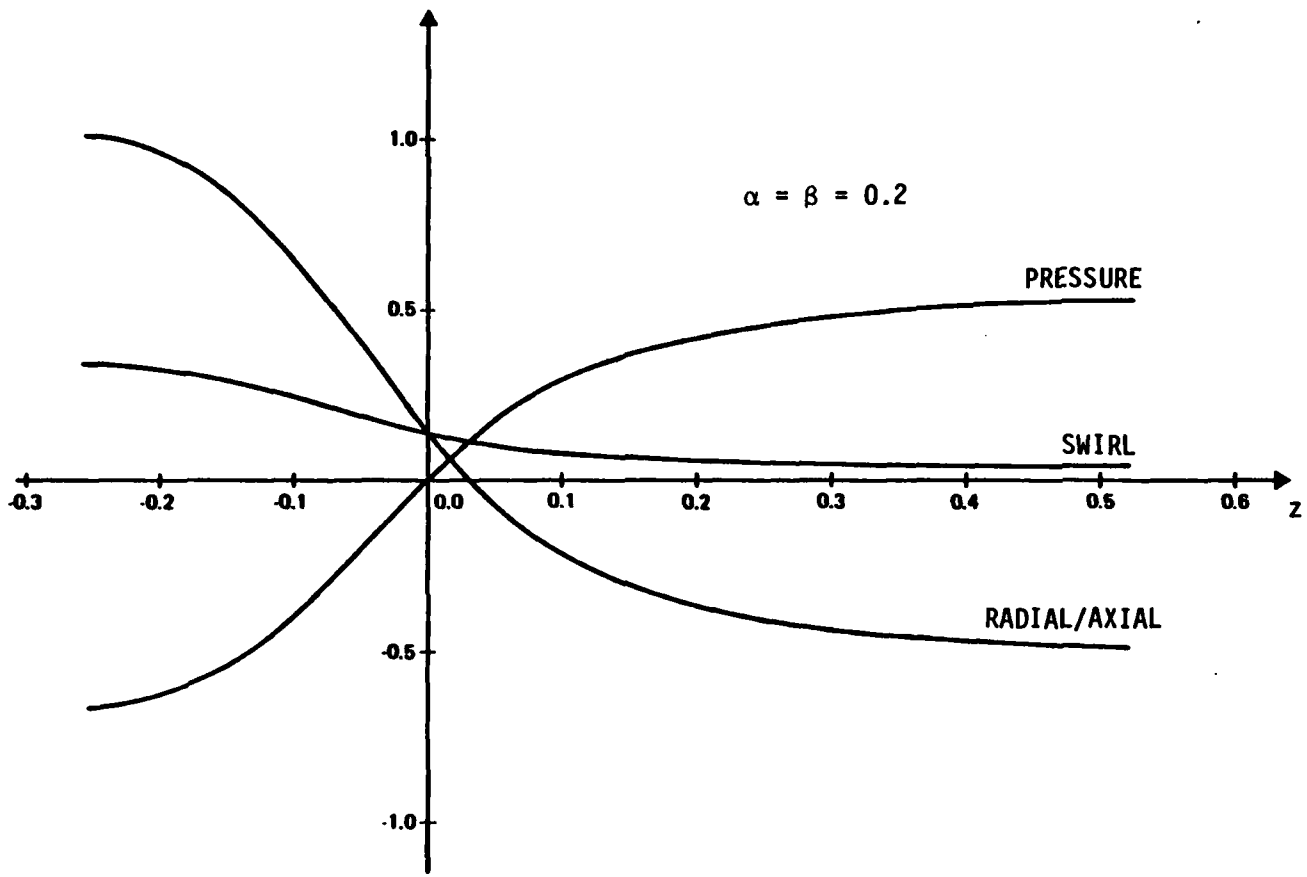

FIGURE 5. The solution to the boundary-value problem posed by equations (3.1.7) - (3.1.9), for $\alpha = 0.2$, $\beta = 0.2$, and $R_0' = 2$, given in figure 4, is further studied. The "pressure" denotes the value of $(1 - R^{-2})$; the "swirl" denotes the value of $\alpha R^{-3}(1 + R'^2)^{-\frac{1}{2}}$; the quantity "radial/axial" denotes the value of "swirl" minus "pressure", i.e., the value of the second term on the right-hand side of (3.1.7) before solution for the second derivative.

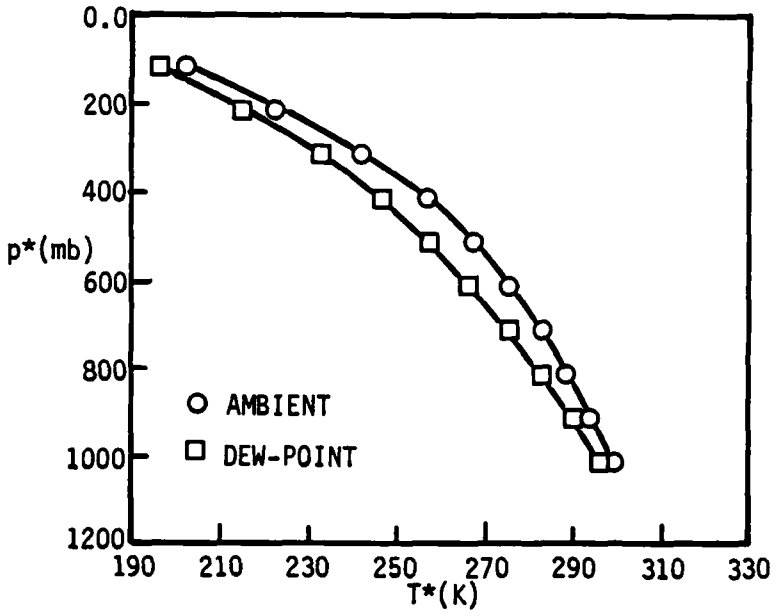

FIGURE 6a. The mean pressure-temperature relationship for the convectively unstable ambient in the West Indies for September (Jordan 1957).

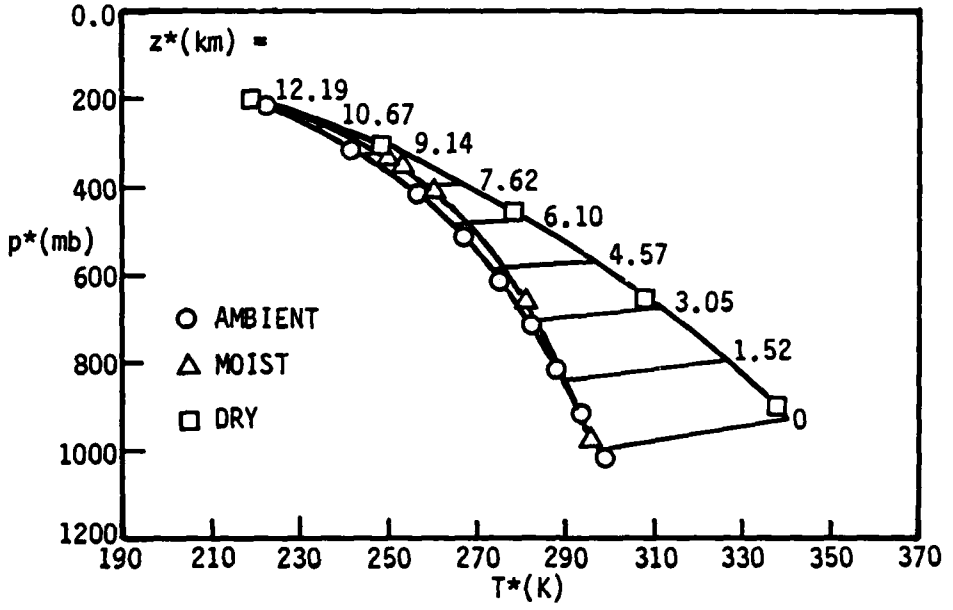

FIGURE 6b. Pressure-temperature relationships.

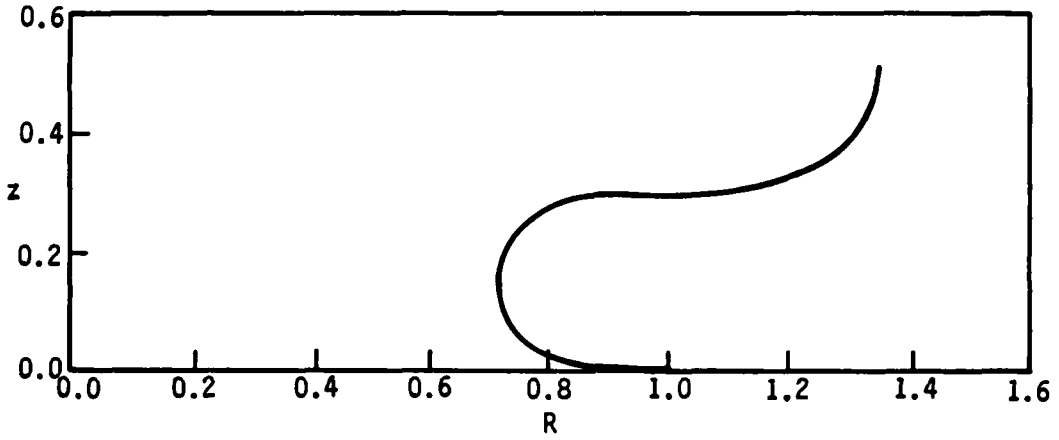

FIGURE 7. The radial displacement of the outer edge of the eyewall R, i.e., the "ambient edge" contiguous to the potential vortex, as a function of height above ground level z, for a tornado-like case.

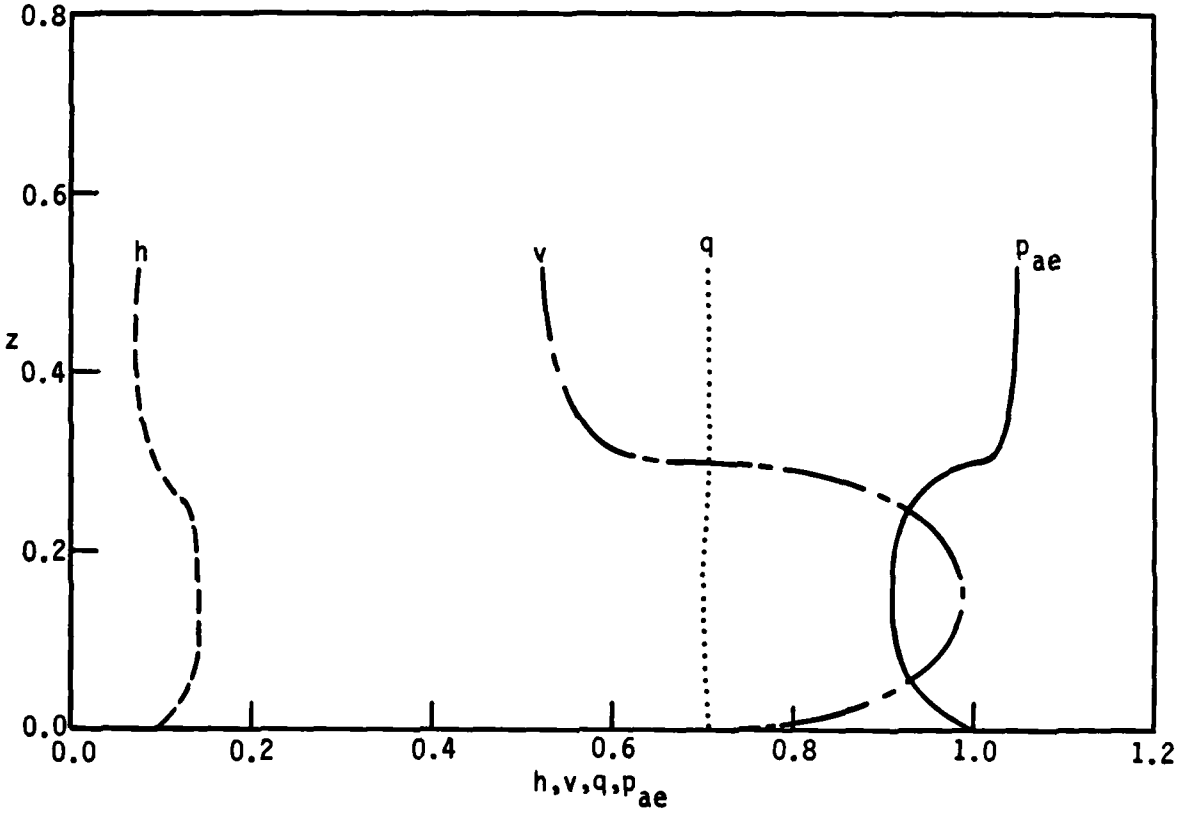

FIGURE 8. For the case of figure 7, the separated-layer thickness h, the transversely averaged swirl speed v, the transversely averaged radial-axial-flow speed q, and the pressure at the ambient edge of the separated layer p_{ae}, as functions of of altitude above ground level z. The pressure in the eye p_{eye} is held at unity.

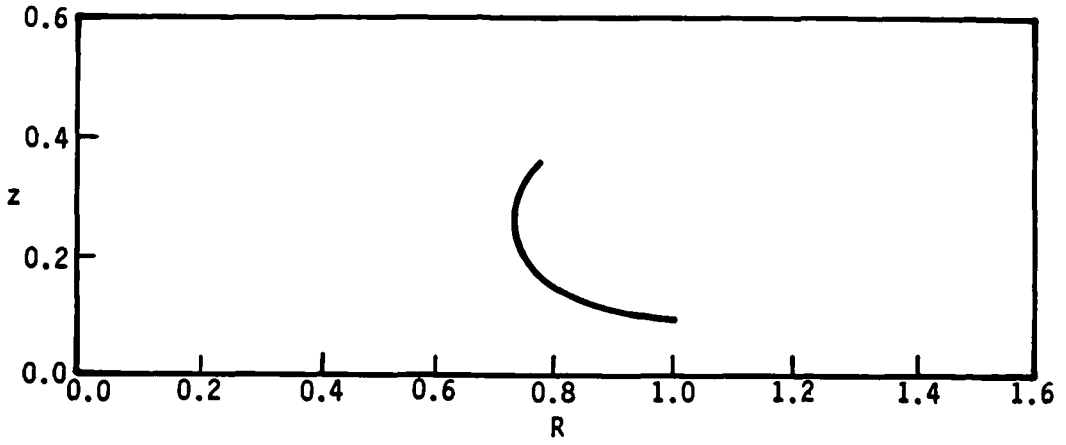

FIGURE 9. The radial displacement of the outer edge of the eyewall R as a function of height above sea level z, for a hurricane-like case.

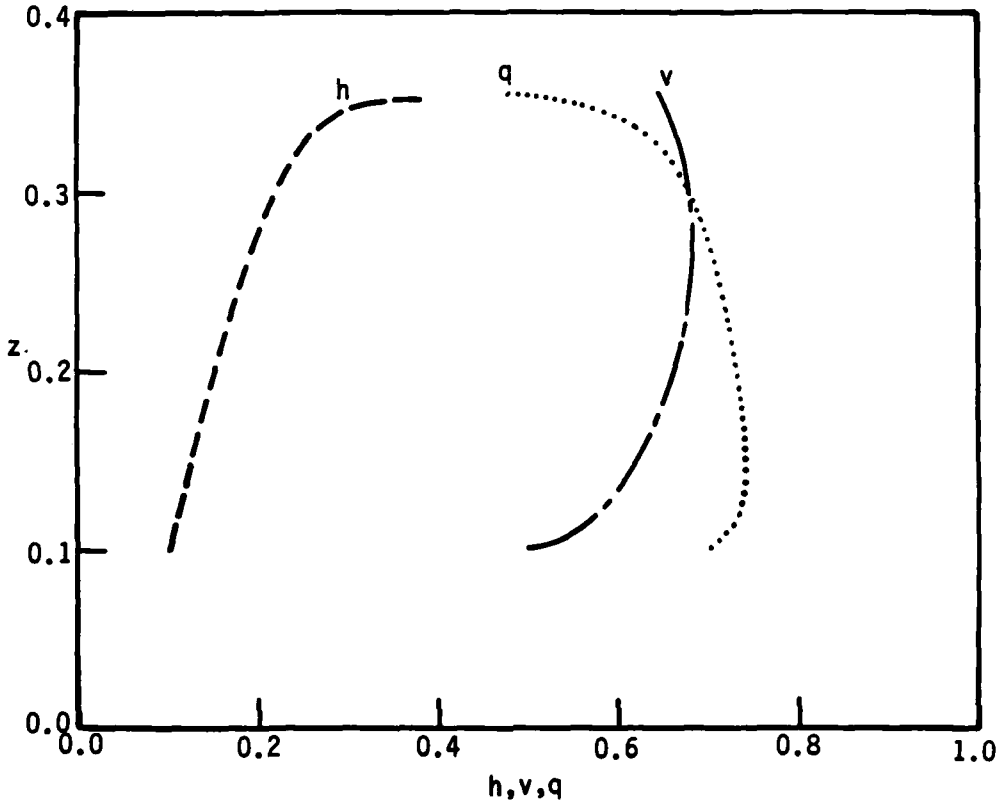

FIGURE 10. For the case of figure 9, the separated-layer thickness h, the transversely averaged swirl v, and the transversely averaged radial-axial-flow speed q, as functions of altitude above sea level z.

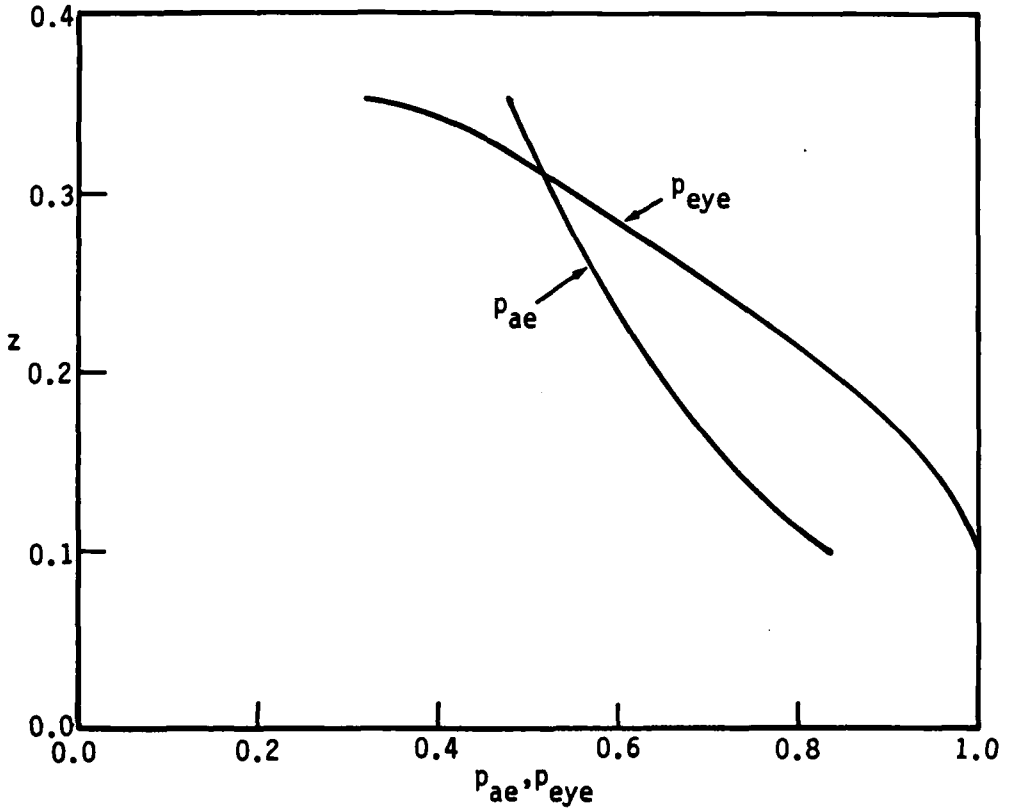

FIGURE 11. For the case of figure 9, the pressure at the ambient edge of the separated layer p_{ae} and the pressure in the eye p_{eye}, as functions of altitude above sea level z.

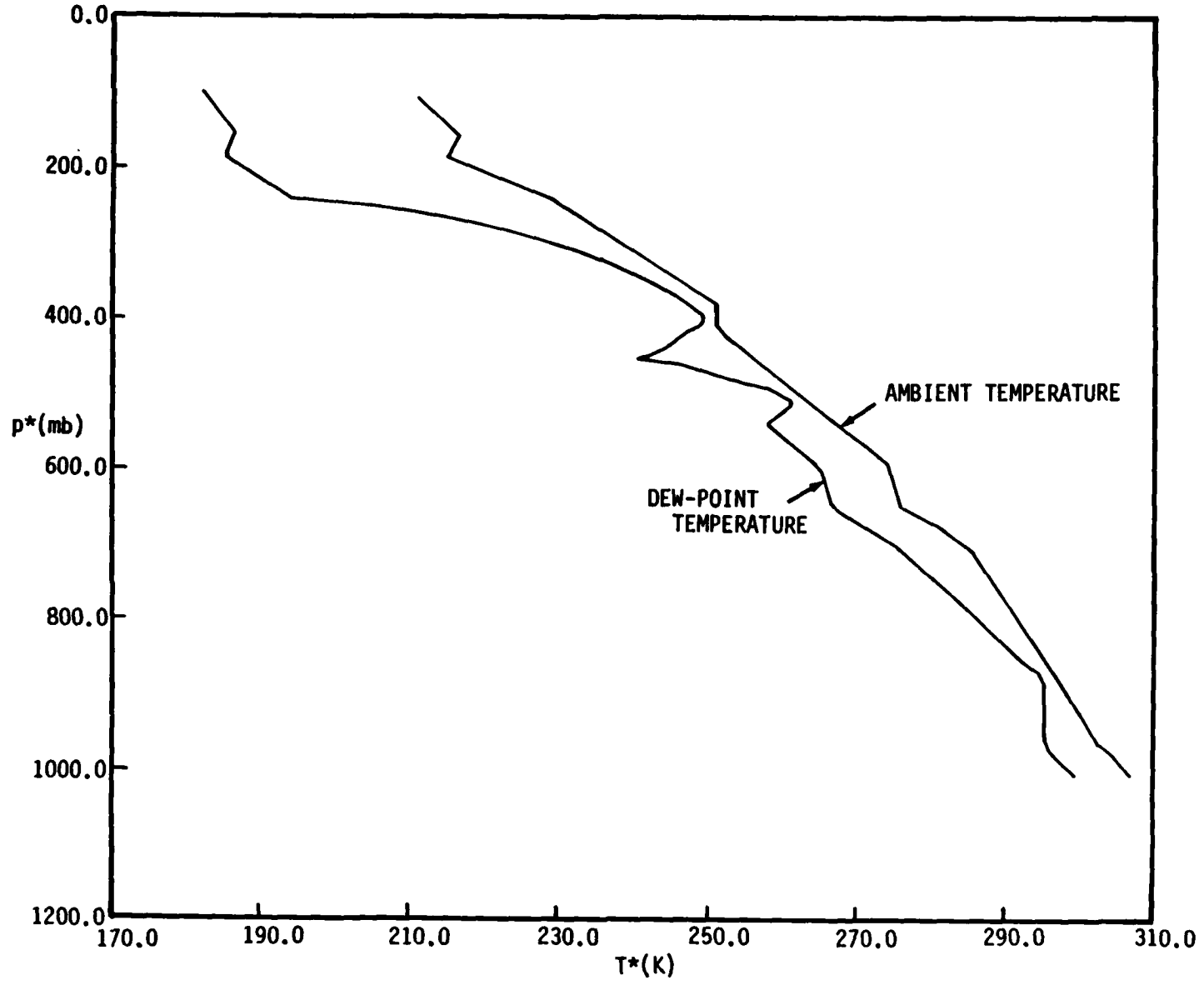

FIGURE 12. Highly convectively unstable ambient (measured in the vicinity of a tornado) at St. Cloud, MN, on July 22, 1967 at 1715Z.

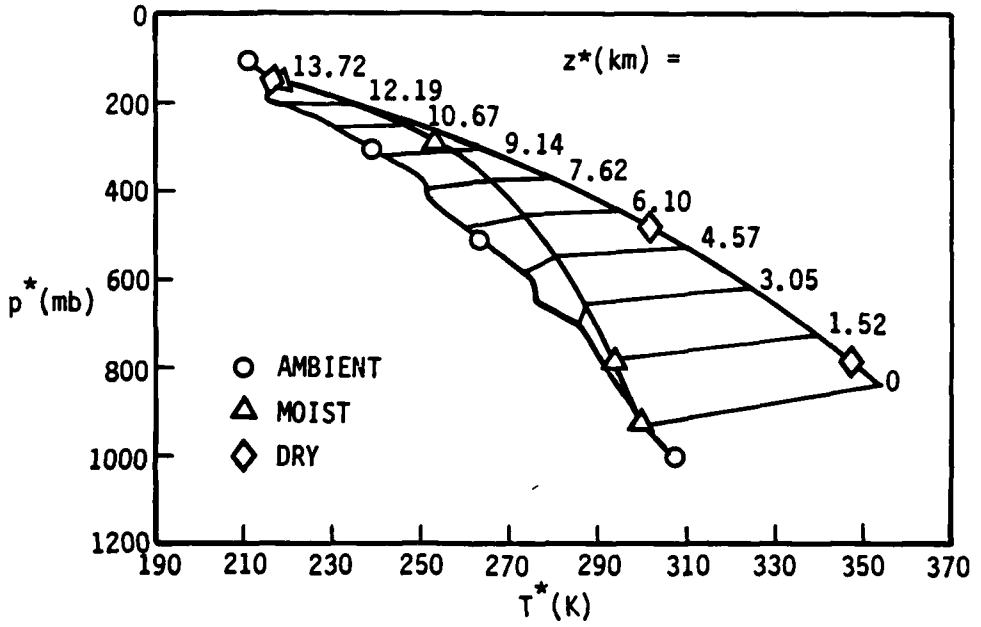

FIGURE 13. Pressure-temperature relationships for the ambient of figure 12, for ground-level air raised on a moist adiabat to its level of neutral stability (i.e., to the tropopause as defined here), and for tropopause-level air compressed dry-adiabatically. Heights are associated by means of hydrostatics, with z*=0 being ground level. The fractional heights displayed are the result of conversion from engineering units to SI convention.

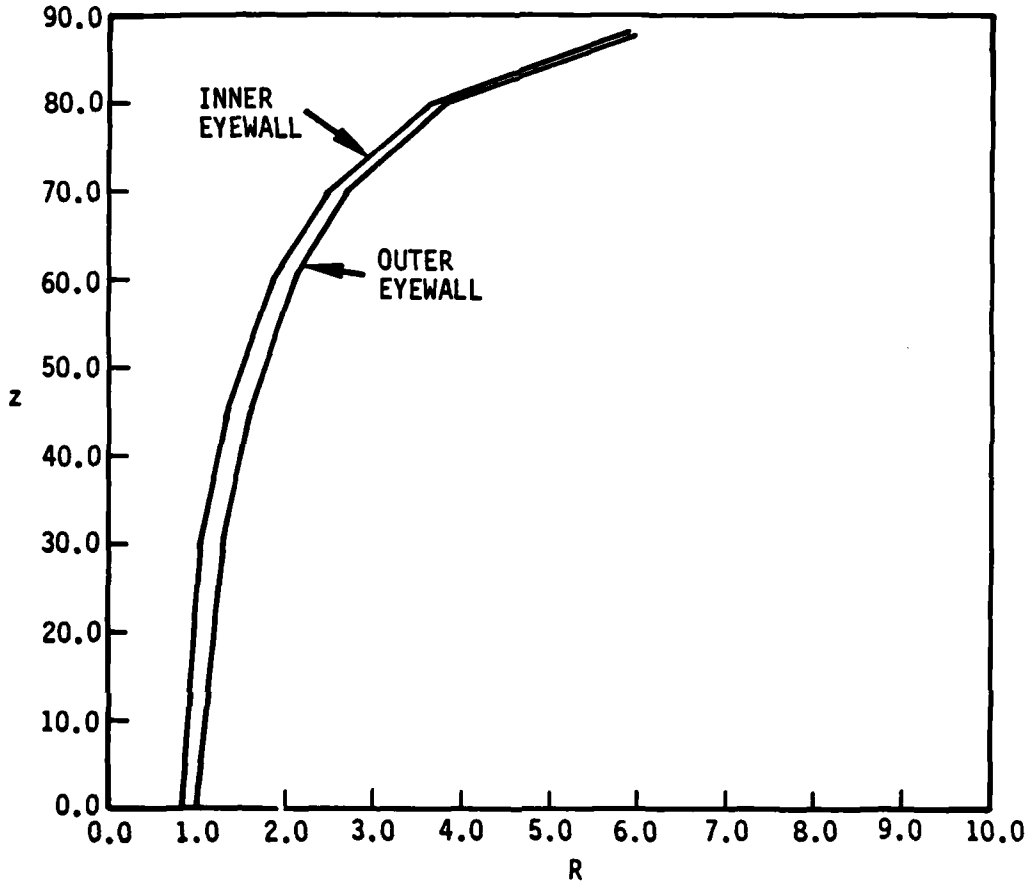

FIGURE 14. For the case of figure 12 with a fully inserted eye, the adopted radial displacement R of the outer eyewall (i.e., the eyewall edge contiguous to the potential vortex) as a function of altitude z, where the completion-of-turnaround height is taken as z = 0. The inner eyewall position is the site of the eyewall edge contiguous to the eye; the inner edge is located by subtracting the eyewall thickness h(z) in a direction perpendicular to the local tangent to R(z).

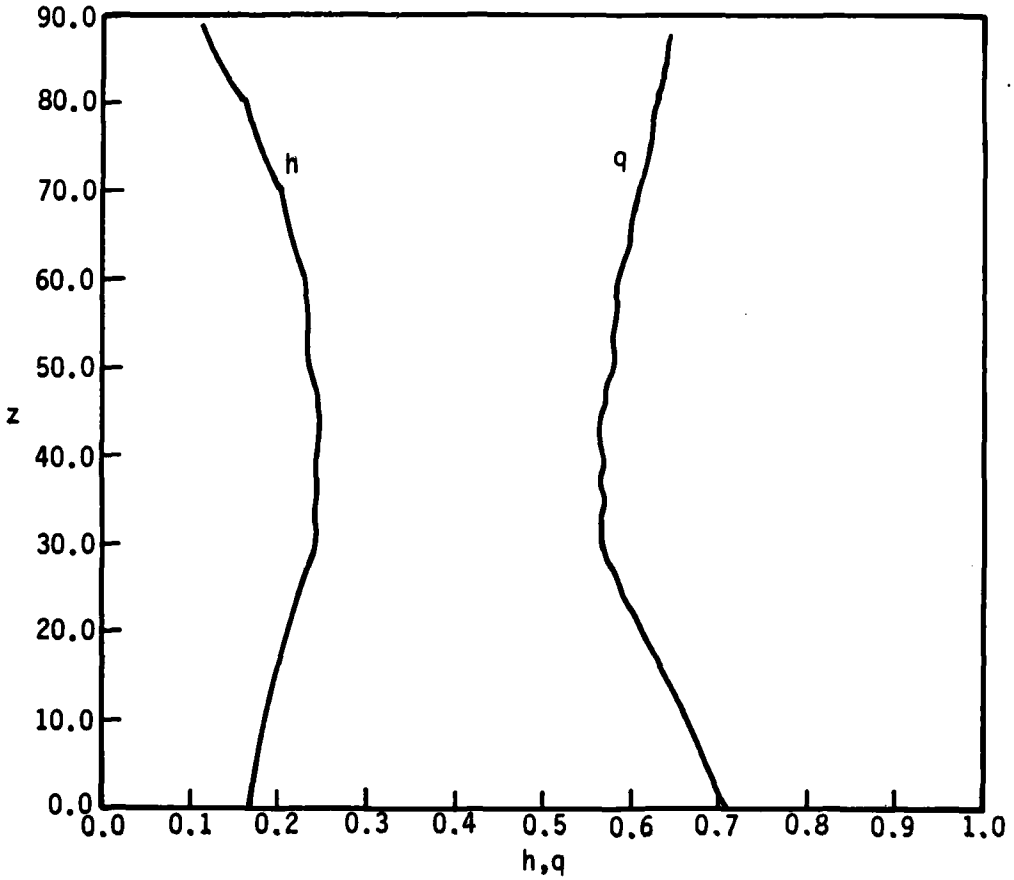

FIGURE 15. For the case of figure 12 with a fully inserted eye, the eyewall thickness h, and the transversely averaged eyewall radial-axial-flow speed q, as functions of altitude z, for the R(z) adopted in figure 14.

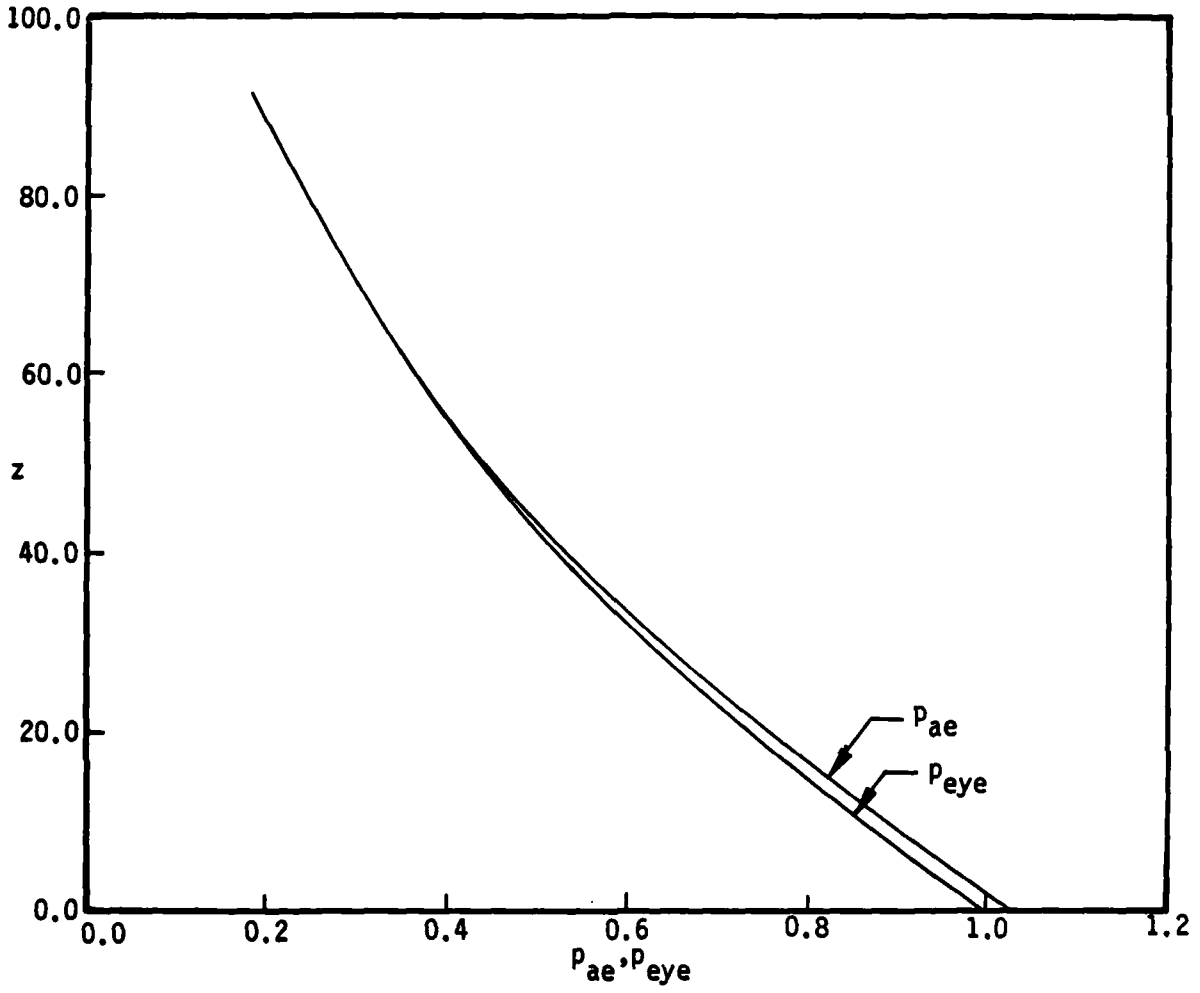

FIGURE 16. For the case of figure 12 with a fully inserted eye, the pressure in the eye p_{eye} and the pressure at the ambient edge of the eyewall p_{ae} as functions of altitude z, for the R(z) adopted in figure 14.

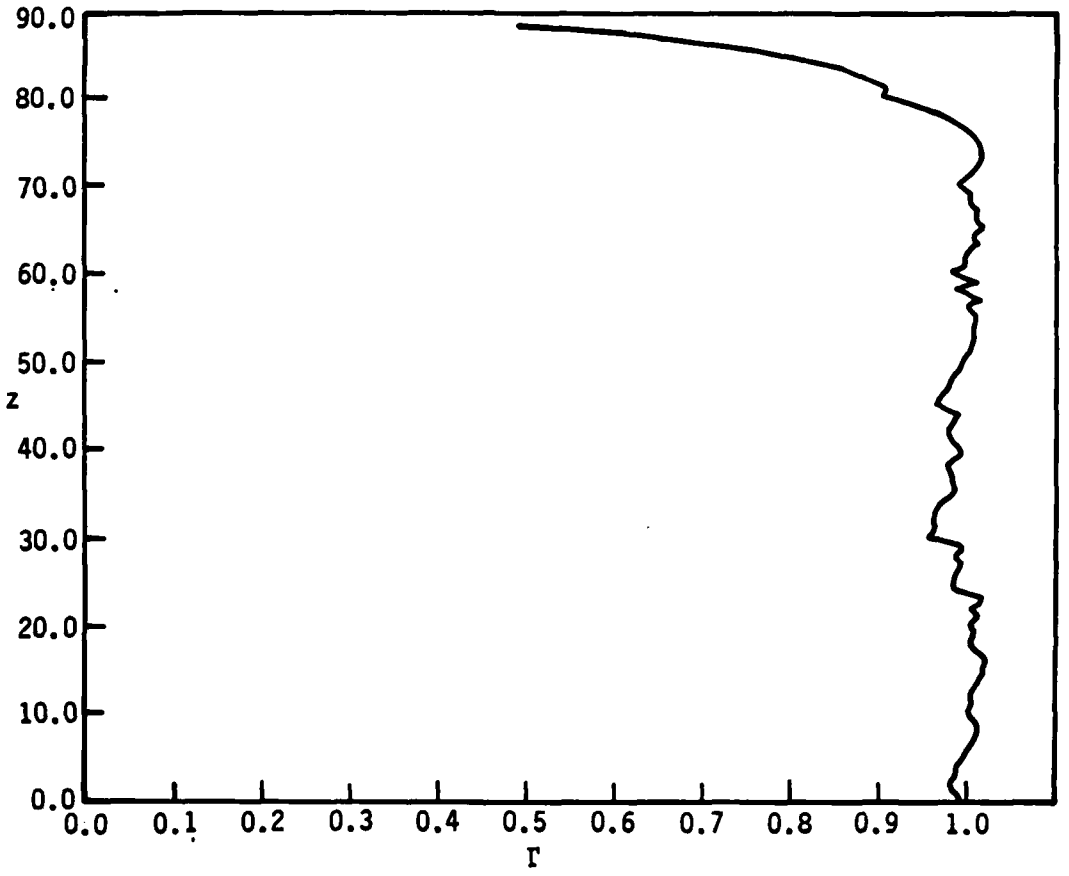

FIGURE 17. For the case of figure 12 with a fully inserted eye, the angular momentum Γ as a function of altitude z, for the R(z) adopted in figure 14. The "jitter" is attributed to simplistic numerical procedure.

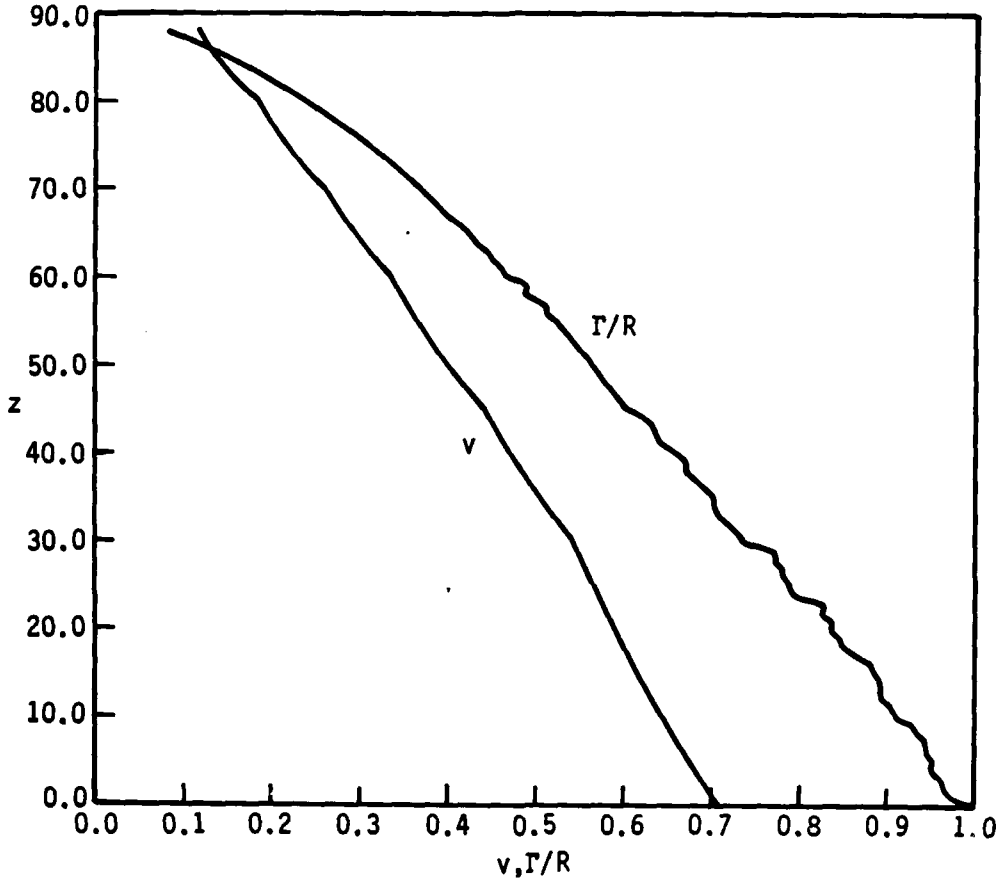

FIGURE 18. For the case of figure 12 with a fully inserted eye, the transversely averaged eyewall swirl speed v, and the swirl speed of the potential vortex at the eyewall edge (Γ/R), as functions of altitude z. Maintaining $(\Gamma/R) > v$ until high in the troposphere constrains the choice of R(z) adopted (figure 14).

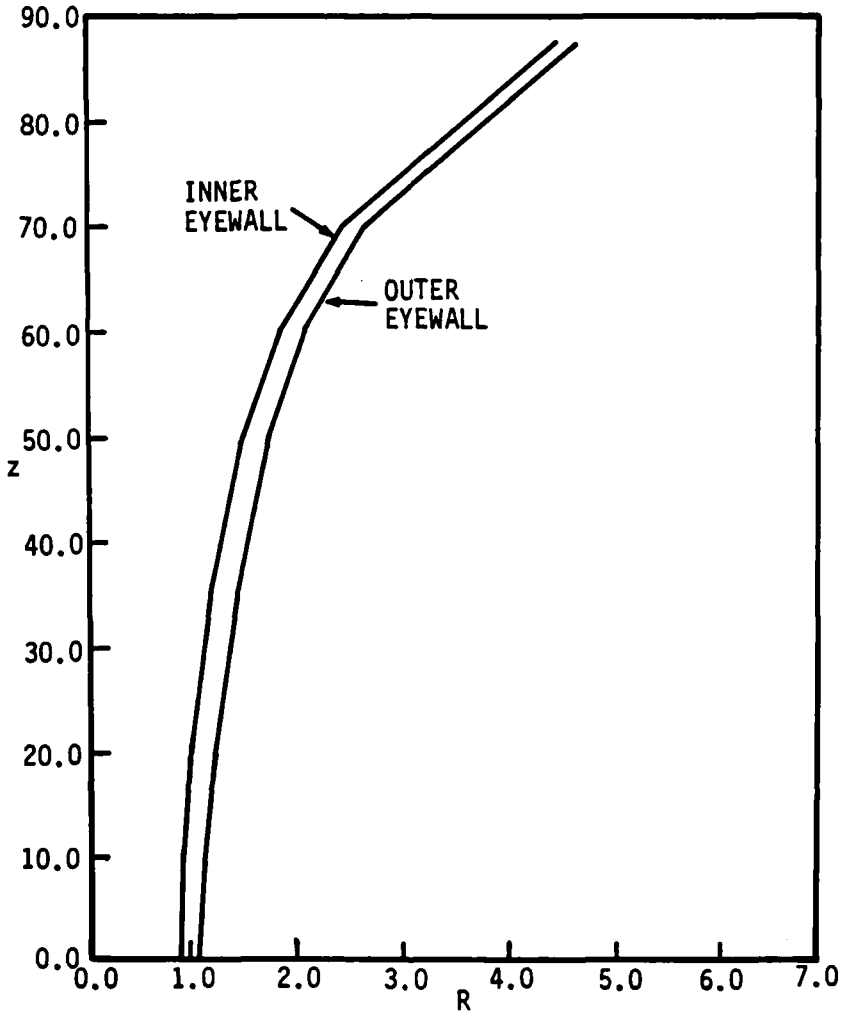

FIGURE 19. For the case of figure 12 with a 90% inserted eye, the adopted radial displacement R of the outer eyewall as a function of altitude z.

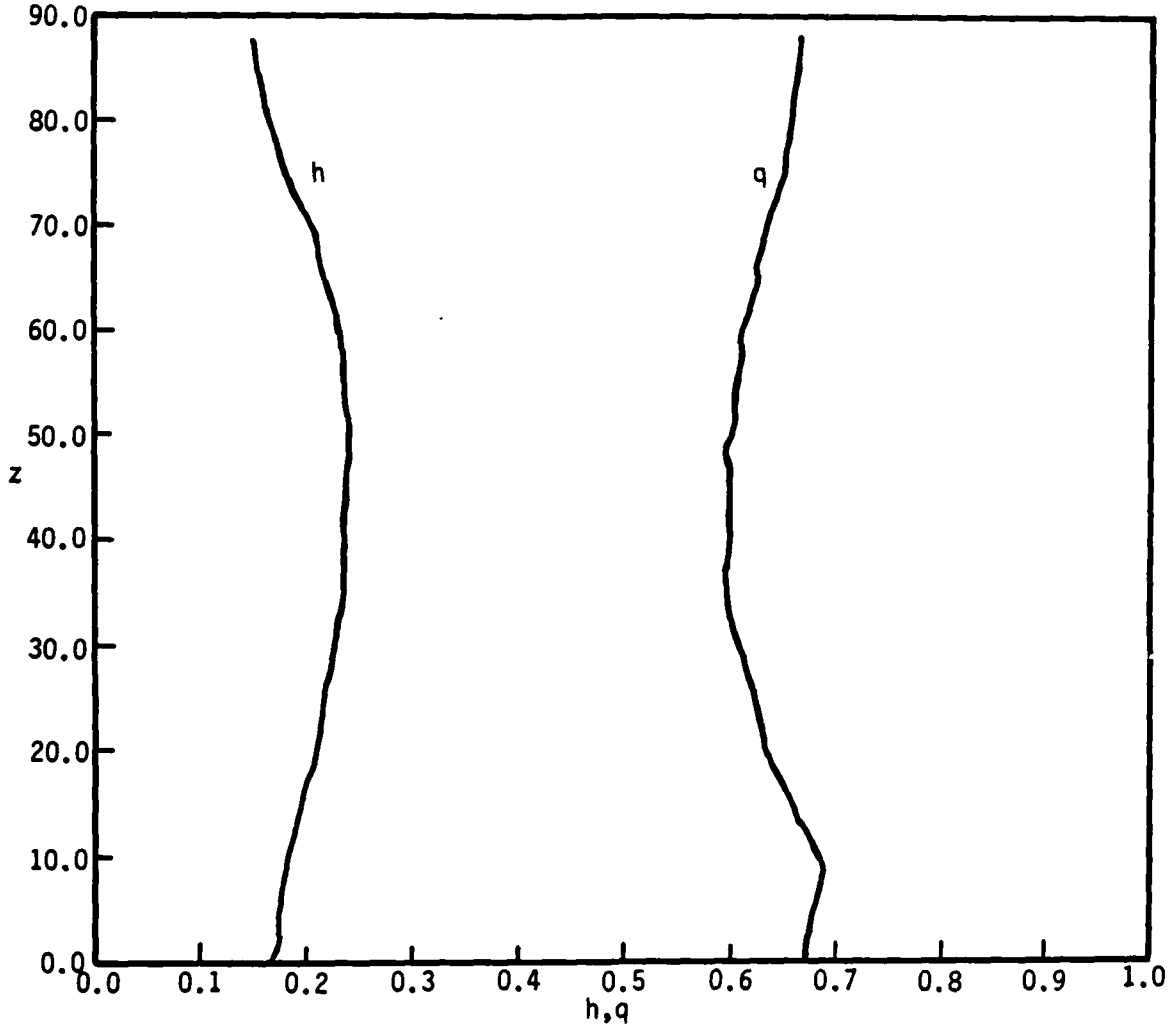

FIGURE 20. For the case of figure 12 with a 90% inserted eye, the eyewall thickness h, and the radial-axial-flow speed q, as functions of altitude z, for the R(z) adopted in figure 19.

AD-A138 242 CONDITIONS FOR TWO-CELL STRUCTURE IN SEVERE VORTICAL STORMS(U) TRW SPACE AND TECHNOLOGY GROUP REDONDO BEACH CA G F CARRIER ET AL. FEB 84 TRW-35524-6003-UT-00 2/2

UNCLASSIFIED N00014-79-C-0508 F/G 4/2 NL

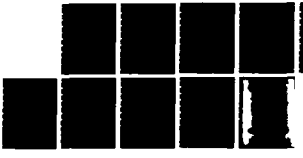

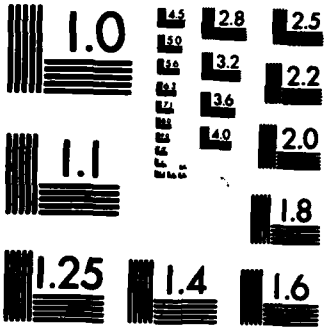

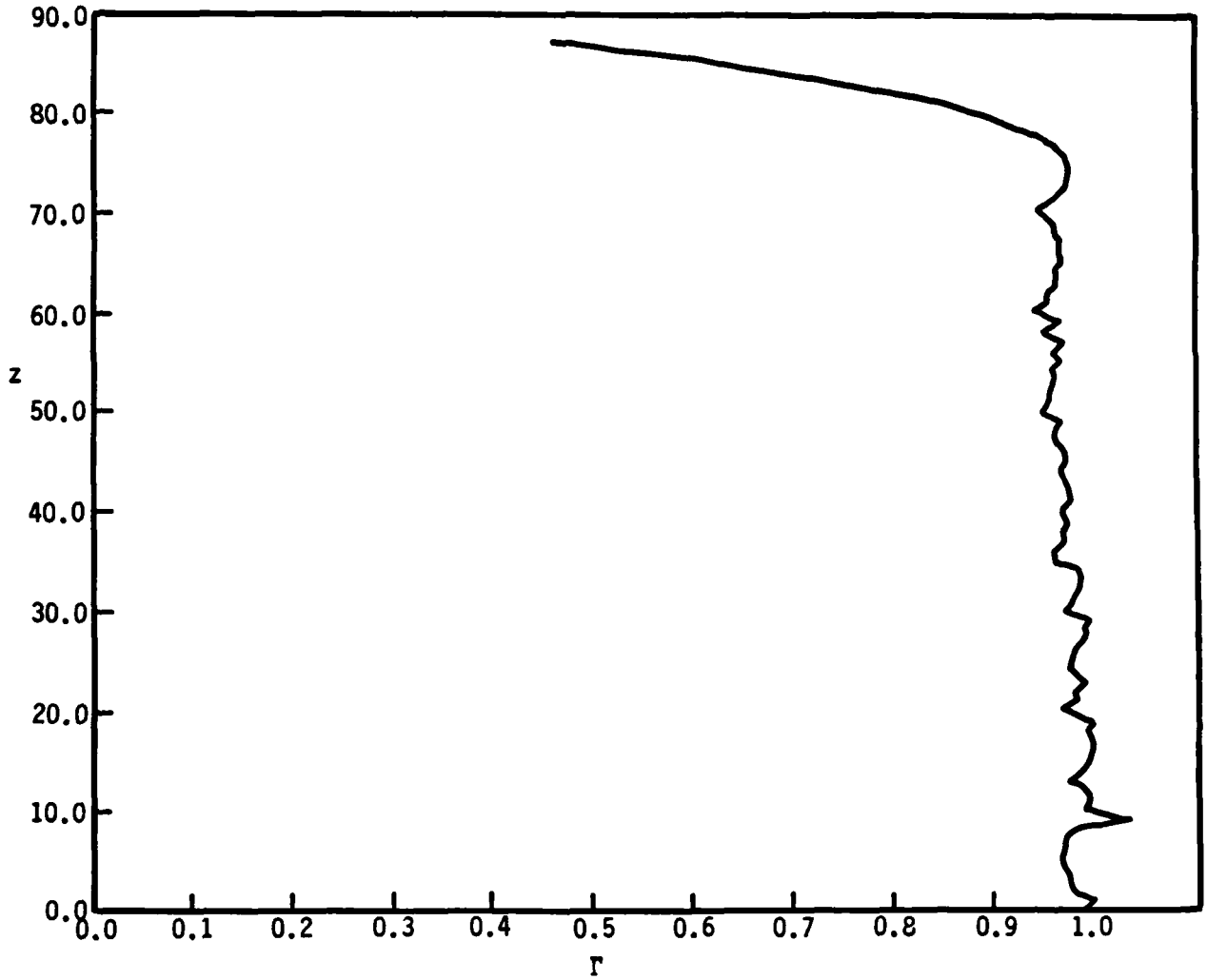

FIGURE 21. For the case of figure 12 with a 90% inserted eye, the angular momentum Γ as a function of altitude z, for the R(z) adopted in figure 19.

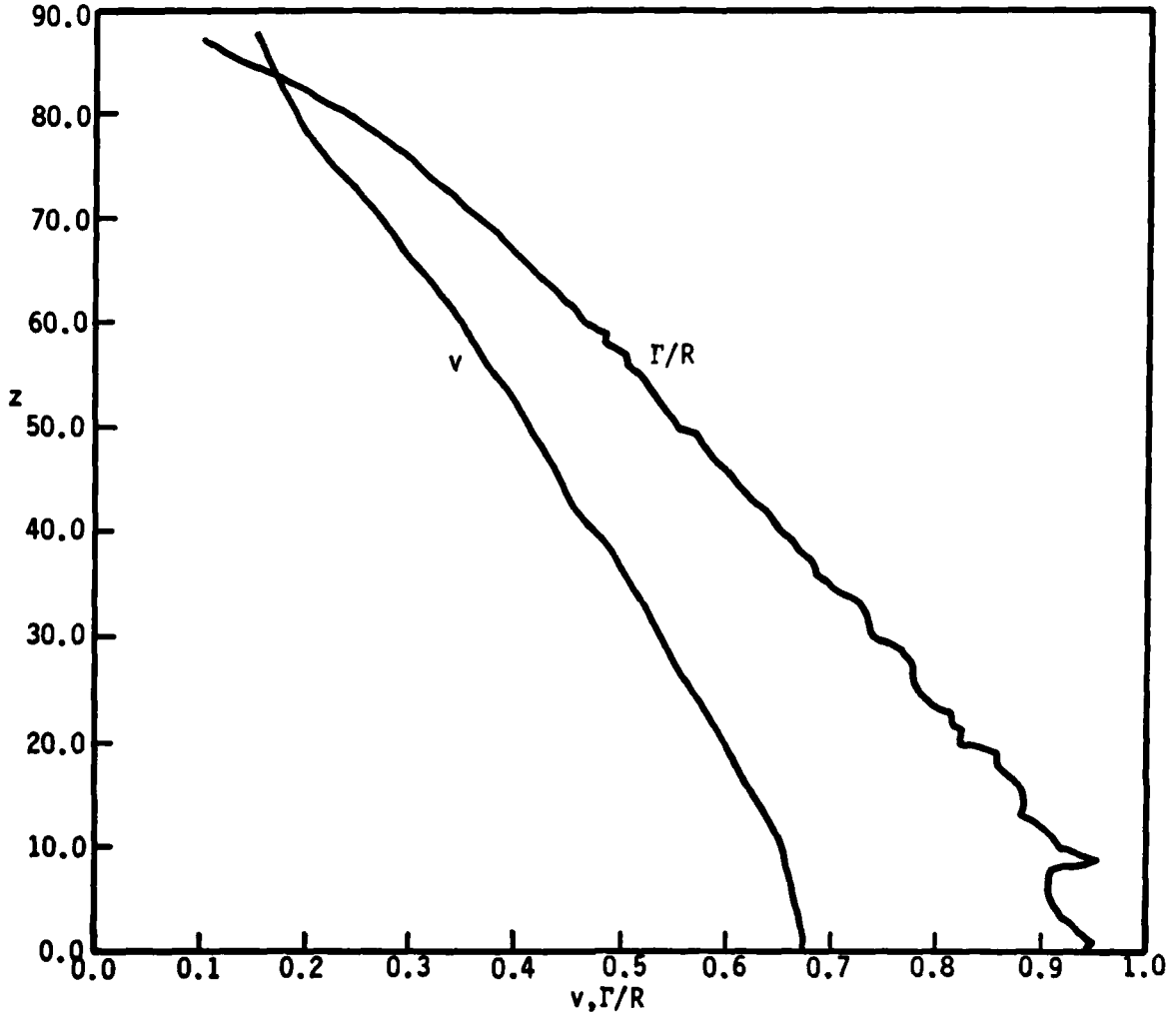

FIGURE 22. For the case of figure 12 with a 90% inserted eye, the eyewall swirl speed v, and the swirl speed of the potential vortex at the eyewall edge (Γ/R), as functions of altitude z. Satisfaction of the stability constraint (Γ/R) > v through most of the troposphere furnishes a strong constraint on the iteratively-arrived-at selection of R(z) presented in figure 19.

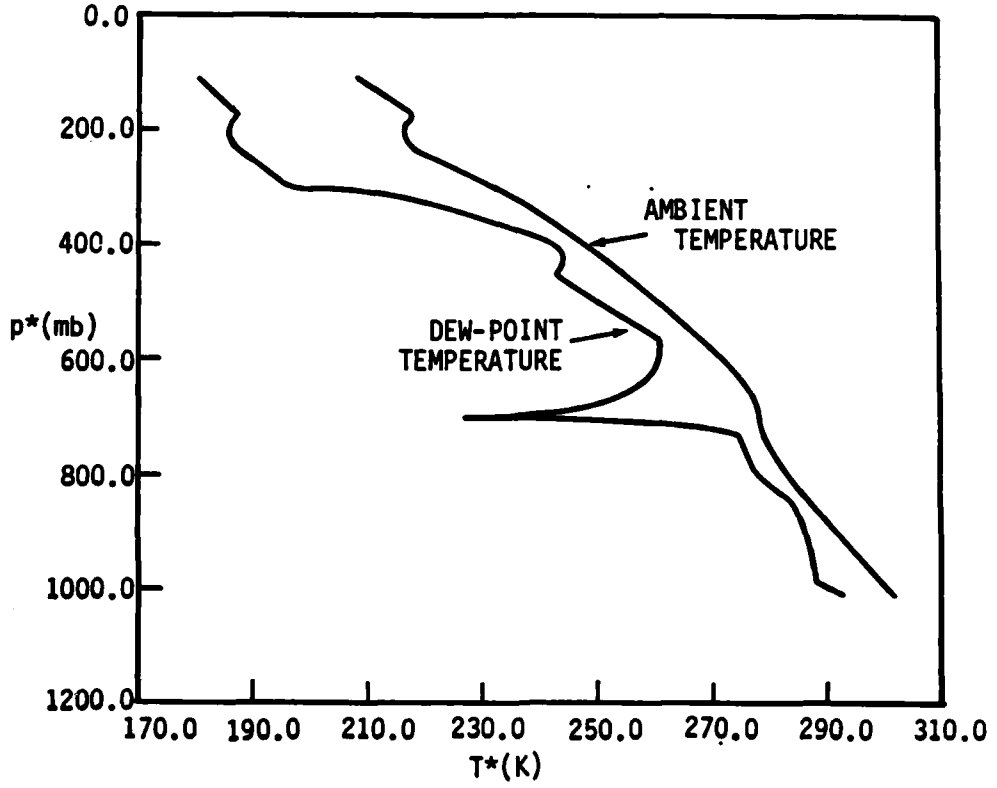

FIGURE 23. Moderately convectively unstable ambient (measured in the vicinity of a tornado) at Jackson, MS, on April 17, 1978 at 2300Z.

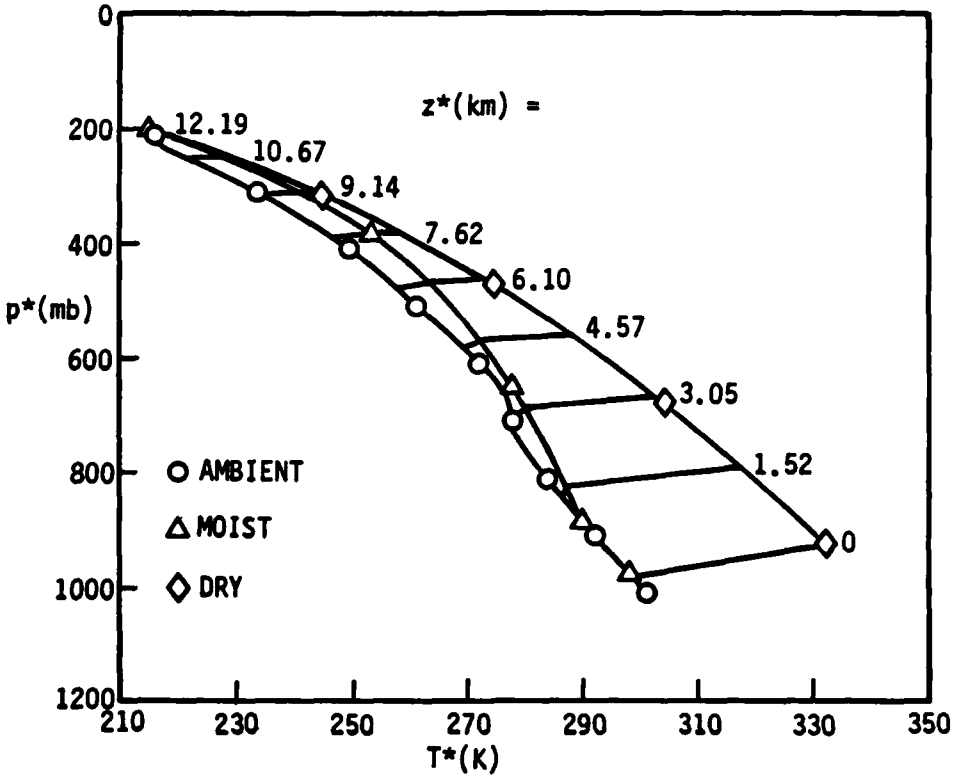

FIGURE 24. Pressure-temperature relationships for the ambient of figure 23, for ground-level air raised on a moist adiabat to its level of neutral stability (i.e., to the tropopause as defined here), and for tropopause-level air compressed dry-adiabatically. Heights are associated by means of hydrostatics, with $z^* = 0$ being ground level. The fractional heights displayed are the result of conversion from engineering units to SI convention.

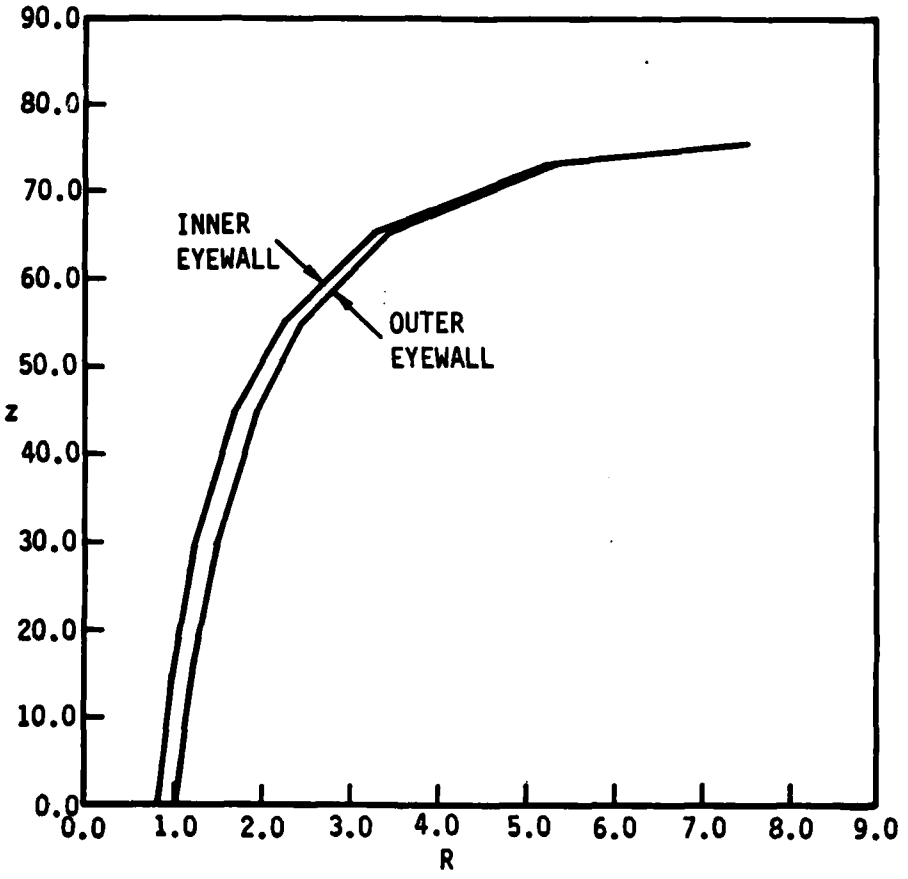

FIGURE 25. For the case of figure 23 with a fully inserted eye, the adopted radial displacement R of the outer eyewall (i.e., the eyewall edge contiguous to the potential vortex) as a function of altitude z, where the completion-of-turnaround height is taken as $z = 0$. The inner eyewall position is the site of the eyewall edge contiguous to the eye; the inner edge is located by the eyewall thickness in a direction perpendicular to the local tangent to R(z).

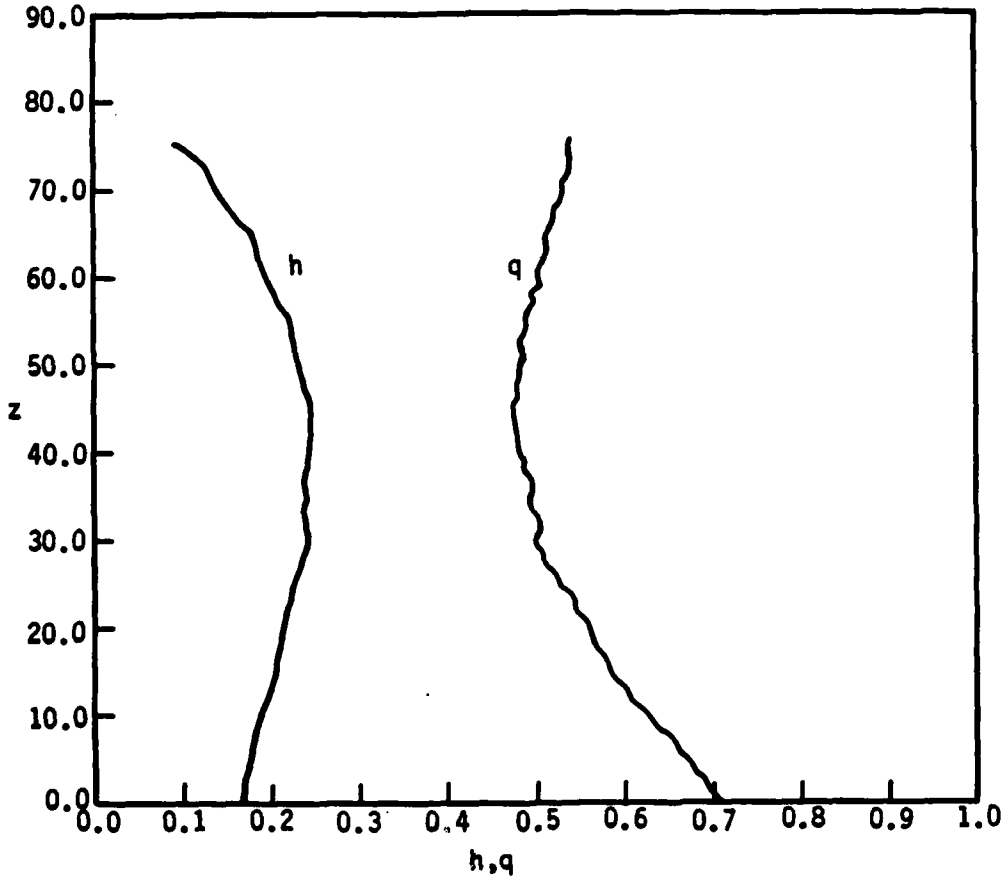

FIGURE 26. For the case of figure 23 with a fully inserted eye, the eyewall thickness h, and the transversely averaged eyewall radial-axial-flow speed q, as functions of altitude, for the R(z) adopted in figure 25.

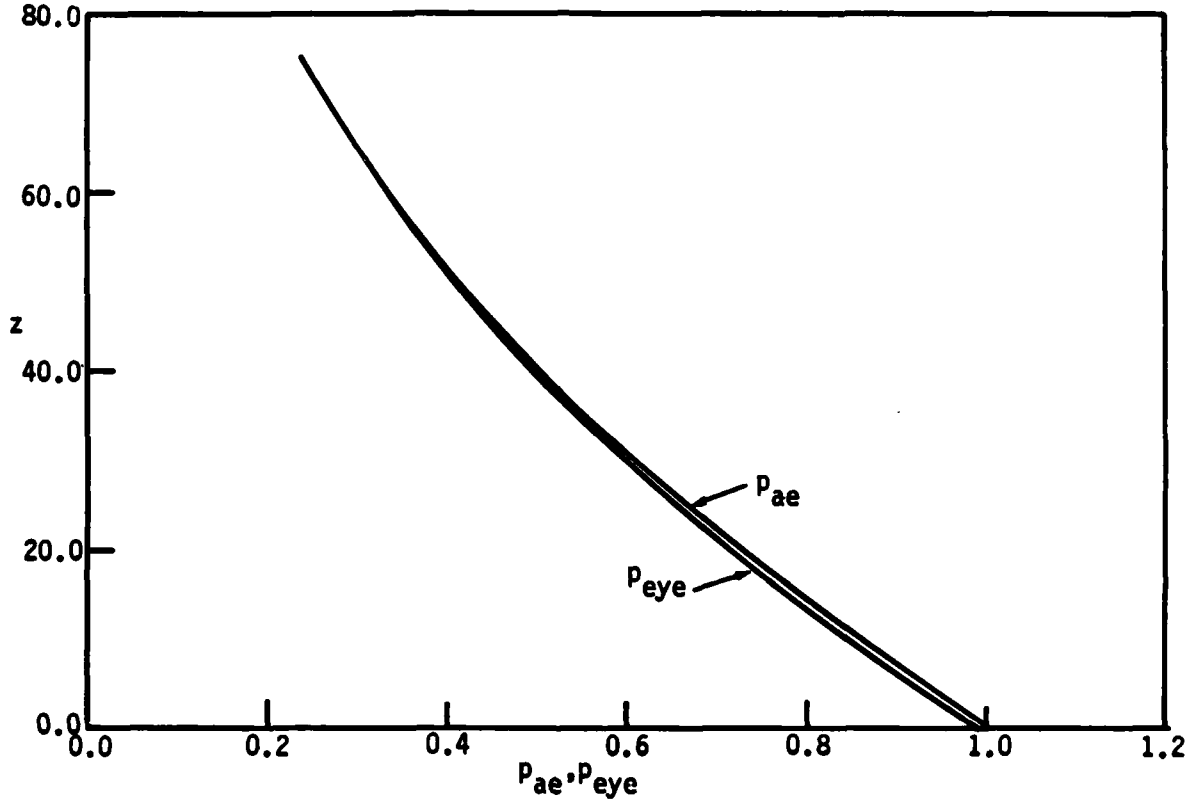

FIGURE 27. For the case of figure 23 with a fully inserted eye, the pressure in the eye p_{eye} and the pressure at the ambient edge of the eyewall p_{ae} as functions of altitude z, for the R(z) adopted in figure 25.

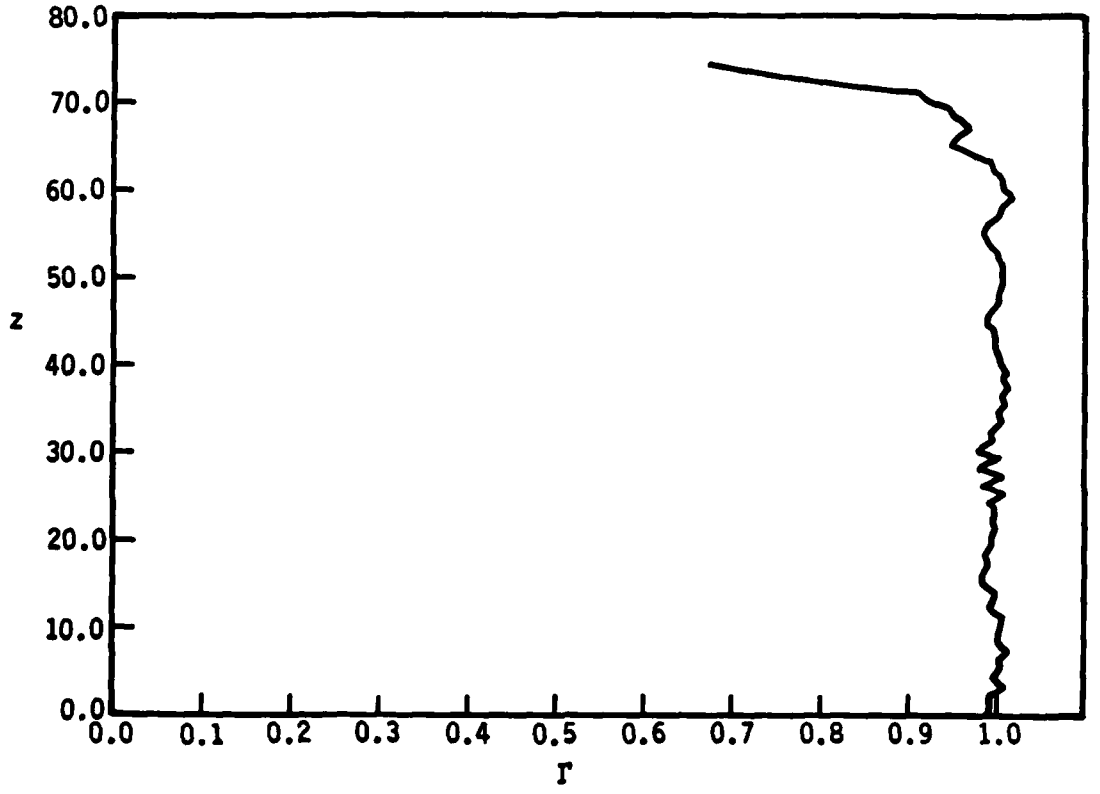

FIGURE 28. For the case of figure 23 with a fully inserted eye, the angular momentum Γ as a function of altitude z, for the R(z) adopted in figure 25. The "jitter" is attributed to simplistic numerical procedure.

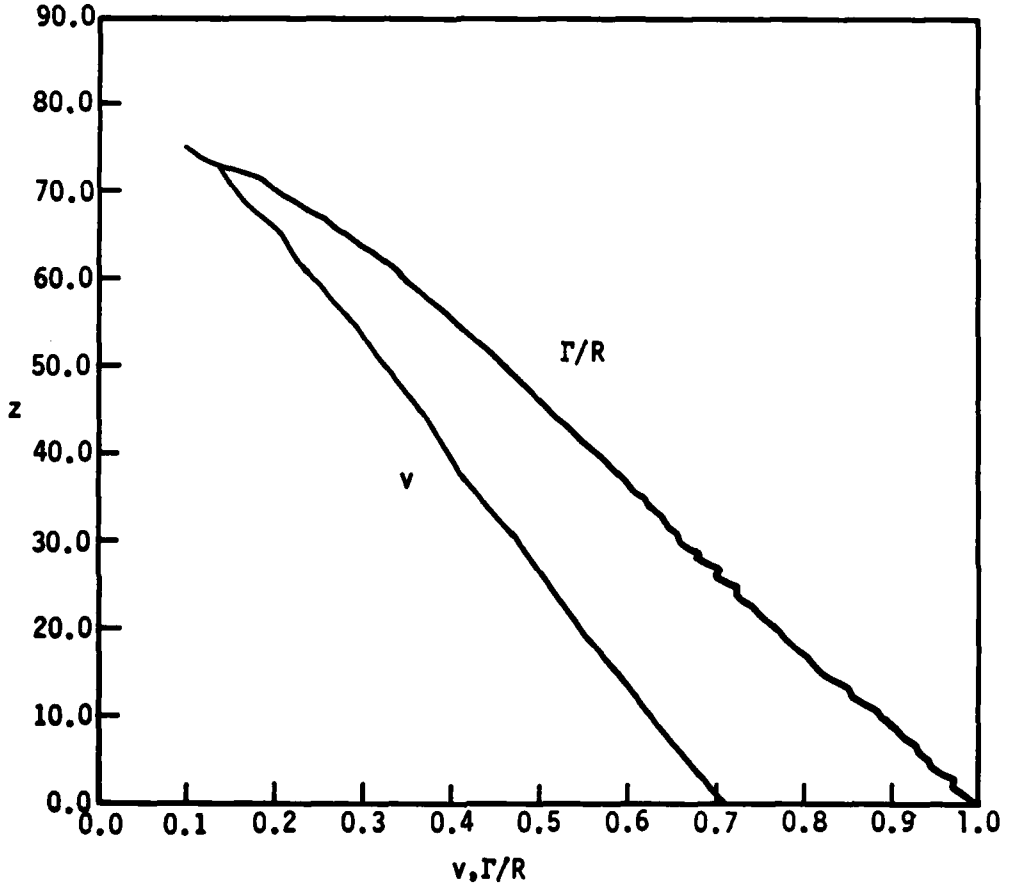

FIGURE 29. For the case of figure 23 with a fully inserted eye, the transversely averaged eyewall swirl speed v, and the swirl speed of the potential vortex at the eyewall edge, as functions of altitude z. Maintaining (Γ/R) > v until high in the troposphere constrains the choice of R(z) adopted (figure 25).

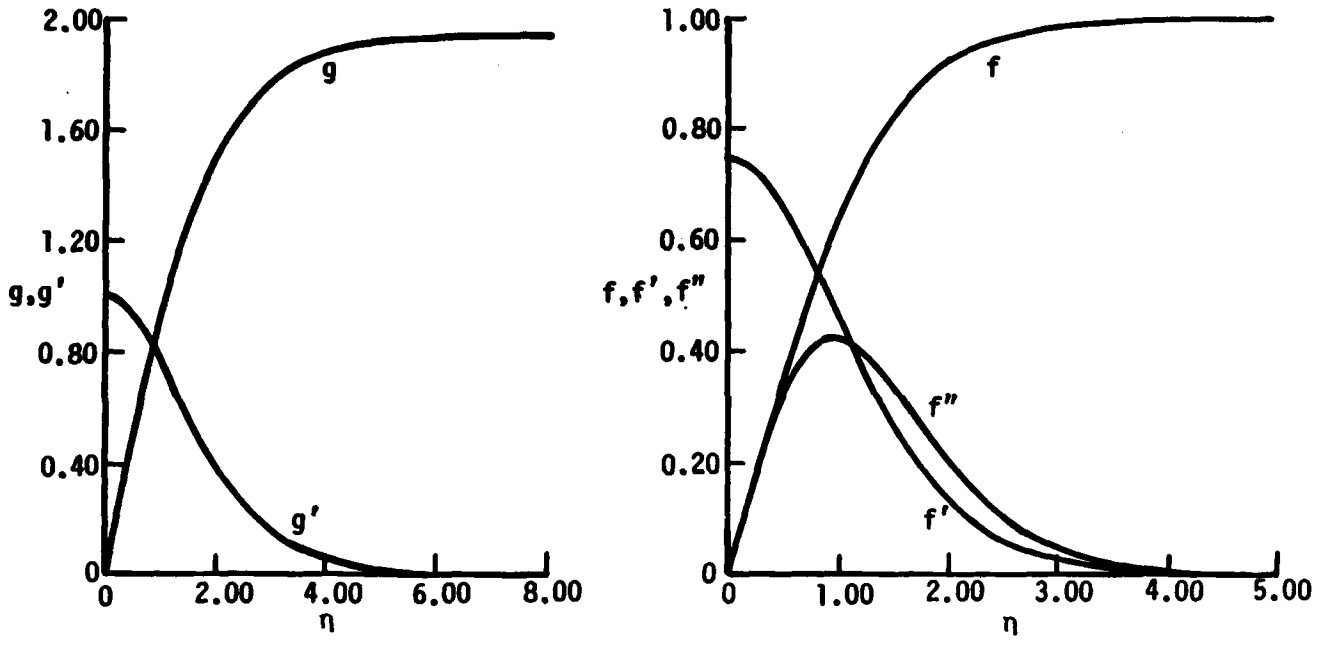

FIGURE 30. For constant viscosity, numerical results for the outer, thicker portion of the inflow layer under the high-speed part of the inviscid vortex. Left, results related to the radial and axial flow components. Right, results related to the swirl velocity component. The similarity independent variable η is large for large distance normal to the wall.

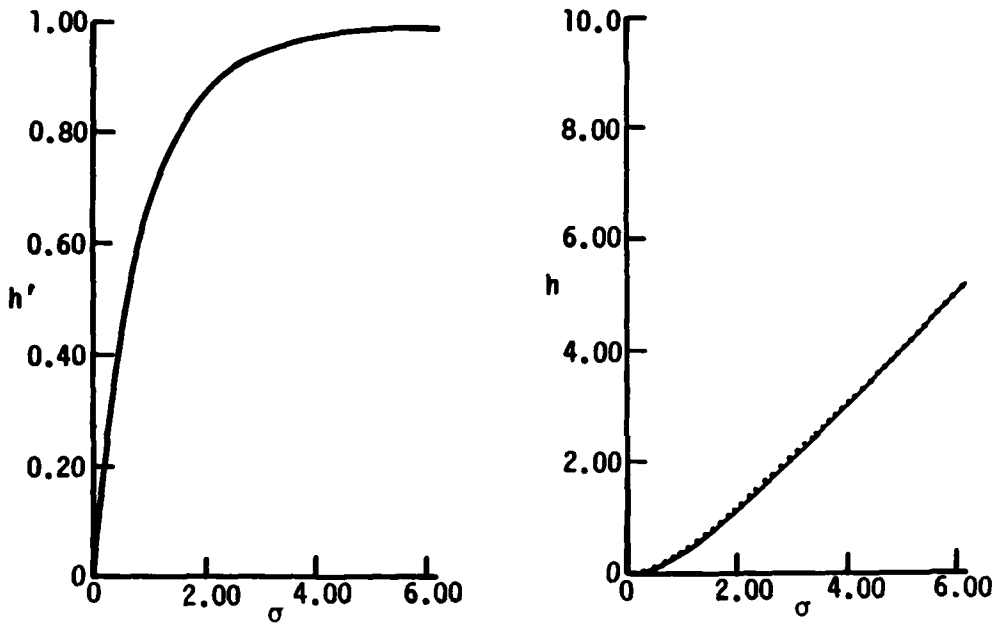

FIGURE 31. For constant viscosity, results related to the radial inflow in the thin, effectively nonrotating sublayer immediately contiguous to the wall, under a rapidly swirling vortex. Left, $h'(\sigma)$, as computed numerically. Right, a comparison of numerically computed results (dotted line) and the approximate analytic expression discussed in the text (solid line) for $h(\sigma)$. The similarity independent variable σ is large for large distance normal to the wall.

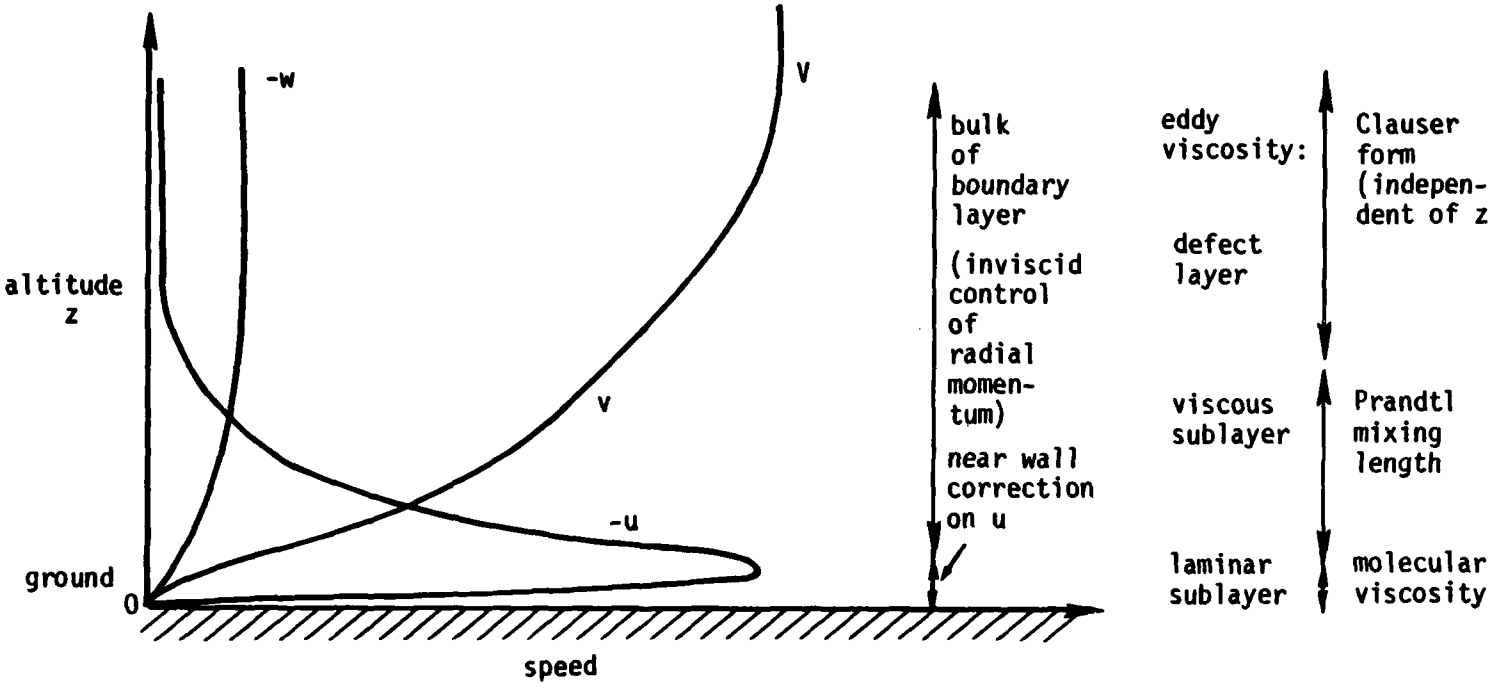

FIGURE 32. A schematic of the axial profile of radial velocity component u, azimuthal velocity component v, and axial velocity component w, at a radial distance r from the center of the vortex, at which the impressed swirl V is large.

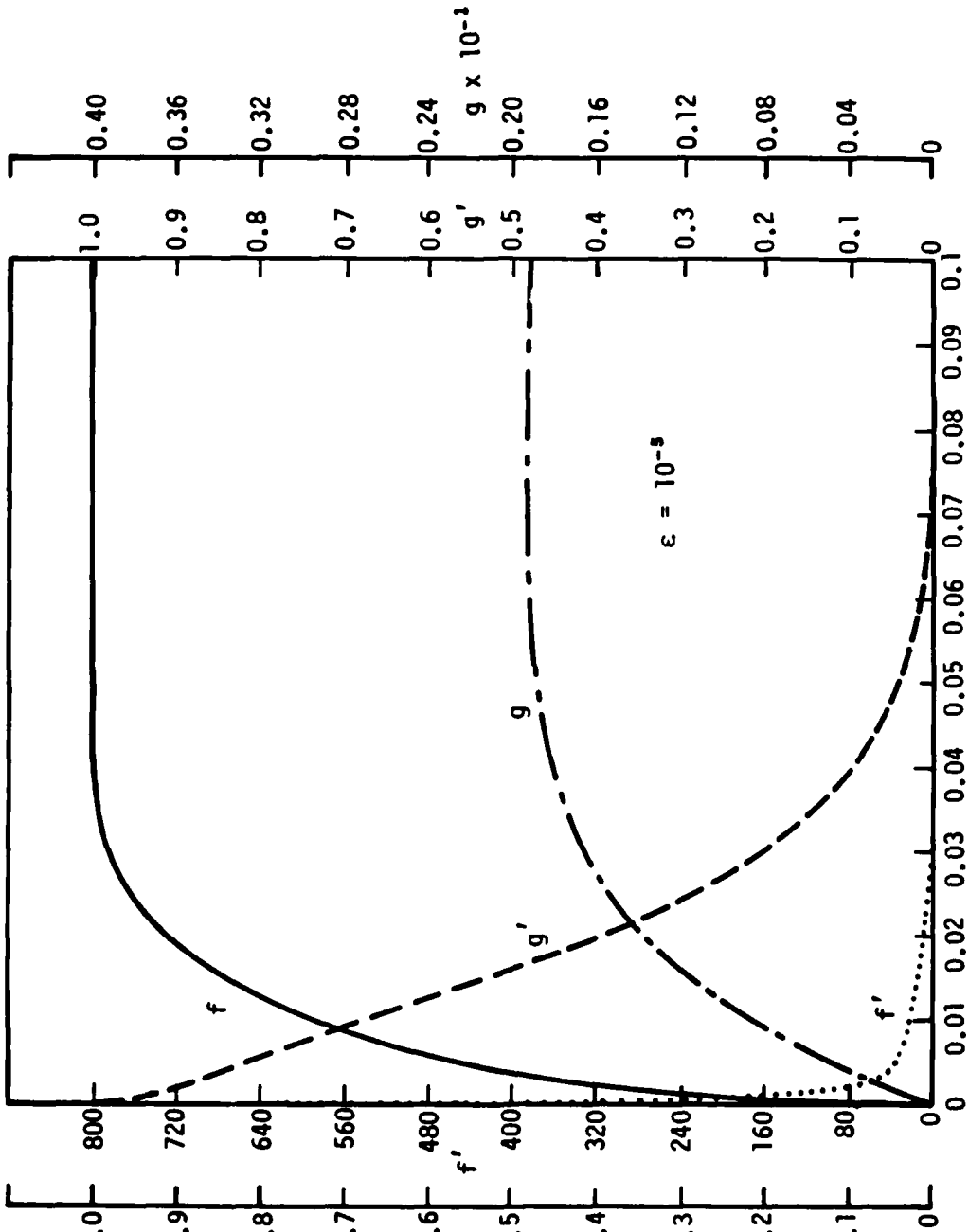

FIGURE 33. Numerical results, for inverse Reynolds number $\varepsilon = 10^{-5}$, for the turbulent boundary layer under a rapidly swirling vortex.

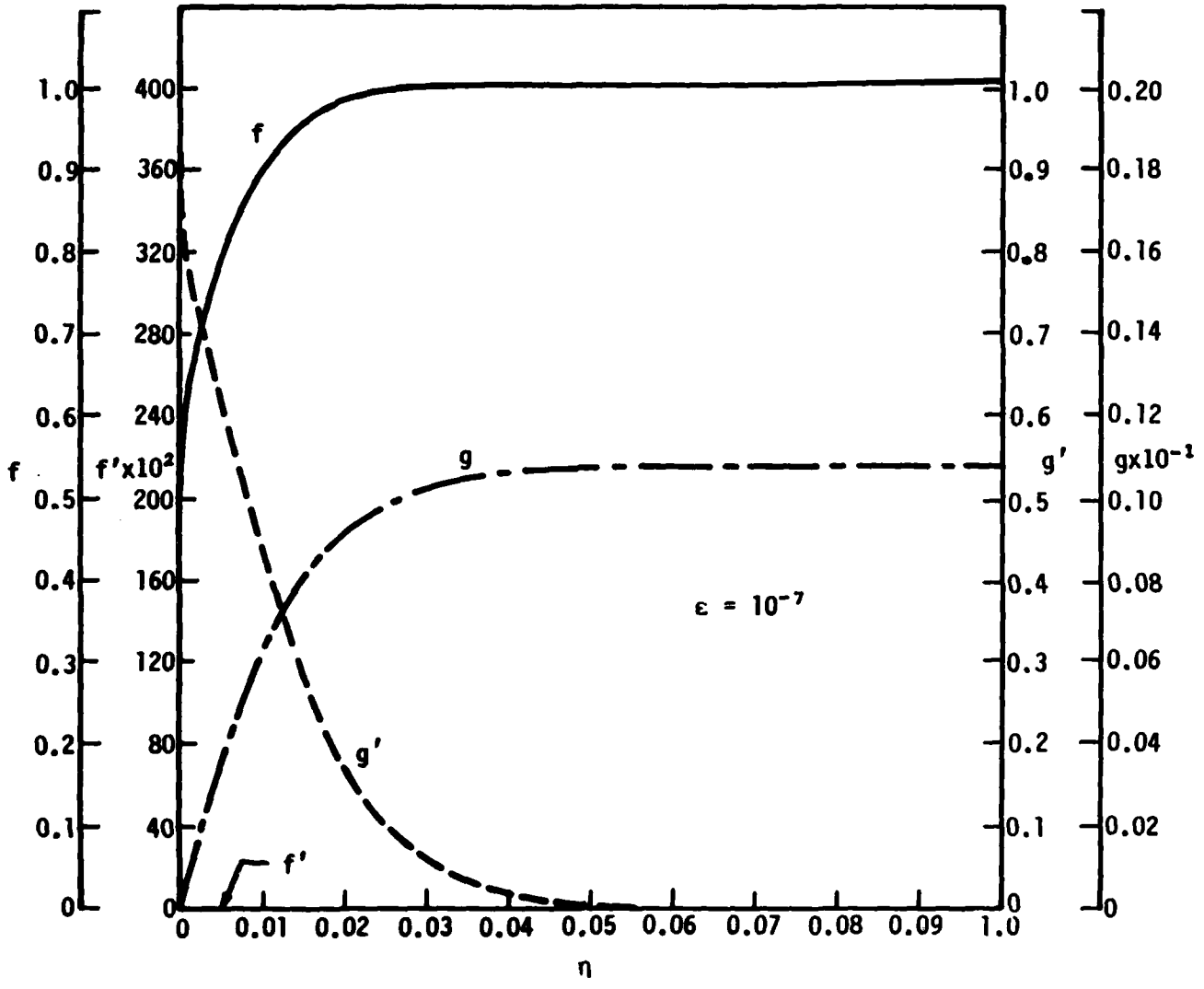

FIGURE 34. Numerical results for inverse Reynolds number $\varepsilon = 10^{-7}$, for the turbulent boundary layer under a rapidly swirling vortex.

α	β	α/β	$R'(0) \equiv R_0'$	$(R^-)_{calc}$	$(R^-)_{\alpha=0}$	$(R^+)_{calc}$	$(R^+)_{\alpha=0}$
0.1	0.1	0.0	2.0	0.791	0.789	1.264	1.266
0.0	0.1	0.0	5.0	0.754	0.751	1.326	1.329
0.0	0.1	0.0	10.0	0.742	0.738	1.348	1.352
0.0	0.1	0.1	100.0	0.732	0.727	1.366	1.372
0.0	0.2	0.0	2.0	0.718	0.714	1.392	1.397
0.0	0.2	0.0	5.0	0.671	0.664	1.489	1.497
0.0	0.2	0.0	10.0	0.656	0.647	1.524	1.533
0.0	0.2	0.0	100.0	0.644	0.632	1.553	1.565
0.1	0.1	1.0	2.0	0.820	0.789	1.295	1.266
0.1	0.1	1.0	5.0	0.777	0.751	1.348	1.329
0.1	0.1	1.0	10.0	0.762	0.738	1.366	1.352
0.1	0.1	1.0	100.0	0.750	0.727	1.381	1.372
0.1	0.2	0.5	2.0	0.748	0.714	1.422	1.397
0.1	0.2	0.5	5.0	0.695	0.664	1.510	1.497
0.1	0.2	0.5	10.0	0.677	0.647	1.541	1.533
0.1	0.2	0.5	100.0	0.663	0.632	1.567	1.566
0.1	0.5	2.0	2.0	0.876	0.846	1.212	1.181
0.1	0.5	2.0	5.0	0.841	0.818	1.244	1.223
0.1	0.5	2.0	10.0	0.828	0.808	1.254	1.237
0.1	0.5	2.0	100.0	0.818	0.800	1.264	1.250
0.2	0.1	2.0	2.0	0.845	0.789	1.325	1.266
0.2	0.1	2.0	5.0	0.796	0.751	1.369	1.329
0.2	0.1	2.0	10.0	0.779	0.738	1.384	1.352
0.2	0.1	2.0	100.0	0.765	0.727	1.396	1.372
0.2	0.2	1.0	2.0	0.774	0.714	1.452	1.397
0.2	0.2	1.0	5.0	0.716	0.664	1.530	1.497
0.2	0.2	1.0	10.0	0.695	0.647	1.558	1.533
0.2	0.2	1.0	100.0	0.678	0.632	1.581	1.566
0.2	0.4	0.5	2.0	0.685	0.615	1.652	1.606
0.2	0.4	0.5	5.0	0.617	0.550	1.789	1.772
0.2	0.4	0.5	10.0	0.594	0.528	1.838	1.832
0.2	0.4	0.5	100.0	0.578	0.509	1.877	1.887

TABLE 1. Numerical results (denoted "calc") for extrema of the turnaround from integration of the initial-value problem (3.1.7)-(3.1.9). Results for $(R^{\pm})_{\alpha=0}$ are from (3.1.16). Also, calculated results for $R^{\pm}$ for $R_0' = 100$ are within 2% of results for $R_0' \to +\infty$, for α,β studied.

ε	σ	η_1	$f'(0)$
10^{-4}	$1.35 \cdot 10^{-2}$	$6.18 \cdot 10^{-3}$	$1.17868 \cdot 10^{2}$
10^{-5}	$6.90 \cdot 10^{-3}$	$3.85 \cdot 10^{-3}$	$6.24682 \cdot 10^{2}$
10^{-7}	$2.88 \cdot 10^{-3}$	$2.395 \cdot 10^{-3}$	$2.56536 \cdot 10^{4}$
10^{-9}	$1.637 \cdot 10^{-3}$	$1.805 \cdot 10^{-3}$	$1.36583 \cdot 10^{6}$
10^{-11}	$1.034 \cdot 10^{-3}$	$1.436 \cdot 10^{-3}$	$9.72465 \cdot 10^{7}$

TABLE 2. Properties of the approximate selfsimilar solution for the turbulent boundary layer under the high-speed portion of a potential vortex.

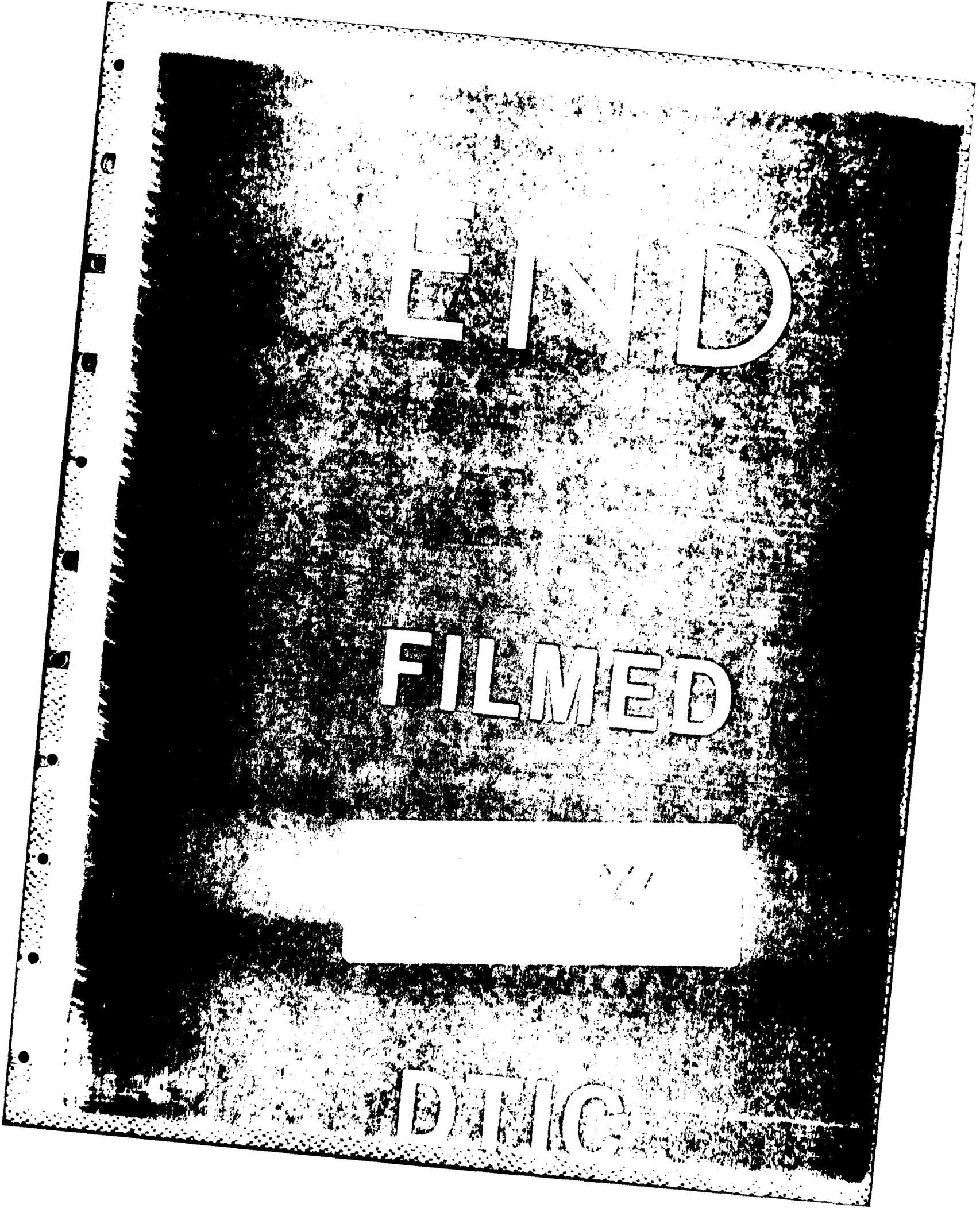
END
FILMED
DTIC